# Developing models of T cell mediated injury to the bone marrow niche

Daniel Octavius Jasper North

*Green Templeton College*

Weatherall Institute of Molecular Medicine




*Thesis submitted for the degree of Master of Science (by Research) in Medical Sciences*

University of Oxford

Trinity 2025

## Abstract

Haematopoiesis takes place within a tightly regulated niche, which provides the microanatomical, metabolic and immunological context for normal haematopoietic function. Several diseases characterised by bone marrow failure are mediated by T cell mediated inflammation within the bone marrow niche. These include poor graft function following allogeneic stem cell transplantation (alloSCT), immune effector cell-associated haematotoxicity following chimeric antigen receptor T cell therapy and immune aplastic anaemia. A mechanistic understanding of the cause of bone marrow failure in these conditions is required to facilitate the rational development of new interventions to improve patient outcomes.

These mechanistic insights are impeded by limitations in existing pre-clinical models, which calls for the development of novel tractable model systems. Bone marrow stromal populations are a target for graft-vs-host disease (GVHD) following alloSCT with implications for both stromal and haematopoietic function. We hypothesise that the injury to bone marrow stromal populations by alloreactive T cells can be used as the basis for new models to explore the impact of T cell mediated injury to the haematopoietic niche. The work presented in this thesis is nested within a larger project with the following aim:

*To develop and mechanistically interrogate tractable models of T cell mediated injury to the haematopoietic niche, to identify novel targets for the treatment of cytopenias following cellular therapies, and related conditions.*

The scope of the work presented in this thesis is the initial development of these model systems; a murine model of GVHD optimised to study the impact of GVHD on the haematopoietic niche, and an *in vitro* system using human iPSC-derived bone marrow organoids.

Prior studies exploring the impact of GVHD on haematopoiesis in mice used models characterised by severe systemic illness and short survival, which limits the study of engrafting haematopoiesis. This limitation was circumvented by selecting a transplant model characterised by a mild GVHD phenotype and carefully titrating the dose of graft T cells. This resulted in a phenotype in the GVHD cohort relative to controls characterised by anaemia, changes to bone marrow stromal population architecture and a trend towards a reduction in $CD201^{+}$ long-term haematopoietic stem cells. Bone marrow failure and pancytopenia were not observed in these experiments, but these results will guide ongoing model development.

A recently published protocol to generate human iPSC-derived bone marrow organoids was established within our laboratory. This will form the basis of an experimental system reacting primary donor T cells against organoids to explore T cell mediated injury to the bone marrow niche in a novel model system using human tissue. An attempt was also made to generate an MHC class I/II K/O iPSC line, to generate hypo-immune organoids for use as a negative control within this experimental system.

## Acknowledgements

I would like to thank my supervisors, Professor Ronjon Chakraverty, Dr Adam Wilkinson and Dr Abdullah Khan. Undertaking this work has been a wonderful opportunity, and I am grateful for their guidance, expertise and support throughout this project. I would also like to express my thanks to Associate Professor Bethan Psaila and Professor Andrew McMichael for their contributions to my thesis committee.

This project was made possible by a Scholarship awarded by The Haematology Society of Australia and New Zealand in partnership with Maddie Riewoldt's Vision. It is a privilege to be supported by an organisation dedicated to improving the lives of patients and families impacted by bone marrow failure syndromes.

This work was facilitated by the generous support of many collaborators. I would like to thank Jackie-Sloan Stanley and Christian Babbs in the WIMM transgenic core facility for their time and expertise. I would also like to thank the WIMM flow core facility and in particular Kevin Clark for his patience and humour. From the Psaila group, I would like to thank Dr Yuqi Shen, Dr Natalie Jooss, Ms Aude Olijnik and Ms Zoe Wong. I am grateful not just for the training, but for your boundless welcome and friendship. I would also like to thank the members of the Wilkinson and Chakraverty groups, in particular Dr Andrew McIntyre, Dr Leonid Olender and Ms Elisa Armbrecht.

Most importantly, I would like to thank my family, and in particular my wife Gayle. Without your love and support none of this would have been possible.

## Table of Contents


*1. Introduction and Background* ..... *11*

**1.0 Overview** ..... **11**

**1.1 Haematopoiesis and the Haematopoietic Niche** ..... **12**

1.1.1 Traditional 'branching tree' models of haematopoiesis ..... 12
1.1.2 Single cell technologies and new models of haematopoiesis ..... 14
1.1.3 Haematopoiesis in a spatial context ..... 15
1.1.4 Niche support for haematopoiesis ..... 15
1.1.5 Non-haematopoietic populations in the bone marrow niche ..... 17

**1.2 Inflammation in the Haematopoietic Niche** ..... **21**

1.2.1 Emergency myelopoiesis and stress haematopoiesis ..... 21
1.2.2 Inflammation and HSC fitness ..... 22
1.2.3 Bone marrow stroma and inflammation ..... 24

**1.3 T Cell Mediated Inflammation in the Haematopoietic Niche in Human Disease** ..... **26**

1.3.1 Poor graft function following alloSCT and bone marrow GVHD ..... 26
1.3.2 Immune effector cell-mediated haematotoxicity ..... 29
1.3.3 Immune aplastic anaemia ..... 31
1.3.4 Other conditions ..... 31

**1.4 Applications and Limitations of Existing Model Systems** ..... **33**

**1.5 Project Aims and Objectives** ..... **35**

*2. Materials and Methods* ..... *37*

**2.0 Murine Model Development** ..... **37**

2.0.1 Animals ..... 37
2.0.2 Equipment and analysers ..... 37
2.0.3 Cellular product method development ..... 38
2.0.4 Buffers and reagents ..... 41
2.0.5 Endpoint flow cytometry panel development ..... 42
2.0.6 General transplantation experiment procedures ..... 42
2.0.7 Radiation dose titration ..... 43
2.0.8 Syngeneic transplant and non-transplanted littermates ..... 44
2.0.9 T cell dose titration ..... 44
2.0.10 Peripheral blood timepoint workflows ..... 45
2.0.11 Endpoint workflows ..... 46
2.0.12 Statistical Methods ..... 49
2.0.13 Software and analysis ..... 50

**2.1 Organoid Differentiation** ..... **51**

2.1.1 Overview ..... 51
2.1.2 HiPSC handling ..... 51
2.1.3 Phase I – Mesodermal induction ..... 53
2.1.4 Phase II – Stromal and haematopoietic commitment ..... 53
2.1.5 Day 5 – Hydrogel embedding ..... 54
2.1.6 Phase III – Vascular sprouting ..... 55
2.1.7 Phase IV – Hydrogel extraction and individual organoid culture ..... 55
2.1.8 Organoid digestion and analysis ..... 56
2.1.9 HiPSC CRISPR editing ..... 57

*3. Murine Model Development* ..... *59*

**3.0 Introduction and approach** ..... **59**

**3.1 Results** ..... **65**
3.1.1 Cell product method development ..... 65
3.1.2 Transplant endpoint flow cytometry panel development ..... 66
3.1.3 Radiation dose titration ..... 69
3.1.4 Syngeneic transplantation and aged matched litter mates ..... 72
3.1.5 T cell dose titration #1 ..... 76
3.1.6 T cell dose titration #2 ..... 78

**3.2 Discussion and Summary** ..... **88**

***4. Contributions to a Human iPSC-Derived Bone Marrow Organoid Model of Stromal Graft-vs-Host Disease*** ..... ***94***

**4.0 Introduction** ..... **94**

**4.1 Results** ..... **99**
4.1.1 Organoid differentiation technique replication ..... 99
4.1.2 MHC class I/II K/O hiPSC editing ..... 102

**4.2 Discussion** ..... **102**

***5 Discussion*** ..... ***105***

**5.0 Findings and Limitations** ..... **105**
5.0.1 Murine Model – Limitations due to underpowered experiments ..... 105
5.0.2 Murine Model – Peripheral blood phenotype ..... 106
5.0.3 Murine Model – T cell kinetics and endpoint timing ..... 110
5.0.4 Murine Model – Bone marrow haematopoietic and stromal findings ..... 111
5.0.5 Organoid model – progress and limitations ..... 114

**5.1 Future Directions** ..... **117**
5.1.1 Murine model optimisation ..... 117
5.1.2 Organoid model development ..... 121

**5.2 Conclusion** ..... **122**

***Appendices*** ..... ***124***

**Appendix 1 – Flow Cytometry Panels** ..... **124**

**Appendix 2 – Organoid Reagents** ..... **129**
Appendix 2 Section 1 – Component Reagents ..... 129
Appendix 2 Section 2 – Reagent Production ..... 130

***References*** ..... ***132***

## Table of Figures

Chapter 1

Figure 1. 1: Serial inflammatory insults irreversibly degrade HSC fitness. .....24

Figure 1. 2: Stromal GVHD in the haematopoietic niche post alloSCT. .....27

Chapter 2

Figure 2. 1: Example flow plots from a pre-infusion c-Kit$^{+}$ purity check.....40

Figure 2. 2: Simplified schematic of stepwise hydrogel embedding. .....55

Chapter 3

Figure 3. 1: Schematic representation of planned GVHD mouse model. .....61

Figure 3. 2: Representative gating for haematopoietic stem cell (HSC) and multipotent progenitor (MPP) populations. .....67

Figure 3. 3: Representative gating for lineage committed progenitor populations. 68

Figure 3. 4: Representative gating for bone marrow T cell populations. .....69

Figure 3. 5: Radiation dose titration peripheral blood analyses. .....71

Figure 3. 6: Donor chimerism by radiation dose in haematopoietic subpopulations. .....72

Figure 3. 7: Serial measurements of haematological parameters from individual non-transplanted 129 mice. .....74

Figure 3. 8: Haematological parameters following syngeneic transplantation compared with non-transplanted litter mates. .....75

Figure 3. 9: Stromal population architecture and phenotype following syngeneic transplantation compared with non-transplanted litter mates. .....76

Figure 3. 10: Peripheral blood analyses from T cell dose titration #1. .....77

Figure 3. 11: Clinical parameters by T cell dose from T cell dose titration #2.....79

Figure 3. 12: Peripheral blood analyses from T cell dose titration #2. .....81

Figure 3. 13: Peripheral blood T cell kinetics in mice randomised to the GVHD cohort.....82

Figure 3. 14: Bone marrow haematopoietic populations between GVHD and no GVHD cohorts. .....85

Figure 3. 15: Stromal population architecture between GVHD and no GVHD cohorts. ....86
Figure 3. 16: Representative gating to define bone marrow stromal populations...87
Figure 3. 17: Bone marrow T cell analyses between GVHD and no GVHD cohorts. 88

**Table 3. 1:** Peripheral blood haematological parameters over time in non-transplanted 129S2/SvHSD mice. ....73

Chapter 4
Figure 4. 1: Schematic of a bone marrow organoid T cell injury model. ....96
Figure 4. 2: Sequential images of developing organoids. ....99
Figure 4. 3: Cellular architecture of organoids by flow cytometry.....100
Figure 4. 4: Representative gating for hiPSC-derived bone marrow organoids.....101

Chapter 5
Figure 5. 1: Schematic representation of planned c-Kit$^{+}$ dose titration experiment. ....119

## List of Abbreviations

| | |
|---|---|
| 129S2/SvHsd | 129 |
| Acute graft-vs-host disease | aGVHD |
| Anaemia of chronic disease | ACD |
| Aplastic anaemia | AA |
| Allogeneic stem cell transplantation | alloSCT |
| Biomedical services | BMS |
| C57BL/6 | B6 |
| Chemically defined lipids | CDL |
| Chimeric antigen receptor T cell | CAR-T cell |
| Chronic graft-vs-host disease | cGVHD |
| Common lymphoid progenitors | CLP |
| Common myeloid progenitor | CMP |
| Complete blood count | CBC |
| CXCL12 Abundant Reticular Cell | CAR Cell |
| Dulbecco's modified Eagle medium | DMEM |
| Foetal bovine serum | FBS |
| Graft-vs-host disease | GVHD |
| Granulocyte macrophage progenitor | GMP |
| Haematopoietic stem cell | HSC |
| Haemophagocytic lymphohistiocytosis | HLH |
| Human induced pluripotent stem cell | hiPSC |
| Immune effector cell-associated haematotoxicity | ICAHT |
| Integrated DNA Technologies | IDT |
| Interferon | IFN |
| Knock out | K/O |
| Leptin-receptor$^+$ MSCs | LepR$^+$ MSCs |
| Lineage negative, c-Kit$^+$, CD86$^+$ | L86K |
| Lineage negative, c-Kit$^+$, Sca-1$^+$ | LSK |
| Lipopolysaccharide | LPS |
| LT-Haematopoietic stem cell | LT-HSC |
| Lymphocytic choriomeningitis virus | LCMV |
| Megakaryocyte erythroid progenitor | MEP |
| Mesenchymal stromal/stem cell | MSC |
| Multipotent progenitor | MPP |
| National Institutes of Health | NIH |
| Pathogen associated molecular pattern | PAMP |
| Phosphate buffered saline | PBS |
| Ribonucleoprotein | RNP |
| Single cell RNA sequencing | scRNAseq |

| | |
|---|---|
| Small guide RNAs | sgRNAs |
| Stem cell factor | SCF |
| Stem Cell Technologies™ | SCT |
| Standard Deviation | SD |
| T cell receptor | TCR |
| Toll like receptor | TLR |
| Von Willebrand Factor | vWF |
| Ultra-low attachment | ULA |
| Weatherall Institute of Molecular Medicine | WIMM |
| Wild type | WT |

# 1. Introduction and Background

## 1.0 Overview

This project involved the preliminary development of two novel models of T cell mediated injury to the haematopoietic niche. Haematopoiesis takes place within a tightly regulated niche which provides the microanatomical, immunological and metabolic environment required for haematopoietic function (1, 2). This niche is defined by stromal populations and primarily located within the bone marrow in adult mammalian life. 'Stress haematopoiesis' and 'emergency haematopoiesis' describe the demand-adapted responses of the haematopoietic system to various stressors ranging from infection or sterile inflammation, to major haemorrhage (3, 4). There is increasing evidence that rather than a bystander role, stromal components of the niche are active contributors to the modulation of haematopoiesis by inflammatory stress (5-7).

Despite a body of evidence implicating niche inflammation in the pathogenesis of a range of haematopoietic conditions, the contributions of the adaptive immune system to these processes remain under characterised (8-10). It is clear that T cell mediated injury to the haematopoietic niche is centrally implicated in human diseases characterised by bone marrow failure; including aplastic anaemia (AA), poor graft function following allogeneic stem cell transplantation (alloSCT), haematotoxicity following chimeric antigen receptor (CAR) T cell therapy and haemophagocytic lymphohistiocytosis (HLH) (11-14). These conditions are challenging to treat, with a significant burden of morbidity and

mortality. Progress towards improving patient outcomes is hampered by a lack of adequate pre-clinical model systems. New tractable models are required to facilitate mechanistic interrogation of T cell mediated haematopoietic injury, to guide targeted therapeutic interventions.

The aim of this project is to begin the development of two new model systems utilising the reaction of alloimmune T cells against bone marrow stromal populations to model T cell mediated injury to the haematopoietic niche. The first model is a modification of a conventional murine model of graft-vs-host disease (GVHD) optimised to study the interactions between stromal populations and engrafting haematopoiesis in the setting of GVHD. The second utilises the reaction of primary donor T cells against human induced pluripotent stem cell (hiPSC) derived bone marrow organoids as novel method of exploring T cell-stroma interactions in human tissue.

## 1.1 Haematopoiesis and the Haematopoietic Niche

### 1.1.1 Traditional 'branching tree' models of haematopoiesis

Haematopoietic stem cells (HSCs) are defined by their capacity for long-term self-renewal and ability to reconstitute all haematopoietic lineages, with *in vivo* competitive transplantation assays remaining the 'gold-standard' for the experimental evaluation of HSC function (15). HSCs can also by characterised by other features that are distinct from more mature populations, such as quiescence, a metabolic program defined by glycolysis and reduced mitochondrial activity, or a

dependence on autophagy as a regulator of cell state (16-18). In traditional models of haematopoiesis, rare HSCs sit at the apex of a branching hierarchy before undergoing stepwise differentiation via intermediate progenitor states. This process ultimately results in the constant production and replacement of billions of terminally differentiated peripheral blood cells daily, across the lifespan of an organism (19). Beneath HSCs in this hierarchy are a population referred to as multipotent progenitors (MPPs), defined by lineage-bias, a capacity to repopulate all mature lineages and a lack of capacity for indefinite self-renewal on serial transplantation (20, 21). MPPs then differentiate into short-lived lineage committed progenitors which directly produce the mature effector cells of the peripheral blood (22-24).

While insights from *in vivo* transplantation assays suggest a central physiological role for HSCs in haematopoiesis, this may not reflect the role of HSCs outside of the context of transplantation. A growing body of evidence suggests that in the steady-state HSCs act as a functional 'reserve' population, occasionally entering the cell-cycle to replace the MPP pool (25). It is likely that relatively long-lived MPP populations provide the amplification and turn-over driving day-to-day haematopoiesis. By placing expression of diphtheria toxin A under the control of a Cre-ER$^{T}$ restricted to HSCs, Schoedel and colleagues developed a mouse model where tamoxifen administration could be used to rapidly and efficiently deplete HSCs from steady-state haematopoiesis (26). A sustained >90% loss of HSCs had no measurable impact on whole bone marrow cellularity, or peripheral blood white cell counts. However, recovery from 5-FU induced myelodepletion failed in tamoxifen treated animals. These results suggest a key role of HSCs in recovery from

cytotoxic stress, but significant redundancy in the steady state. Similar results regarding the involvement of HSCs in steady-state haematopoiesis were seen in a study by Sun et al. using an inducible sleeping-beauty transposon to facilitate labelling and clonal-tracing of haematopoietic cells *in vivo* without manipulation or transplantation (27). Over more than one year of follow-up most peripheral haematopoiesis was derived from long-lived multipotent and lineage restricted populations without a capacity for long-term engraftment. Indeed, <5% of clones identified among immunophenotypic HSCs could be detected in mature peripheral blood populations. These studies suggest that insights into HSC biology from transplantation assays may not be generalisable to other physiological contexts.

### 1.1.2 Single cell technologies and new models of haematopoiesis

Insights from contemporary single cell RNA sequencing (scRNAseq) technologies combined with new methods of single-cell lineage tracing have disrupted the traditional unidirectional model of haematopoietic differentiation via step-wise transition through defined intermediates, arguing in favour of a fluid model of continuous differentiation. These findings include evidence of the production of mature populations directly by HSCs without transition through intermediate states, bidirectionality in differentiation hierarchies, lineage-commitment of individual cells within pluripotent populations and heterogeneous differentiation pathways leading to overlapping mature cell fates (28-31). An exploration of the evolving complexity in our understanding of haematopoietic cell fate decisions is beyond the scope of this discussion but has been recently comprehensively reviewed (19, 32).

### 1.1.3 Haematopoiesis in a spatial context

Despite these caveats, a branching tree model of haematopoiesis remains a useful conceptual framework for understanding haematopoiesis in health and disease. Over the last 30 years, the ability to segregate haematopoietic subpopulations into functionally homogeneous groupings based on cell surface marker expression has become sufficiently refined to allow the analysis of these populations by flow-cytometry to stand in for functional assays in many experimental contexts (20, 22-24, 33). The landmark finding that $CD150^{+}$, $CD48^{-}$, $CD41^{-}$ cells represent a rare population highly enriched for HSCs allowed their identification with a simple two-colour stain amenable to conventional fluorescence microscopy (34). This has facilitated the study of haematopoiesis within a spatial context and an appreciation for the complex regulation of haematopoiesis by the non-haematopoietic populations which define the bone marrow niche.

### 1.1.4 Niche support for haematopoiesis

Interspersed throughout the bone marrow are mesenchymal stromal/stem cells (MSCs), forming a dense reticular network and interfacing with many haematopoietic populations, including the majority of immunophenotypic HSCs (35). MSC populations have been identified as the primary sources of key cytokines required for HSC maintenance, including stem cell factor (SCF), and CXCL12. SCF (also known as KIT ligand), signalling through its receptor c-Kit is a key regulator of HSC maintenance and localisation. Disruption of c-Kit:SCF interactions with a

monoclonal antibody is sufficiently effective at mobilising HSCs from the bone marrow niche to facilitate transplantation (36). Studies using White Spotting 41 mice characterised by a partial loss of c-Kit function demonstrate the requirement of SCF:c-Kit signalling for maintenance of the steady-state HSC pool and promotion of HSC quiescence (37). Alternative splicing results in soluble and membrane bound isoforms of SCF. Biallelic loss of *Kitl* which encodes SCF is lethal in late gestation, however studies demonstrating haematopoietic defects in *Sld* mice characterised by a loss of only the membrane bound isoform of SCF have long been interpreted as providing evidence that SCF must act locally, in the context of a niche environment (38). More recent studies suggests that soluble SCF, produced ubiquitously by systemic endothelial populations, may be sufficient for the support of haematopoiesis in some settings (39). In work by the Jacobsen group, the marrow of long bones harvested from foetal *Kitl* knock-out (K/O) mice form haematopoietic niches similar to wildtype (WT) foetal long bones when developed as renal subcapsular ossicles in WT adults, suggesting that membrane bound expression of SCF is dispensable in this context. While this model is unlikely to reflect physiological haematopoiesis, these findings highlight the need for caution in generalising results between model systems in this field.

CXCL12 (also known as stromal derived factor-1) is a chemokine, and it is thought that CXCL12 signalling via the expression of its receptor CXCR4 on HSCs is a key regulator of both HSC localisation and maintenance (40). Disruption of CXCR4 with a small molecule inhibitor is sufficient to mobilise HSCs into the peripheral blood in both mice and humans (41) and conditional K/O of *Cxcr4* in haematopoietic populations depletes HSCs from the bone marrow of adult mice (42). It has also

been demonstrated that a systemic depletion of CXCL12 results in a marked reduction in HSCs. Ding and Morrison explored the implications of conditional *Cxcl12* K/O from specific stromal populations (43); deletion of *Cxcl12* from Leptin-receptor$^+$ MSCs (LepR$^+$ MSCs) or endothelial cells resulted in a loss of bone marrow retention of HSCs, or loss of HSC persistence respectively. Further evidence for the role of CXCL12 in HSC localisation is provided by demonstrating that the conditional deletion of *Cxcl12* from a subpopulation of LepR$^+$ MSCs results in the redistribution of HSCs to niches defined by MSCs with intact *Cxcl12* expression (44).

### 1.1.5 Non-haematopoietic populations in the bone marrow niche

The study of MSC populations in the bone marrow niche is complicated by controversy surrounding the most appropriate way to classify them, with different definitions overlapping significantly, and different conceptual frameworks leading to what at times appear contradictory results. Three MSC populations have emerged in the literature as having a key role in the support of haematopoiesis. These are LepR$^+$ MSCs, CXCL12-abdundant reticular (CAR) cells, and Nestin$^+$ MSCs; described and characterised by the Morrison, Nagasawa and Frenette groups respectively (1, 40, 45).

While LepR$^+$ MSCs are characterised by expression of the leptin receptor, and CAR cells are characterised by high levels of CXCL12, it is likely that these two identification strategies have converged on the same population of cells. It has been shown that >90% overlap exists between LepR$^+$ MSCs and cells highlighted by high expression of *Cxcl12* (43). Indeed, its has been demonstrated that LepR$^+$ MSCs have

100-fold greater expression of *Cxcl12* compared with other stromal populations. Recent studies employing scRNAseq have validated the likely overlap between these two populations, with cells expressing both LepR and CXCL12 clustering as a distinct population on unbiased dimensionality reduction (46). LepR$^{+}$ MSCs are spindle shaped cells which form an intercalated network throughout the bone marrow. These cells are a non-redundant source of a range of haematopoietic growth factors, including SCF, CXCL12, IL-7, CSF-1 and pleotropin (43, 47-50). Rather than a uniform population, it is likely that LepR$^{+}$ MSCs are heterogenous with many functionally distinct subpopulations; these include pluripotent stem cells with a capacity to regenerate adipogenic, osteogenic and chondrogenic lineages (51).

Nestin$^{+}$ cells were first described using a *Nestin*-GFP reporter strain, which identifies two distinct population, Nes-GFP$^{dim}$ cells which overlap substantially with LepR$^{+}$ MSCs, and rare Nes-GFP$^{bright}$ cells with a periarteriolar distribution (52). The discovery that the Nes-GFP$^{bright}$ but not Nes-GFP$^{dim}$ cells overlap significantly with NG2$^{+}$ pericytes has facilitated their functional interrogation using NG2-CreER$^{TM}$ mouse strains (53). HSCs adjacent to Nes-GFP$^{bright}$ cells are more likely to be quiescent and less susceptible to depletion by 5-FU. Selective depletion of NG2$^{+}$ cells is sufficient to deplete HSCs from the marrow and redistribute them away from arterioles. Furthermore, on entering the cell cycle HSCs have been shown to relocate away from Nes-GFP$^{bright}$ cells/arterioles.

These observations have led to a model conceptualising the haematopoietic niche as two distinct microenvironments. A central marrow niche, defined by sinusoidal endothelial cells, megakaryocytes and LepR$^{+}$ MSCs, where the majority

of HSCs reside (35), and an endosteal niche for a quiescent reserve population of HSCs, defined by Nes-GFP$^{bright}$ pericytes, arterioles and sympathetic nerve fibres (52-54). This dual-niche model has also been described in terms of perisinusoidal and periarteriolar niches, based on the endothelial subpopulation enriched in each microenvironment. This model is supported by data demonstrating that functionally heterogenous HSCs appear to segregate to endosteal and central marrow niches. Studies with *vWF-eGFP* mice have demonstrated that immunophenotypic HSCs can be subdivided into two functional sub-groupings, a von Willebrand Factor (vWF)$^{+}$ HSC population with a myeloid/megakaryocyte lineage bias and limited lymphoid reconstitution, and vWF$^{-}$ HSCs with a lymphoid (or 'balanced') lineage bias (55). Spatial studies with this reporter strain reveal a peri-arteriolar/endosteal distribution for vWF$^{-}$ HSCs, and a peri-megakaryocytic/central marrow distribution for vWF$^{+}$ HSCs (56). Selective depletion of Nestin$^{+}$ MSCs reduced numbers of vWF$^{-}$ but not vWF$^{+}$ HSCs. These studies suggest the existence of anatomically and functionally distinct niches, regulating heterogenous HSC subpopulations.

However, the functional relevance of the endosteal niche as a reservoir of quiescent HSCs has been challenged by widely cited authors (1). This critique was based on a landmark study which subdivided HSCs (identified by $\alpha$-catulin expression) into dividing and non-dividing cells on the basis of Ki-67 staining (35). Both dividing and non-dividing HSCs were enriched in the central marrow, and located in close proximity to LepR$^{+}$ MSCs. Furthermore, neither dividing nor non-dividing HSCs were observed to have a spatial relationship with either arterioles or endosteal surfaces. This controversy is unresolved and is likely to reflect the complexity and heterogeneity of the bone marrow niche, and the impact of subtle

changes in experimental design on study interpretation in this field. The argument that the localisation of HSCs with relation to specific stromal populations provides evidence of a micro-anatomically defined niche has also come under further scrutiny with the advent of sophisticated techniques for the quantitative analysis of spatial relationships in complex tissues (2). It has recently been demonstrated that while the vast majority of steady-state HSCs are close to central marrow niche constituents (including $LepR^+$ MSCs, sinusoids and megakaryocytes), there is no evidence that there is a closer relationship between HSCs and these populations than exists with randomly distributed dots (57). The same study also demonstrated no change in the distribution between dormant and non-dormant HSCs, and no closer relationship between dormant HSCs and $NG2^+$ cells than random dots. These authors argue that the spatial relationship between HSCs and stromal populations in the marrow may simply reflect the relative abundance of these cell types.

While MSC populations are likely to represent a key stromal component of the haematopoietic niche, there is evidence that crucial contributions to the regulation of haematopoiesis come from other stromal populations, as well as mature haematopoietic populations. These include endothelial cells, adipocytes, sympathetic nerves, osteoblasts, megakaryocytes and regulatory T cells (45, 58, 59). A comprehensive consideration of these populations, and the emerging evidence that haematopoietic cells also support the normal function of stromal populations in the niche are beyond the scope of this discussion (60).

## 1.2 Inflammation in the Haematopoietic Niche

### 1.2.1 Emergency myelopoiesis and stress haematopoiesis

A fundamental hallmark of the inflammatory response is an increase in mature granulocytes both in peripheral blood, and at the site of tissue injury (61). 'Emergency myelopoiesis' describes the mechanisms by which the bone marrow rapidly generates and expels granulocytes in the setting of inflammatory stress (4). 'Stress haematopoiesis' is the broader set of processes underpinning the demand-adapted response of the haematopoietic system to diverse stressors, ranging from cytotoxic insult to major haemorrhage (62). Pathogens can directly regulate haematopoiesis. HSCs express Toll-like receptors (TLRs), and enter the cell-cycle in direct response to pathogen associated molecular patterns (PAMPs) such as lipopolysaccharide (LPS) (63). The transition of HSCs from quiescence into cell-cycling is also activated by a range of inflammatory cytokines, including IL-1$\beta$, INF-$\gamma$, TNF-$\alpha$, and IL-6 (64-67).

Inflammatory signals have different impacts throughout haematopoietic hierarchy, as shown by the example of G-CSF, a key regulator of both basal and stress granulopoiesis (68). In HSCs, G-CSF encourages cell-cycling and bone marrow egress (69). Alternatively, in lineage committed granulocyte-macrophage precursor (GMP) populations, G-CSF signalling guides cell fate decisions towards granulopoiesis at the expense of monocyte/macrophage differentiation (70). In the MPP compartment, a subset of MPP3 cells can rapidly respond to peripheral granulocyte depletion or LPS both by preferential differentiation into GMPs, and by amplifying this signal via the secretion of proinflammatory cytokines (71). This

process generates a self-reinforcing feedback loop and pushes other MPP populations towards granulopoiesis, including otherwise lymphoid biased MPP4s (72, 73). IL-1β signalling also regulates the activity of GMP populations to facilitate the coordinated rapid production of neutrophils in response to stress (74). In stress conditions GMP populations demonstrate biphasic behaviour, first adopting a program of self-renewal leading to dense local clusters of GMPs. These clusters then differentiate in a coordinated fashion, leading to cluster resolution and the bulk production of mature neutrophils.

Stress haematopoiesis does not simply represent an acceleration of basally activated differentiation pathways, but rather a coordinated redirection of resources to meet the needs of the moment. This process involves the reversal of cell fate decisions in populations which would otherwise not contribute to the production of the required cells, and bypasses of intermediate differentiation states between HSC/MPP populations and mature effectors (4). While the haematopoietic system has remarkable scope to respond to stress in a demand-adapted fashion, there is evidence that this occurs at the expense of HSC fitness.

### 1.2.2 Inflammation and HSC fitness

The finding that exposure to inflammatory stress degrades the fitness of HSCs in serial competitive transplantation assays has been observed in a range of models of inflammation, including LPS injection, mycobacterium infection, and exposure to inflammatory cytokines including IL-1β, IFN-γ, and others (10, 65, 75-77). The impact of inflammation on HSC fitness was elegantly demonstrated in a recent

study by the Milsom group (78). Cohorts of mice were subject to between 8 and 24 weeks of sterile inflammatory challenge, followed by between 5 to 20 weeks of recovery; HSCs from these mice were then harvested and subject to evaluation of functional fitness through serial transplantation assays. Sequential rounds of inflammatory challenge resulted in a cumulative numerical depletion of HSCs, and cumulative degradation of HSC fitness (Figure 1.1).

Another key finding of this study was that there was no evidence of any recovery of the regenerative capacity of mouse HSCs after resolution of the inflammatory challenge, even after 20 weeks of observation post treatment. Similarities between the phenotype of HSCs exposed to sterile inflammation and aged HSCs led these authors to postulate that the cumulative irreversible impact of inflammatory challenges across the lifespan may contribute to haematopoietic aging, a concept echoed by other authors (79).

While fitness on competitive transplantation assays is the gold standard for demonstrating HSC exhaustion in murine models, peripheral cytopenias define bone marrow failure in a clinical setting. Most studies demonstrating the suppressive effect of inflammation on haematopoietic function either do not measure or do not observe a peripheral blood phenotype. The link between inflammation induced HSC exhaustion and peripheral cytopenias has been best demonstrated in a model of chronic mycobacterium infection in mice, which results in haematopoietic collapse and cytopenias after 3-4 months of follow-up (10).

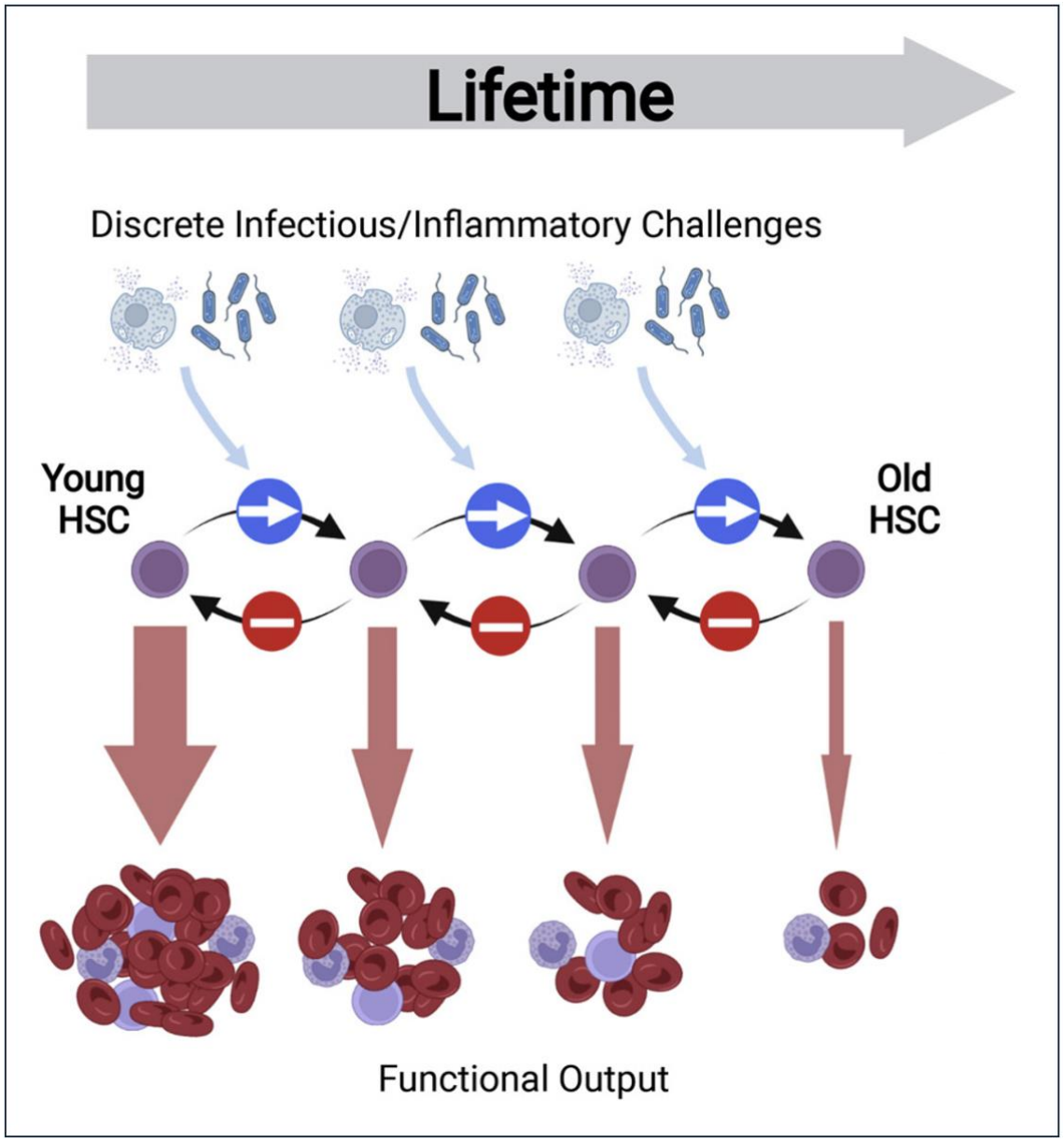



**Figure 1. 1:** Serial inflammatory insults irreversibly degrade HSC fitness.

Sequential inflammatory insults deplete HSC numbers and degrade HSC function in a cumulative and irreversible manner. It has been suggested that the burden of cumulative inflammatory insults across the lifespan may account for the degradation of HSC reconstitution capacity which is one of the hallmarks of haematopoietic aging. Figure adapted from Bogeska et al. 2022 (78).

### 1.2.3 Bone marrow stroma and inflammation

Bone marrow stromal populations are not bystanders in the response of the haematopoietic system to inflammation; stroma has been shown to act as a

translator of pathogen signals in the niche into coordinated stress responses. Stromal cells produce IL-6 following exposure to the fungal pathogen *C. albicans*, resulting in increased granulocyte production in an *in vitro* haematopoiesis-stroma co-culture model (80). The regulation of myelopoiesis by stroma-derived IL-6 has also been demonstrated in murine models of *T. gondii* infection (81). The secretion of G-CSF by endothelial cells secondary to TLR-4 activation is required for neutrophil production in response to LPS. In contrast, *Tlr4* K/O in haematopoietic cells or hepatocytes is insufficient to suppress emergency granulopoiesis (7, 82). In response to niche inflammation $LepR^+$ MSCs take on a proinflammatory phenotype (5); a study recently released in pre-print by the Passegué group makes the argument that this emergent population then regulates the function and distribution of bone marrow myeloid populations (83). Inflammatory $LepR^+$ MSCs produce IL-1β, a cytokine implicated in haematopoietic aging via the chronic activation of emergency myelopoiesis signalling pathways. Disruption of stromal IL-1β signalling either via K/O or blocking antibody mitigates the impact of ageing on haematopoiesis in mouse models (5). Understanding how both haematopoietic and non-haematopoietic populations in the niche respond to stress is required for the rational development of novel treatments for diseases mediated by inflammation within the bone marrow microenvironment.

## 1.3 T Cell Mediated Inflammation in the Haematopoietic Niche in Human Disease

A number of diseases are characterised by bone marrow failure and cytopenia secondary to T cell mediated inflammation within the haematopoietic niche. These include complications of cellular therapies such as poor graft function following alloSCT or immune effector cell-associated haematotoxicity (ICAHT), as well as immune aplastic anaemia (AA). While distinct clinical entities, these conditions are linked by the contribution of activated T cells to their pathophysiology, and the high burden of morbidity and mortality among patients who do not response to currently available therapies.

### 1.3.1 Poor graft function following alloSCT and bone marrow GVHD

AlloSCT is a treatment where HSCs from a healthy donor are transplanted into a recipient, with the goal of donor HSCs reconstituting haematopoiesis and facilitating normal life-long haematopoietic function (84). AlloSCT is most commonly used for haematological malignancies, where the treatment rationale is the recognition and eradication of cancer cells by donor T lymphocytes; this is called the graft-vs-leukaemia (GvL) effect (85). The recognition of host antigens by donor T cells leading to tissue injury is known as GVHD, a potentially devastating complication impacting >30% of patients undergoing alloSCT (86, 87).

Poor graft function following alloSCT describes a failure of normal haematopoietic function characterised by prolonged peripheral blood cytopenias

despite the persistence of donor haematopoiesis (12). This is distinct from graft failure, where transplanted haematopoiesis does not persist, and these entities can be separated by measurement of donor chimerism. Poor graft function impacts 5-25% of alloSCT (12, 88). The current standard of care for poor graft function is infusion of $CD34^{+}$ selected donor cells, with reported response rates in retrospective series of 69-82% (89-91). Outcomes for patients who do not respond to this intervention are poor with only 22% 5-year survival.

There is evidence that GVHD impacting stromal populations within the bone marrow niche contributes to poor graft function following alloSCT (Figure 1.2) (92).

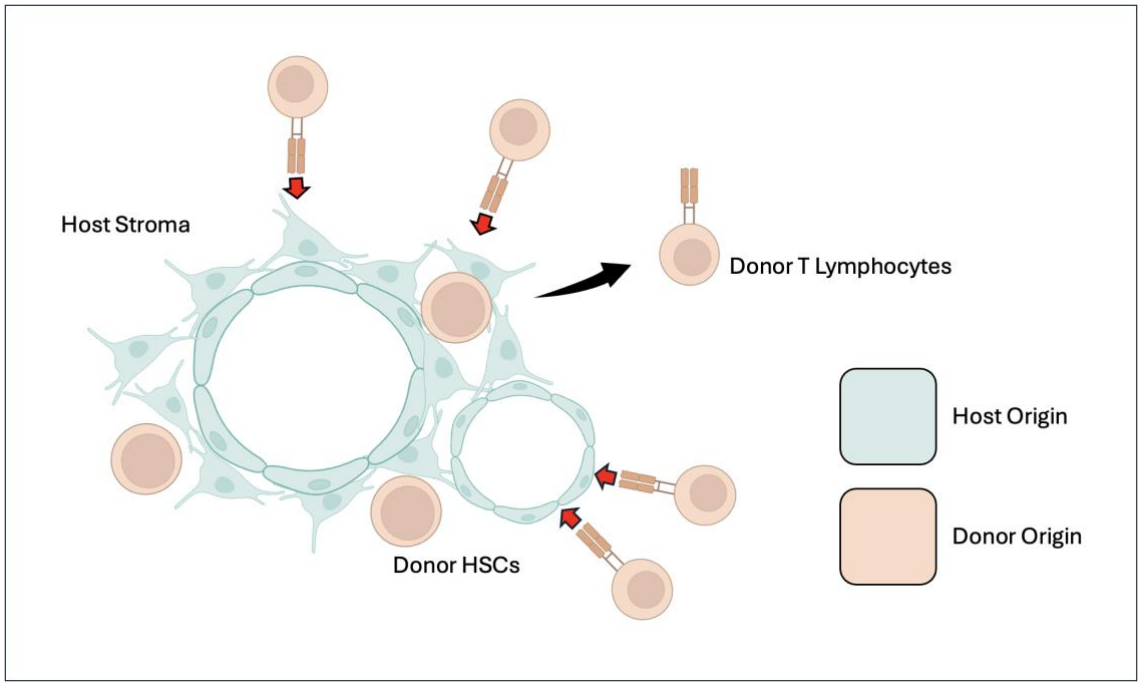



**Figure 1. 2:** Stromal GVHD in the haematopoietic niche post alloSCT.

The haematopoietic niche post alloSCT is a unique immunological interface. Donor haematopoiesis engrafts in and is supported by a niche defined by stromal cells of recipient origin. Donor T lymphocytes can recognise and injure host stromal populations, with implications for both stromal and haematopoietic function. Figure created using BioRender.com

GVHD is a risk factor for poor graft function and is particularly associated with persistent thrombocytopenia (12, 93). A nested case control series comparing bone marrow biopsies from patient with poor graft function vs normal graft function following alloSCT revealed a reduction in $CD146^+$ MSCs, a population identified as a likely human ortholog of murine $LepR^+$ MSCs (94, 95). Bone marrow endothelial cells and osteoblasts were also depleted in the context of poor graft function. In other cohort studies, it has been demonstrated that bone marrow T cells in patients with poor graft function are less likely to be naïve and are enriched for $Th_1$ and $Th_{17}$ populations, as well as $CD8^+$ T cells skewed towards a type I immune response (96, 97). Shono and colleagues analysed the relationship between clinical GVHD, idiopathic cytopenias and loss of bone marrow osteoblasts in a prospective case series of 57 alloSCT patients (98). This study identified a subset of patients with chronic GVHD (cGVHD) and loss of bone marrow osteoblasts on histological examination, among whom 10/11 had concurrent idiopathic peripheral blood cytopenias. It has also been demonstrated that bone marrow stromal cells collected from patients with acute GVHD (aGVHD) have impaired *in vitro* colony forming ability compared with stroma collected from patients without aGVHD (99). Murine models have demonstrated depletion of $LepR^+$ MSCs, sinusoidal endothelial cells and osteoblasts in the setting of aGVHD (99-101). These models also demonstrate that aGVHD resulted in reduced bone marrow cellularity and peripheral blood cytopenias (102). In aggregate there is evidence in both clinical and preclinical studies that bone marrow stromal populations are depleted in the setting of GVHD, with implications for graft function following alloSCT.

### 1.3.2 Immune effector cell-mediated haematotoxicity

Chimeric antigen receptor T cell (CAR-T) therapy involves re-engineering a patient's T cells to target cell-surface antigens expressed by their cancer. This technology has revolutionised the management of haematological malignancies in recent years, achieving durable remissions in patients who otherwise would not have had available treatments (103). CAR-T is associated with a number of unique toxicities, of which a syndrome of prolonged cytopenia known as ICAHT is among the most common and difficult to treat (13). ICAHT is graded from mild (grade 1) through to life-threatening (grade 4) based on the depth and duration of neutropenia, and classified based on timing from CAR-T infusion into early (occurring prior to day 30) or late (occurring after day 30) (104). The incidence of severe or life-threatening ICAHT has been reported at 22%, with an associated increase in non-relapse mortality at 12 months of 14%, compared with 4% in patients with absent or non-severe ICAHT (105). This is largely driven by a marked increase in the incidence of fatal infections in CAR-T patients with prolonged neutropenia. Patients with ICAHT typically exhibit a biphasic pattern, with initial recovery of counts followed by a secondary incidence of cytopenia. A small subset develop 'aplastic' ICAHT, associated with markedly reduced bone marrow cellularity and a cytopenias persisting up to years from CAR-T infusion (106).

The aetiology of ICAHT is unclear, though risk factors for its development implicate inflammatory stress and reduced haematopoietic reserve (107). Pre-infusion cytopenias or inflammatory markers (CRP and ferritin) inform the CAR-HAEMATOTOX score, a validated predictive tool to identify those patients at increased risk of ICAHT. It is likely that disruption of bone marrow stromal

populations by the action of the CAR-T product is also contributory. $CD271^+$ has been identified as an alternative to $CD146^+$ for identifying $LepR^+$ MSC equivalents in human bone marrow (108). $CD271^+$ cells are less frequent at D28 post CAR-T in patients with ICAHT, compared with matched case-controls with normal haematopoietic recovery (109). This study also demonstrated that bone marrow levels of the key stroma-derived factors CXCL12 and SCF at D28 are reduced in ICAHT patients. Strati and colleagues performed scRNAseq on bone marrow aspirates collected from 11 patients with, and 5 patients without ICAHT following CAR-T for lymphoma (110). Pathway analysis between clusters identified in ICAHT patients compared with the equivalent clusters seen in non-ICAHT patients revealed an IFN-γ response signature in most cell populations. This effect was particularly pronounced in HSCs. Bone marrow from ICAHT patients was also enriched for a population of oligoclonal $CD8^+$ cells with evidence of increased expression of *IFNG* and *TBX21*, a regulator of IFN gene expression. Given the known suppressive effect of IFN-γ on HSC function, this raises the possibility that ICAHT is contributed to by the impact of T cell derived IFN-γ on HSC populations (76).

While the majority of ICAHT patients will have spontaneous resolution of their cytopenias, the increased burden of non-relapse mortality in those patients with severe ICAHT highlights the need to generate new therapeutic strategies for this group. This effort is undermined by the current lack of model systems of ICAHT in the literature.

### 1.3.3 Immune aplastic anaemia

Immune AA is an acquired bone marrow failure syndrome, with an incidence of ~2 per million people in the developed world (111). Patients with AA present with peripheral cytopenias and markedly reduced cellularity on bone marrow examination, and mortality is driven by opportunistic infections in the setting of prolonged neutropenia. The aetiology of AA is incompletely understood, but clinical evidence and the success of immunosuppressive therapy directed at T cells implicates the depletion of HSCs by self-reactive T lymphocytes in the pathogenesis of this condition. Specific HLA antigens contribute to AA. Specific HLA polymorphisms are associated with an increased incidence of AA, and 10-15% of patients have evidence of 'escape-clones' characterised by loss-of-heterozygosity in the region of chromosome 6 containing HLA alleles (112, 113). Antigens associated with EBV infection can mimic epitopes present on HSCs, and molecular mimicry following viral infection has been proposed as a mechanism for the failure of tolerance driving AA (114). Immune suppression, marrow stimulation with TPO agonists and stem cell transplantation are the mainstays of treatment for AA (115). These treatments are effective in most patients however toxicity limits their use in elderly individuals. With a median age at diagnosis of 60 years, 70-80% 5-year survival is observed in patients aged <60 at diagnosis, compared with only 38% in patients aged 60 years or older (116).

### 1.3.4 Other conditions

A number of other diseases characterised by peripheral cytopenias are mediated by the action of T cells within the haematopoietic niche. Two examples are HLH and

cytopenias following viral infection. HLH is a rare, life-threatening condition characterised by severe systemic inflammation and pancytopenia. HLH is a syndrome with many potential triggers, involving a failure of negative feedback leading to the run-away activation of $CD8^+$ T lymphocytes and the massive release of inflammatory cytokines (117). IFN-γ released by $CD8^+$ T cells has been highlighted as contributory to cytopenia secondary to HLH. In a preclinical model of HLH driven by lymphocyte choriomeninigitis virus (LCMV) infection in perforin-deficient (*pfp*$^{-/-}$) mice, depletion of either $CD8^+$ T cells or IFN-γ rescued pancytopenia (118).

The link between viral infection and suppressed haematopoiesis ranging from transient mild cytopenias to bone marrow failure has long been recognised (119); though with the exception of parvovirus B19 which directly infects erythroid progenitors, the specific mechanisms by which viruses impair haematopoiesis are poorly understood (120). Isringhausen et al. used a mouse model to demonstrate that viral cytopenias are associated with disruption of haematopoietic and stromal populations by the action of $CD8^+$ T cells (121). Mice infected by LCMV had destruction of $LepR^+$ MSCs by bone marrow infiltrating $CD8^+$ T lymphocytes. Virus specific $CD8^+$ T cells produced IFNγ, and IFNγ resulted in decreased bone marrow cellularity and impaired repopulating fitness of HSCs.

Given the range of serious medical conditions driven by T cell mediated injury to the haematopoietic niche, there is a clear need for effective preclinical models of this pathophysiology.

## 1.4 Applications and Limitations of Existing Model Systems

A number of murine models of T cell mediated bone marrow failure have been developed. While they have provided important insights, they have limitations which call for the development of novel experimental systems.

The Young group have developed a model which has been widely used in preclinical studies of aplastic anaemia (122, 123). Infusion of lymphocytes from an MHC-mismatched donor mouse into a recipient results in the rapid depletion of haematopoiesis by alloreactive T cells, leading to bone marrow hypocellularity and pancytopenia (124). Like clinical AA patients, cytopenia in this model can be prevented using cyclosporin or infusion of anti-thymocyte globulin. Depletion of haematopoiesis in this model system occurs rapidly, and is driven by direct interactions between $CD8^+$ T lymphocytes and HSC populations (125). This mirrors the pathophysiology of AA but is unlikely to reflect the mechanisms of bone marrow failure in conditions such as poor graft function post alloSCT and ICAHT which do not involve direct interactions between T cells and HSCs. This model also does not facilitate exploring the implications of injury to stromal populations for haematopoietic function.

Two groups have analysed the impact of severe GVHD on haematopoiesis in mouse models (101, 102). Both models use MHC-mismatched donor and recipient mice, and comparisons are performed between a control cohort who receive bone marrow cells without additional lymphocytes, and a GVHD cohort that receive an additional infusion of lymphocytes to induce GVHD. These mice rapidly develop systemic manifestations of GVHD, and analyses are performed between D21 and

D28 post-transplant due to short survival within the GVHD cohorts. These systems demonstrate that GVHD results in reduced bone marrow cellularity, peripheral pancytopenia and marked suppression of B cell lymphopoiesis. Changes to stromal populations are observed, with loss of osteoblasts seen in both studies. Variable results were seen regarding the impact of GVHD on $LepR^{+}$ MSCs, with Lin and colleagues demonstrating a marked reduction in this population, in contrast to the findings of the Matsushima group who saw no appreciable changes (99). In a recent study using one of these model systems, a JAK inhibitor used clinically in the treatment of GVHD called ruxolitinib was shown to attenuate the impact of GVHD on engrafting haematopoiesis (99). Ruxolitinib was shown to increase the transfer of mitochondria from recipient stromal populations to donor HSCs, which may have contributed to improved haematopoietic function in this experiment.

While these models provide a platform to explore the impact of T cell mediated inflammation on stromal and haematopoietic function, the severity of GVHD employed in these experiments introduces limitations. Mice in the GVHD cohorts of these studies survive between 21 – 28 days; this is insufficient time for transplanted HSCs to engraft and reconstitute mature effector populations, in particular T lymphocytes which can take 4-8 weeks to be measurable in peripheral blood. At this early timepoint, measured bone marrow and peripheral blood populations are likely in part to reflect the persistence of lineage committed progenitors, rather than the output of transplanted HSCs (22). Mice in these studies are also critically ill at experiment endpoint; because severe illness has a depressive effect on haematopoiesis, these models do not allow the impact of T cells on the haematopoietic niche to be separated from this systemic effect (126).

Another inherent limitation of any mouse model of GVHD is that fundamental differences exist between murine and human T cell biology (127, 128). New developments in 3D cell culture techniques using human tissue, including novel hiPSC-derived organoids, provide an opportunity to address this limitation.

## 1.5 Project Aims and Objectives

An unmet clinical need and the limitations of existing pre-clinical models call for the development new tractable models of T cell mediated injury to the haematopoietic niche. Murine models of AA have successfully used MHC-mismatched T cells to deplete haematopoiesis, and there is clear evidence that bone marrow stromal populations are a target for GVHD. With these observations in mind, we hypothesised that alloreactive T cells targeting bone marrow stromal populations could be used as the basis of novel models of T cell mediated injury to the haematopoietic niche.

The work presented in this dissertation is nested within a larger project with the following aim:

*To develop and mechanistically interrogate tractable models of T cell mediated injury to the haematopoietic niche, to identify novel targets for the treatment of cytopenias following cellular therapies, and related conditions.*

This aim will be addressed through the delivery of four discrete objectives:

1. To develop tractable models of T cell mediated injury to the haematopoietic niche both *in vivo* and in hiPSC-derived bone marrow organoids.
2. To characterise these models at high resolution, using scRNAseq and flow cytometry.
3. To interrogate the mechanisms by which T cells injure bone marrow stromal populations, and the implications of these interactions for haematopoietic function.
4. To use these model systems to trial novel targeted interventions, with the goal of identifying candidate approaches for clinical translation.

The scope of this body of work is restricted to the first of these objectives. Chapter 3 details the systematic development of an *in vivo* model. This model is an adaptation of a conventional murine model of GVHD, optimised to explore the impact of alloreactive T cells within the haematopoietic niche both on stromal populations, and engrafting haematopoiesis.

Our collaborators in the Psaila group have recently developed a method for differentiating hiPSCs into bone marrow organoids, which include haematopoietic and stromal populations analogous to the central marrow niche (129, 130). We intend to develop an experimental system where primary donor T cells are reacted against bone marrow organoids, to facilitate modelling the mechanisms of T cell mediated injury to the haematopoietic niche in a novel *in vitro* system using human tissue. Chapter 4 details the foundational work towards the development of this organoid model.

# 2. Materials and Methods

## 2.0 Murine Model Development

### 2.0.1 Animals

Transplant recipient animals were wildtype 129S2/SvHsd (129)s, with initial breeding pairs purchased from Envigo RMS LLC prior to breeding in house. $CD45.1^+$ C57BL/6 (B6) donors were B6.SJL-*Ptprc*$^a$*Pepc*$^b$*/BoyJ* purchased as required from the Oxford biomedical services (BMS) core colony. $CD45.1^+/CD45.2^+$ heterozygous donors were bred in house from $CD45.1^+$ B6 males and WT B6 females purchased from Envigo RMS LLC. Antibody titration experiments were performed using young adult WT B6 mice kindly donated by the Simmons group at the Weatherall Institute of Molecular Medicine (WIMM). All animals were housed at the animal facility at BMS JR Hospital, and work was performed in accordance with the Animals (Scientific Procedures) Act of 1986, under PPL1874268. All animals were humanely killed either at the occurrence of a prespecified humane endpoint, or at the scheduled experimental endpoint by a rising concentration of $CO_2$ prior to cervical dislocation.

### 2.0.2 Equipment and analysers

Magnetic enrichments were performed using a Miltenyi MidiMACS™ cell separation system. Cell counting was performed using an Invitrogen Countess 3 automated cell counter. Irradiation for radiation dose titration and syngeneic transplantation

experiments was performed using a calibrated caesium-137 radiation source at BMS JR. Irradiation for T cell dose titration experiments was performed using a calibrated X-ray irradiator at the Oxford Functional Genetics Facility. Peripheral blood counts were performed using a scil VET abc Plus™ veterinary haematology analyser kindly provided by the Patel Group at the WIMM. Flow cytometry analysis was performed using a BD LSR Fortessa X50 at the WIMM flow cytometry core facility.

### 2.0.3 Cellular product method development

Workflows for c-Kit$^+$ enrichment of bone marrow cells were adapted from a previously described method (131). Following humane killing, hind limbs, pelvises and vertebrae were harvested from donor animals and cleaned with scalpel and Kimwipes™. All samples were kept on ice following collection unless otherwise specified. Each donor mouse was processed in parallel. Haematopoietic cells were released by gentle crushing in a mortar and pestle in phosphate buffered saline (PBS), prior to homogenisation into a single cell suspension by agitation with an 18G needle and syringe. Cells were sequentially filtered at 100μm and 70μm into a 50mL centrifuge tube. Cells were pelleted by centrifuging (all centrifuging in murine workflows were performed with the following settings unless otherwise specified: Centrifuge tubes: 440rcf, 5 min, 4°C, 96-well plates: 700rcf, 2 min, 4°C). Cell pellets were resuspended, prior to filtration at 50μm into a 15mL volume. Cell counts were performed on this volume.

Cells were pelleted by centrifuging and resuspended in 500μL PBS. Anti-c-Kit APC Abs (eBioscience 17-1171-83) were added to each sample at a dose of 0.2μL/$10^7$ cells, prior to incubation at 4°C for 30 min. Following incubation, 5mL of PBS was added prior to filtration at 50μm. Cells were then pelleted and resuspended in 500μL of PBS, prior to the addition of anti-APC microbeads (Miltenyi 130-090-855) at 0.2μL/$10^7$ cells. Incubation was then performed at 4°C for strictly 15 minutes. Cells were washed in 13mL of PBS prior to centrifuging and resuspension in 2mL of PBS. The cell suspension was passed through a 50μm filter into a Miltenyi LS column for positive magnetic selection. Cells were eluted from the LS column with 5mL of PBS, and the column was washed with an additional 5mL PBS by repeating the elution step. Cells from different donor mice were pooled at this stage of the enrichment for experiments with >1 donor. To quantify the T cell depletion achieved by this procedure, an enrichment was performed as detailed above with an aliquot sampled at each stage of the enrichment process. Quantification of live c-Kit$^+$ cells and T lymphocytes in these aliquots was performed by flow cytometry. The protocol was repeated a number of times to determine the reproducibility of the c-Kit$^+$ cell purity and T cell depletion in the post-enrichment product.

As c-Kit$^+$ purity varied between enrichments, a check of enrichment efficiency was built into the pre-injection workflow of each experiment. Prior to injection, c-Kit$^+$ cell purity was checked by flow cytometry based on the anti-c-Kit APC antibody used in the enrichment process. An aliquot of the final elution product was compared to an aliquot from LS column run-off used to define a c-Kit negative population, to generate an estimate of enrichment efficiency (Figure 2.1).

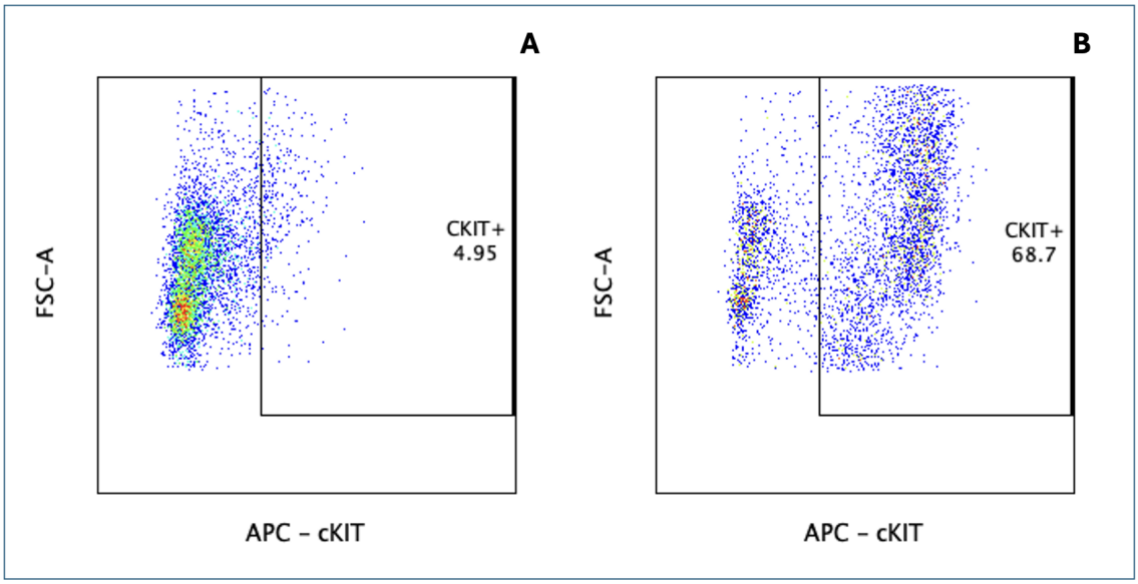



**Figure 2. 1:** Example flow plots from a pre-infusion c-Kit⁺ purity check.

The incorporation of an anti-c-Kit APC conjugated antibody into the c-Kit⁺ cell enrichment workflow facilitated estimation of enrichment efficiency by flow cytometry. All plots shown are following debris and doublet exclusion. **A** The LS column run-off following c-Kit⁺ positive magnetic selection was used to define a c-Kit⁺ gate. **B** The c-Kit⁺ cell purity of the final enrichment product was estimated from the proportion of cells positive for APC. Cell dose in the experiment shown in this example was estimated at a post enrichment purity of ~70%.

Following measurement of enrichment efficiency, cells were pelleted and resuspended at the desired concentration for injection.

A workflow was developed for the isolation of T cells from donor spleens. After humane killing, spleens were removed from donor animals. For experiments with >1 donor animal, different spleens were processed in parallel. Spleens were macerated by gently passing them through a 100µm mesh filter into a sterile 60mm Petrie dish containing ACK lysing buffer using the plunger of a 1mL syringe. After maceration, Petrie dish contents were washed with PBS into a 50mL centrifuge tube. ACK lysis was quenched with 5mL of PBS, and cells homogenised into a single cell suspension by pipetting and filtered at 70µm. Cells were pelleted and then resuspended in 5mL of ACK lysis buffer for a 5-minute incubation period. Cells were centrifuged then resuspended in 5mL of PBS prior to filtration at 50µm into a 15mL

centrifuge tube. 5mL of PBS was then used to wash the original centrifuge tube and filter, resulting in a 10mL cell suspension each donor spleen. Cell counts were then performed. Cells were then enriched using a CD3$\varepsilon^+$ microbead kit (Miltenyi 130-094-973) in accordance with manufacturer's instructions. Following enrichment, cells were pelleted and resuspended at the desired concentration for injection. For experiments with >1 donor spleen, the cellular products from each donor spleen were pooled and homogenised prior to injection.

Five replications of this protocol were performed to determine the reproducibility of the post enrichment CD3$^+$ T cell yield and purity.

### 2.0.4 Buffers and reagents

MACS buffer was prepared by adding 1% heat inactivated foetal bovine serum (FBS) (Sigma Cat: 4135) and 1% 100mM EDTA (Sigma Cat: 03690) to PBS. Stroma buffer was prepared by the addition of 10% FBS to Hanks' Balanced Salt Solution (HBSS) (Gibco Cat: 14175-053). These buffers were prepared in the week prior to each experiment and stored at 4°C until use.

Digestion-mix was prepared by dissolving dispase II (Roche Cat: 04943078001) and collagenase IV (Gibco Cat: 17104-019) in stroma buffer. The final concentration of dispase II and collagenase IV for digestion is 1mg/mL, and 200IU/mL respectively. Digestion-mix was prepared at double-strength the evening prior to each endpoint, stored at 4°C and brought to room temperature prior to use.

Antibody master-mixes were prepared fresh the morning of each experiment by adding the required volume of antibody to MACS buffer and 10% Brilliant Stain

Buffer Plus (BD Cat: 566385). A working stock of mixed biotinylated lineage antibodies (lin-biotin cocktail) was prepared fresh every three months and stored at 4°C until use. Antibody panels are summarised in appendix 1.

### 2.0.5 Endpoint flow cytometry panel development

Two haematopoietic panels and one T cell panel were developed to facilitate analysis of bone marrow populations at the experimental endpoint. Haematopoietic panels were developed to define HSC/MPP and lineage committed progenitors respectively, using widely used immunophenotypic models of murine haematopoiesis (20, 22). These panels were supplemented by the inclusion of CD201 and CD86 to render them robust to inflammation. A T cell panel was developed to define $CD4^+$ and $CD8^+$ T cell populations and characterise their activation state based on the expression of adhesion molecules CD44 and CD62L (132). These panels all incorporated CD45.1 and CD45.2 to facilitate the separate analysis of donor and recipient haematopoiesis. Additional panels to define bone marrow stromal and peripheral blood populations were already available within the laboratory at project outset. Representative gating is shown in Chapter 3. All flow cytometry panels used are detailed in appendix 1.

### 2.0.6 General transplantation experiment procedures

All transplants were performed with 129 recipients, aged 10-12 weeks on transplant D0. Where possible, equal numbers of male and female recipients were utilised,

with recipients randomised to treatment allocation with sex as a blocking factor. No blinding was performed. Transplant recipients received 0.5 x $10^6$ c-Kit$^+$ cells, isolated on the day of transplantation from male CD45.1$^+$ B6 donors unless otherwise specified. GVHD experiments included the addition of CD3$\varepsilon^+$ splenocytes isolated from either CD45.1$^+$ or CD45.1/2$^+$ male B6 donors. All donor animals were aged 8-16 weeks on D0. Mice were conditioned for transplantation by irradiation at a dose of 9Gy unless otherwise specified, delivered in two fractions separated by four hours, followed immediately by cell product infusion by tail vein injection. Cell products were agitated by vortexing immediately prior to drawing up for injection, and injections were delivered in a uniform 200μL volume. Enrofloxacin anti-microbial prophylaxis was provided in drinking water for 28 days following irradiation. Mice were weighed prior to irradiation, daily for 14 days post transplantation, and then weekly until experimental endpoint. In GVHD experiments, mice underwent a weekly clinical assessment using a validated tool (133). Any mice with >15% loss of weight or clinical evidence of moderate/severe GVHD were humanely killed. Peripheral blood was sampled every 14 days, with the final sample collected on transplant D56. Animals were killed after eight weeks for endpoint analyses.

### 2.0.7 Radiation dose titration

An experiment was conducted to identify an optimal radiation dose to condition 129 recipients for transplantation. Four male and four female recipients were

randomised to 7.5Gy or 9Gy doses of radiation, prior to c-Kit$^+$ cell product injection with no graft T cells. Experimental procedures were conducted as described earlier.

### 2.0.8 Syngeneic transplant and non-transplanted littermates

An experiment was performed to characterise normal unperturbed haematopoiesis in our model system, and the artifact introduced into analyses by irradiation and transplantation in the absence of GVHD. Four male and four female littermates were randomised either to syngeneic transplantation with 0.5 x$10^6$ c-Kit$^+$ cells with no graft T cells from a male 129 donor, or no transplantation. Experimental procedures were conducted as described earlier.

### 2.0.9 T cell dose titration

Pilot experiments were performed to identify an appropriate dose of graft T cells to induce GVHD in this model system. In the first T cell titration experiment, six male and seven female recipients were randomised to T cell doses of 0, 5x$10^4$, 1x$10^5$ and 5x$10^5$ in addition to c-Kit$^+$ bone marrow cells. T cells for this experiment were isolated from CD45.1$^+$ donors. A repeat T cell dose titration was performed, randomising six male and seven female recipients to doses of 0, 1x$10^6$ or 5x$10^6$ graft T cells, isolated from CD45.1/CD45.2 heterozygous donors to facilitate differentiation between CD45.1$^+$ c-Kit$^+$ bone marrow derived T cells, and co-transplanted graft T cells. Experimental procedures were conducted as described earlier.

### 2.0.10 Peripheral blood timepoint workflows

At peripheral blood timepoints 50μL of blood was collected from each experimental animal by tail vein incision into microvette tubes containing lithium heparin gel. Peripheral blood samples were handled at room temperature unless otherwise specified. Complete blood counts (CBCs) were measured with a veterinary haematology analyser in accordance with manufacturer's instructions. Following CBC measurement, the remaining blood was transferred into Eppendorf tubes, and red lysis performed with 1mL of ACK buffer per sample, with a 15 min incubation. Cells were then pelleted by centrifuging, the supernatant removed, and a secondary red cell lysis performed with 700uL ACK buffer per sample, with a 15 min incubation. Cells were centrifuged, then resuspended in 100uL of PBS and transferred to 96 well plates for staining.

Peripheral blood chimerism was analysed using a flow cytometry panel developed by colleagues in the Wilkinson group, with minor modifications (131). All staining was performed in 100uL volumes. Viability staining was performed using Zombie Green™ (Biolegend cat: 423111) at a concentration of 1:1000, for 10 min at room temperature. Cells were then centrifuged, washed in MACS buffer, and stained with the antibody master-mix for 30 min at 4°C. Cells were then centrifuged and washed in MACS buffer prior to fixation in 100uL of BD Cytofix™ fixation buffer, at 4°C for 20 min. Cells were then washed and resuspended in MACS buffer and left at 4°C until flow cytometry sample acquisition. Sample acquisition was performed within 48 hours of sample collection.

### 2.0.11 Endpoint workflows

At the prespecified experimental endpoint transplant recipients were humanely killed prior to harvesting of hind limbs and pelvises for endpoint analyses. From each experimental animal, one hind limb and hemipelvis was used for each of the stromal and haematopoietic endpoint workflows. All tissue was kept on ice unless otherwise specified. Stromal and haematopoietic workflows were performed in parallel.

For the haematopoietic endpoint, bones were cleaned with scalpel and Kimwipes™. Haematopoietic cells were released by gentle crushing of the bones with a mortar and pestle in PBS, prior to homogenisation into a single cell solution using an 18G needle and syringe. Cells were then sequentially filtered at 100μm, 70μm and 50μm into a 15mL centrifuge tube. Cells were pelleted by centrifuging, the supernatant removed and red cell lysis performed by resuspension in 2mL ACK lysing buffer followed by 5 min incubation at room temperature. Lysis was quenched with 10mL of PBS, cells centrifuged and resuspended in 10mL of PBS. From this volume, cell counts were performed, prior to centrifuging and resuspension at a concentration of $1x10^7$ cells/mL. Cells were then transferred to 96-well plates for staining.

For the HSC/MPP panel, two wells containing $2.5x10^6$ cells were stained per sample, for the lineage committed progenitor panel one well containing $2.5x10^6$ cells was stained per sample, and for the T cell panel one well containing $1x10^6$ cells was stained per sample. Samples were then centrifuged, and resuspended in 100μL of viability stain (BD Horizon™ Fixable Viability Stain 780, Cat: 565388) at a

concentration of 1:1000, prior to 10mins incubation at room temperature. Cells were then washed in MACS buffer. HSC/MPP panel and T cell panel samples then underwent Fc receptor blocking with anti-CD16/32 (Biolegend 101302) at a dose of 0.5μL/$10^6$ cells in a 50μL volume. As the lineage committed progenitor panel incorporates active staining against CD16/32, blocking was performed with PECy7 conjugated anti-CD16/32 (Biolegend Cat: 101317), at a concentration of 1:200 in 50μL. Incubation with blocking antibodies was performed for 15min at 4°C.

After blocking, the next staining step was performed without removing the 50μL blocking antibody solution. For the T cell panel, 50μL of the staining master-mix was added, made up at double strength resulting in a final staining volume of 100μL at desired antibody concentration. A 30 min incubation was performed at 4°C prior to washing the cells in MACS buffer and fixation.

For HSC/MPP and lineage committed progenitor panels, 0.75μL of lin-biotin cocktail in 50μL of MACS buffer was added to each sample, resulting in a final staining volume of 100μL at the desired concentration. Incubation was performed at 4°C for 30min, prior to washing the cells in MACS buffer. Cells were then resuspended in 100μL of the appropriate staining master-mix, and incubated at 4°C for 90 min (the RAM34 clone included in the haematopoietic and stromal panels requires an extended incubation period (131)). Cells were then washed in MACS buffer and fixed.

For the stromal endpoint workflow, bones were cleaned with a scalpel and Kimwipes™. The ends of long bones were carefully removed with scissors, and the marrow plug flushed with stroma buffer into a 15mL centrifuge tube. Long bones including the chips removed prior to flushing and hemipelvises were then gently

crushed with a mortar and pestle in 2mL of room temperature stroma buffer. The contents of the mortar and pestle were then washed into the 15mL centrifuge tube containing the marrow plug, such that each sample was suspended in exactly 5mL of stroma buffer after crushing. 5mL of the double-strength digestion mix was then added to each sample, resulting in a total volume of 10mL per sample at the desired concentration of digestion mix. Samples were then digested at 37°C for 45min using an orbital incubator with a throw-arm of 50mm at 180RPM. After incubation, digestion was inactivated by the addition of 1mL of 100mM EDTA.

Samples were then filtered through a 100μm filter into a 50mL centrifuge tube, pelleted by centrifuging and the supernatant carefully removed. Red cell lysis was performed by resuspension in 1mL of ACK lysing buffer followed by a 2min incubation at room temperature. Cells were then again passed through a 100μm filter, prior to pelleting and resuspension in 10mL of PBS. Cell counts were measured. Cells were then resuspended at a concentration of $5x10^7$/mL and transferred to a 96-well plate for staining.

For each sample, one well containing $1x10^7$ cells was stained. Cells were first centrifuged and resuspended in 100μL of viability stain (BD Horizon™ Fixable Viability Stain 780, Cat: 565388) at a concentration of 1:1000, prior to 10mins incubation at room temperature. Cells were then washed in MACS buffer, and Fc blocking performed with 5μL of anti-CD16/32 antibody in 100μL of MACS buffer for 15min at 4°C. To this volume, 100uL of BUV395 conjugated anti-CD45 antibody (BD Horizon Cat: 56427) at a concentration of 1:50 was added, resulting in a final staining volume of 200μL with an anti-CD45 concentration of 1:100. Incubation was performed at 4°C for 30min, prior to washing in MACS buffer. Cells were then

resuspended in 100uL of the staining master-mix and incubated at 4°C for 90min. Samples were then washed in MACS buffer, resuspended in 100uL of the streptavidin-conjugated secondary stain and incubated for 30min at 4°C. Cells were then washed and fixed.

All samples underwent fixation in 100uL of BD Cytofix™ fixation buffer, at 4°C for 20 min. Cells were then washed and resuspended in MACS buffer and stored at 4°C until flow cytometry sample acquisition. Sample acquisition was performed within 48 hours of sample collection.

### 2.0.12 Statistical Methods

Descriptive statistics are presented as mean +/- standard deviation (SD) unless otherwise specified. Hypothesis testing was performed using unpaired two-tailed student t-tests. For survival analyses, hypothesis testing was performed using the log-rank test. As the results presented represent exploratory analyses in the context of pilot studies, correction for alpha inflation in the setting of multiple comparisons has not been performed. Power calculations were not performed as the experiments presented in this project were pilot studies with a plan to replicate results with appropriately powered validation experiments. The number of mice included in each experiment was determined on a pragmatic basis, with scale limited by the resources available to safely and successfully execute critical experimental timepoints. The decision not to perform power analyses or adjustments for multiple comparisons limits the strength of the conclusions that

can be drawn from this work, and results should be interpreted with caution until appropriately powered validation experiments are performed.

### 2.0.13 Software and analysis

Flow cytometry data was analysed using FlowJo V10.10.0. Statistical analysis and data visualisation was performed using GraphPad Prism V10.4.0. Figures were developed using BioRender.com.

## 2.1 Organoid Differentiation

### 2.1.1 Overview

HiPSC-derived bone marrow organoids were differentiated following a recently published protocol developed by collaborators in the Psaila group (130). This protocol involves four phases, during each of which a tailored cocktail of cytokines is employed to guide differentiation. Appendix 2 lists the specific components of the reagents employed throughout the protocol, including phase specific differentiation media. Media were prepared fresh on the day of use, with cytokine aliquots thawed immediately prior to use. Phase 1 involves forcing mesodermal commitment through hypoxia and WNT activation on protocol Day 0-3. Phase 2 guides differentiation towards haematopoietic and bone marrow stromal lineage commitment from Day 3-5, prior to hydrogel embedding on Day 5 to provide a 3-dimension structure to facilitate vascular sprouting during phase 3 from Day 7-12. In phase 4, organoids are extracted from hydrogel and cultured individually in 96-well plates, prior to downstream endpoint assays.

### 2.1.2 HiPSC handling

All work was performed with Gibco hiPSCs (ThermoFisher Cat: A18945). All hiPSC work was performed under strict sterile conditions, as hiPSCs require antibiotic-free culture media. Incubation was performed at 37°C, 5% $CO_2$ and atmospheric $O_2$ unless otherwise specified. Plates for hiPSC culture were prepared by coating standard 6-well culture plates with 1mL of Geltrex basement membrane matrix

(ThermoFisher Cat: A1569601). Geltrex was cured at 37°C for 30min – 1hr and then remaining liquid removed. 2mL of room temperature StemFlex culture media (ThermoFisher Cat: A3349401) was then added to each well.

HiPSCs were detached from their current plate prior to passage. Passage was performed from adherent hiPSC colonies at 60-70% confluence. Media was removed by aspiration and wells washed gently with 1mL of room temperature PBS. 1mL of 0.5M EDTA was added to each well and incubated at 37°C for strictly 3min. EDTA was then removed by aspiration, the plate tilted to 45° and adherent cells washed from the well base into suspension with 1mL of StemFlex media in 3-5 passes. Care was taken to keep agitation of the media to a minimum, to facilitate keeping hiPSCs in small clumps rather than a single cell suspension. From this suspension of media, aliquots were collected and added dropwise to the Geltrex coated plates prepared earlier, prior to gentle agitation of the plate by shaking to facilitate uniform distribution of hiPSC clumps across the wells. The volume of the aliquot collected was varied based on the desired frequency of passage, with a 100µL aliquot usually producing a culture at 60-70% confluence within 48-72 hours. After passage cells were returned to the 37° incubator.

Media was changed the day following passage to remove excess debris, or every 48 hours. Media was removed by aspiration, cells washed with 1mL of PBS, and then a 2mL volume of StemFlex added to each well. Cells were visually inspected daily, and passage performed once cells reached optimal confluence.

### 2.1.3 Phase I – Mesodermal induction

Throughout the differentiation, cells were visually inspected daily for the presence of excess debris or contamination. One well of passage # 32 hiPSCs at 60-70% confluence were detached using EDTA as described above. HiPSC were washed from the wall of the well and resuspended in 4mL of StemFlex media supplemented with a ROCK inhibitor at a 1:100 concentration (RevitaCell™, ThermoFisher Cat: A2644501). This suspension was passed dropwise through a pre-wet 150μm filter to remove large aggregates and then divided between two wells of a 6-well ultra-low attachment (ULA) plate (Corning Cat: 3471). Cells were then returned to the incubator overnight.

The following day, the cell suspension was transferred from ULA plates to a 15mL centrifuge tube, pipetting gently to avoid disrupting hiPSC aggregates. Aggregates were then pelleted by centrifuging at 200rcf, for 4min at room temperature. The supernatant was aspirated, and aggregates resuspended in 8mL of phase 1 medium. This cell suspension was divided evenly between 4 wells of the ULA 6-well plate. The plate was placed in a hypoxic incubator, at 37°C, 5% $CO_2$, 5% $O_2$ for 72 hours. The day on which mesodermal induction was initiated by the addition of phase 1 medium and hypoxic incubation was marked as Day 0 of the differentiation.

### 2.1.4 Phase II – Stromal and haematopoietic commitment

On D3 following 72 hours of hypoxic incubation, aggregates in media were transferred into a 15mL centrifuge tube in vertical orientation. Aggregates were

allowed to settle into pellets under gravity over 10min, without centrifugation. Supernatant was removed and pellets resuspended in 8mL of phase 2 medium. 2mL of this suspension was added to each of 4 wells of a 6-well ULA plate. Plates were returned to the normoxic incubator for 48 hours.

### 2.1.5 Day 5 – Hydrogel embedding

On D5, aggregates were embedded in hydrogel (Figure 2.2). The number of aggregates in each well of the 6-well plate were estimated by counting with a light microscope. A number of wells from a 12-well plate were selected for hydrogel embedding, such that 20-30 aggregates would be distributed to each well. Hydrogel components were kept separate and on ice until immediately prior to mixing, as Matrigel® rapidly transitions to a solid on warming above 4°C. Hydrogel base layer mixture was prepared from individual components immediately prior to use. The addition of NaOH and thrombin results in rapid polymerisation, so these components were added last, and hydrogel plating was completed within 2min of the addition of these components. Individual wells of a 12 well plate had 500μL of hydrogel base layer mixture added. The plate containing hydrogel base layers was returned to the incubator for 30-60min to cure.

Aggregates were transferred to a 15mL centrifuge tube and settled into pellets under gravity. Supernatant liquid was removed, and aggregates resuspended in hydrogel organoid layer mixture at a volume of 500μL per well of the 12-well plate. Once again, the hydrogel mixture was prepared from individual components immediately prior to plating. 500μL of the aggregate-hydrogel suspension was

added dropwise to each of the hydrogel base-layers prepared earlier. The plate was returned to the incubator for 30-60min to facilitate the curing of the organoid layer.

1mL of prewarmed phase 3A medium was added dropwise to each well following hydrogel curing. The plate was returned to the incubator for 48 hours.

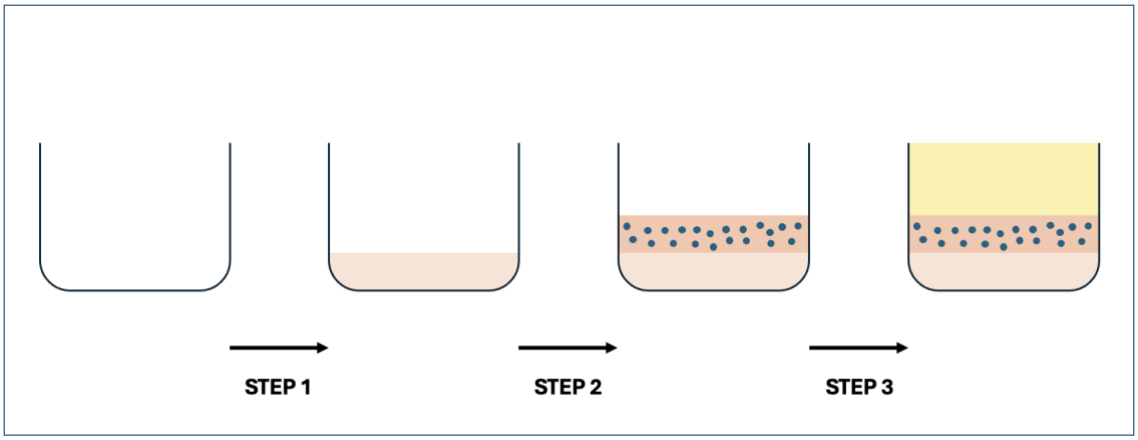



**Figure 2. 2:** Simplified schematic of stepwise hydrogel embedding.

**Step 1:** 500µL of hydrogel base layer mixture is added to a well in a 12-well plate. This is allowed to polymerise at 37°C for 30-60min. **Step 2**: Aggregates are resuspended in hydrogel organoid layer mixture and then 500µL of this suspension plated on top of the base layer. A density of 20-30 aggregates per well is optimal. This layer is allowed to polymerise at 37°C for 30-60 min. **Step 3:** 1mL of phase 3A medium is added to each well. After step 3, three distinct layers should be visible in each well when viewed from side-on.

### 2.1.6 Phase III – Vascular sprouting

On D7, 1mL of phase 3B medium was added to each well. On D10, media was refreshed by removing 1mL of media from each well and replacing it with 1mL of phase 3C medium. Between feeds, plates were returned to the incubator. Between D7-12, vascular sprouts were observed branching into the hydrogel matrix.

### 2.1.7 Phase IV – Hydrogel extraction and individual organoid culture

On D12, organoids were extracted from hydrogels. The number of successful organoids were counted by eye, and the decision made to prepare one ULA 96-well

plate for organoid extraction as an excess of successful sprouts were observed. Hydrogels were disassociated by serial pipetting with a P1000, and this solution transferred to a 15mL centrifuge tube, prior to centrifuging at 200rcf for 2 min. Three layers were visible after centrifugation; a layer of clear media overlying a layer of collagen, and a loose 'pellet' of organoids at the apex of the tube. The media layer was aspirated and set aside for later use (referred to as 'conditioned media' henceforth), and the collagen layer aspirated and discarded. Fresh 'extraction' medium was mixed 70:30 with conditioned media, and this mixture was used to resuspend the organoid 'pellet'. A pasture pipette was then used to manually collect individual organoids from suspension and add them to discrete wells of the 96-well plate. Following this process each well of the 96-well plate contained an individual organoid, suspended in ~100μL of media.

Following hydrogel extraction, organoids were returned to the incubator. Media was refreshed every 72 hours by aspirating and discarding 50μL of media from each well and replacing it with 50μL of freshly prepared phase 4 medium. Organoids were maintained until D21.

### 2.1.8 Organoid digestion and analysis

On D21, organoids were digested to facilitate analysis by flow cytometry. Twelve organoids were pooled for each technical replicate. Pooled organoids were collected into a 15mL centrifuge tube and pelleted by centrifuging at 400rcf for 3min. Supernatant was removed, and organoids resuspended in 1mL of collagenase buffer, containing collagenase D (Merck Cat: 11088858001) at a

concentration of 20mg/mL. Digestion and dissociation were performed by incubating this suspension in a water bath at 37°C for 5min, followed by manual trituration by vigorous pipetting. Repeated cycles of incubation and pipetting were performed until organoids dissociated into a single cell suspension. Digestion was then quashed with a solution of 10mM EDTA in PBS and 5% FBS. Cells were then washed and stained by incubating for 30min in the relevant flow antibody master-mix at 4°C. Sample acquisition was performed immediately following staining. Two panels developed by the Psaila group were utilised to define haematopoietic and stromal populations from the organoids respectively. Three technical replicates were stained for each of these two panels.

### 2.1.9 HiPSC CRISPR editing

HiPSC editing was performed in collaboration with the WIMM transgenic core facility. The approach detailed here was designed and led by the core facility and is reproduced with permission. Editing was performed with the goal of generating a dual K/O MHC class I and II hiPSC line via biallelic CRISPR Cas9 disruption of *β2m,* and *Ciita* respectively. Ribonucleoprotein (RNP) complexes were generated using the Integrated DNA Technologies (IDT) Alt-R®RNP system. crRNAs and tracrRNAs were ordered from IDT and resuspended in TE buffer (IDT Cat: 11-05-01-05) at 100μM. Small guide RNAs (sgRNAs) were prepared by mixing equimolar crRNA and tracrRNA in Nuclease Free Duplex Buffer (IDT Cat: 11-05-01-03). This mix was annealed by incubation at 95°C for 5min, followed by cooling to 25°C at a rate of 1°C/min. SgRNAs were then complexed with HiFi Cas9 V3 (IDT) at equimolar ratios,

and left for 30min at room temperature to generate stable RNPs. The guides used were taken from a prior methods paper detailing a protocol for generating MHC K/O hiPSC lines (134). Specifically, the sequences used to target *β2m* and *Ciita* were 5'-TTCGGCTTCCCATTCTCCGG(TGG)-3' and 5'-GGTCCATCTGGTCATAGAGG(CGG)-3'.

HiPSC transfection was performed using Lipofectamine Stem (Thermofisher Cat: STEM00001). HiPSCs were seeded at 50000 cells/well on 24-well plates coated with Geltrex prepared as described earlier. Commercially available hiPSCs from Stem Cell Technology (SCT Cat: SCTi003-A) were used for editing. Cells were incubated overnight in StemFlex supplemented with RevitaCell™. Cells were then washed with PBS prior to resuspension in Opti-MEM (ThermoFisher Cat: 51985091) for Lipofection. A Lipofection master mix was prepared using 25μL Opti-MEM with 2μL of Lipofectamine Stem per reaction. Equal volumes of Lipofectamine master mix and the RNP mix were incubated together for 10min at room temperature to form lipofection complexes. This mix was added to cells in Opti-MEM and left for four hours prior to supplementation with StemFlex media.

Editing efficiency was estimated by aliquoting from bulk cells and Sanger sequencing, which was performed by the WIMM sequencing core facility. Synthego ICE analysis was used to estimate editing efficiency. To generate colonies with uniform editing, single hiPSCs were isolated by limiting dilution, then were plated onto 24-well plates coated in Geltrex. Colonies were maintained post editing as previously described. 100 independent hiPSC colonies were maintain in culture and then screened for successful editing. To identify colonies with successful editing, each colony was sampled for sanger sequencing.

# 3. Murine Model Development

## 3.0 Introduction and approach

We hypothesise that injury to bone marrow stromal populations by alloreactive T cells can be used as the basis of a mouse model of T cell mediated injury within the haematopoietic niche. GVHD is an independent risk factor for poor graft function following alloSCT (12), and prior studies in mouse models exploring the impact of GVHD on haematopoietic function demonstrated decreased bone marrow cellularity and pancytopenia (101, 102). A limitation of these mouse models is the severe GVHD phenotype employed, which results in a short period of survival post-transplant. This short follow up restricts observations of haematopoietic function to the period immediately following transplantation and prohibits analysis of stably engrafted populations. To circumvent this limitation our approach was to optimise a conventional mouse model of GVHD to survive longer term, via selection of a transplant model characterised by a mild GVHD phenotype and titration of the alloreactive T cell dose (Figure 3.1). From project outset, four criteria were identified as desirable in a model for our purposes:

1. The GVHD cohort in the model needs to have most animals survive long enough for peripheral blood parameters to reflect the output of transplanted HSCs.
2. The model requires a reproducible peripheral blood phenotype characterised by cytopenias.
3. The model requires donor chimerism to be traceable via flow cytometry.

4. Given the broader project focus on bone marrow stromal populations within the niche, the model requires a reproducible bone marrow stromal phenotype measurable using flow cytometry.

Several decisions regarding model design were made at the outset. A B6 donor -> 129 recipient transplant system was selected as the basis for the model. The B6 and 129 mouse strains are two widely used wild-type strains of disparate genetic backgrounds, which share the $H2^b$ haplotype and so are matched at major histocompatibility loci. GVHD in this model is driven by multiple minor histocompatibility antigen mismatches. This transplantation model has previously been extensively used to characterise T cell responses to minor histocompatibility antigens (135). This decision was made on pragmatic grounds, as our group has previously used this model system and observed that with low T cell doses it is capable of generating a reproducible GVHD phenotype without clinically overt end organ manifestations, and thus was likely to be amenable to the generation of a long-lived GVHD model (136). Other pragmatic benefits of a B6->129 transplantation model are the widespread commercial availability of transgenic mouse strains developed from both 129 and B6 wild-type backgrounds, and access to B6 mice expressing the congenic isoform of CD45, CD45.1, which can allow donor chimerism to be easily tracked in haematopoietic cells following transplantation using flow cytometry.

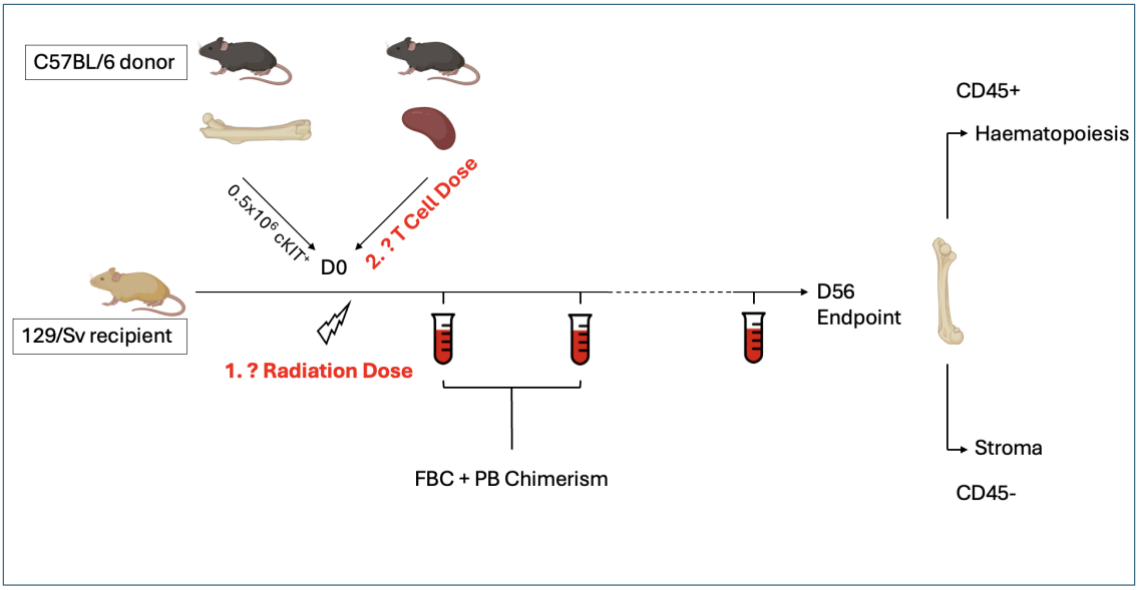



**Figure 3. 1: Schematic representation of planned GVHD mouse model.**

The impact of GVHD on bone marrow stromal populations and engrafting haematopoiesis was explored using a B6->129 minor-HLA mismatch GVHD model. Male and female 129 recipients received $0.5x10^6$ c-Kit$^+$ bone marrow cells isolated from male B6 donors after conditioning with total body irradiation. Recipients randomised to GVHD cohorts received additional graft T cells to induce GVHD. Serial sampling of peripheral blood was performed prior to a scheduled D56 endpoint, when mice were sacrificed to facilitate analysis of bone marrow populations. The optimal radiation dose and T cell dose for this model system were empirically determined through dose titration experiments. Figure created using BioRender.com.

Other decisions that were made at the outset were the bone marrow cell dose and timing of the scheduled endpoint. As controls in this model system would also receive a B6 donor haematopoietic stem cell graft, a method of T cell depletion from bone marrow was required to avoid GVHD occurring in the control cohort. Rather than transplanting T cell-depleted whole bone marrow, we opted to transplant c-Kit$^+$ enriched bone marrow. The c-Kit$^+$ fraction is a population which contains no mature T cells but retains haematopoietic stem and progenitor populations. C-Kit$^+$ cell enrichment was selected as a strategy likely to result in functional T cell depletion, while providing dose consistency for haematopoietic stem and progenitor populations between different experiments. Prior experience with c-Kit$^+$ cell

transplantation led us to select $0.5x10^6$ c-Kit$^+$ cells as a dose likely to result in successful engraftment in most recipients, without requiring an excessive number of donor animals to be sacrificed per experiment. While a 16 week endpoint is frequently recommended for transplantation experiments focused on haematopoietic function (15), we selected an eight week endpoint. This was chosen pragmatically on the basis that this timepoint would be long enough to facilitate studying HSC-derived T cell lymphopoiesis, which frequently is not detectable in peripheral blood in measurable numbers until 6-8 weeks post transplantation, while remaining short enough for sequential experiments to be practically achievable in the context of a student led project. This left the following four sequential steps for model development:

1. Develop reproducible workflows for the generation of the c-Kit$^+$ and CD3$^+$ cellular products.
2. Develop endpoint panels for the analysis of bone marrow haematopoietic and stromal populations by flow cytometry.
3. Identify an appropriate dose of radiation to condition recipient animals for transplantation.
4. Identify an appropriate dose of T cells to generate our desired GVHD phenotype.

Flow cytometry will be a key analysis technology for this model system. Our group has previously developed flow cytometry workflows for the identification of bone marrow stromal populations including LepR$^+$ MSCs, arteriolar endothelial cells and

sinusoidal endothelial cells, based on published models (46). Recent studies have identified that the expression of Sca-1$^+$ identifies a population of LepR$^+$ MSCs which modulate local myeloid populations via the secretion of inflammatory cytokines, and which can be induced by niche IFN signalling (5, 83). Our stromal panel was modified to stratify LepR$^+$ MSCs by Sca-1 expression.

New haematopoietic panels required development. As it was unclear where perturbations in the haematopoietic hierarchy would occur upstream of the peripheral blood phenotype we were attempting to model, the decision was made to develop panels that would allow characterisation of the entire haematopoietic hierarchy, including long-term HSCs (LT-HSCs), MPPs as well as lineage committed progenitors. While several well characterised models exist to immunophenotypically define murine haematopoietic populations, there is a growing body of literature which suggests that the most widely used of these models do not work in the setting of inflammation and may lead to difficulties in interpretation in mice randomised to the GVHD cohort. LT-HSCs are usually immunophenotypically defined as: lineage$^-$, c-Kit$^+$, Sca-1$^+$ (LSK), CD135$^-$, CD150$^+$, CD48$^-$ (SLAM), CD34$^-$ (referred to going forwards as CD34$^-$ SLAM cells). It has been demonstrated that CD34$^-$ SLAM gating is ineffective at identifying functional LT-HSCs in mice with systemic inflammation, and that long term repopulating capacity in this setting is restricted to the subpopulation of CD34$^-$ SLAM gated LT-HSCs expressing CD201 (33). To account for this, we chose to incorporate CD201 into our HSC panel, similar to other groups focused on stress haematopoiesis (137). The LSK gate identifies <0.1% of bone marrow cells, but contains all HSCs and MPPs, and so is frequently used to separate these populations from lineage committed

progenitors. Sca-1 expression is observed on lineage committed myeloid progenitors in the setting of inflammation, which will result in the mischaracterisation of these mature populations as HSC/MPP populations using standard gating strategies (138). Prior studies have demonstrated an expansion in HSC populations with an associated functional deficit in the setting of inflammation, with an associated myeloid lineage bias (65, 76). If the upregulation of Sca-1 on maturing myeloid populations was more frequent in the setting of GVHD than in control conditions, there is a risk that this could result in systemic bias in our analysis suggestive that these changes were present. Other groups have circumvented this issue either by defining HSCs by SLAM marker expression without enrichment by LSK gating, or by substituting Sca-1 for an alternative marker such as ESAM or CD86 (10, 138, 139). We elected to use CD86 as a parallel marker for Sca-1 in our panels, as the published functional validation of the performance of this marker in the setting of inflammation was more comprehensive than was available for ESAM (138). In addition to these changes to facilitate interpretability in the setting of inflammation, panels were developed in line with broadly adopted immunophenotypic models of murine haematopoiesis (20, 22). A panel was also developed to facilitate characterising the cell state of bone marrow T cells.

Prior studies using B6 -> 129 transplantation have used a 9Gy dose of radiation delivered in split fractions to condition recipients for transplantation (140, 141). Local experience suggested that generalising published radiation doses to our institute's irradiator occasionally resulted in the death of large proportions of experimental cohorts due to conditioning stress. As such, the decision was made to empirically determine an appropriate dose of radiation via a dose titration

experiment. After identification of an appropriate dose of radiation to condition recipients, a series of experiments were conducted to determine an appropriate T cell dose to generate our desired GVHD phenotype.

## 3.1 Results

### 3.1.1 Cell product method development

My co-supervisor Adam Wilkinson's group had previously developed a method of c-Kit$^+$ cell enrichment using MACS cell separation (131). Experiments were performed to optimise this technique for transplantation workflows and confirm its efficiency in T cell depletion. Eight repetitions of the c-Kit$^+$ bone marrow cell isolation protocol resulted in a mean (+/- SD) post enrichment purity of 66% (+/- 11.6%). Infrequent yields as low as 40% were observed, so the decision was made to incorporate a quantification of c-Kit$^+$ cells in the post enrichment product by flow cytometry into the pre-infusion workflow of each transplant. An experiment quantifying CD3$^+$ T cell and c-Kit$^+$ cells at each stage of a c-Kit$^+$ cell enrichment were performed. Pre-enrichment bone marrow contained 1.75% T cells, which would correspond to $5.6x10^5$ T cells contaminating each $0.5x10^6$ c-Kit$^+$ cell dose. In four replicate experiments, following c-Kit$^+$ enrichment each $0.5x10^6$ c-Kit$^+$ cell dose contained only 2.5 (+/- 3.2) $x10^3$ T cells. This degree of residual T cell contamination was deemed negligible.

Splenocytes without further enrichment are frequently used to induce GVHD in mouse models, however the spleen contains functional HSC populations in adult mice capable of engrafting following transplantation (142). To avoid splenic HSCs

contributing to chimerism, MACS cell separation was used to isolate $CD3^+$ cells from donor spleens. $CD3\varepsilon^+$ splenocyte enrichment resulted in a mean post-enrichment T cell purity of 82% (+/- 6.6%) across five repetitions of the protocol, with a yield of 10.1 (+/- 3.0) x $10^6$ T cells per donor spleen. All repetitions of this protocol resulted in a post-enrichment T cell purity between 70% and 90%. Given the reproducibility of this method, T cells were dosed on an assumed post-enrichment purity of 80%, with no pre-infusion purity check built into the transplantation workflow.

### 3.1.2 Transplant endpoint flow cytometry panel development

New endpoint panels to analyse the cellular architecture of haematopoietic populations and the memory state of bone marrow T cells were developed. Haematopoietic panels incorporating CD86 as an alternative to Sca-1 were developed due to the concern that Sca-1 upregulation on lineage committed progenitors would be more likely in the setting of GVHD than in control conditions and could become a source of systematic bias. Differential expression of CD45.1 and CD45.2 were employed to separately characterise donor haematopoiesis (expressing CD45.1), graft T cells (expressing CD45.1 and CD45.2) and residual recipient haematopoiesis (expressing CD45.2). Representative gating for two haematopoietic panels, one defining HSC and MPP populations and the other defining lineage committed progenitors are shown in Figure 3.2, and Figure 3.3 respectively.

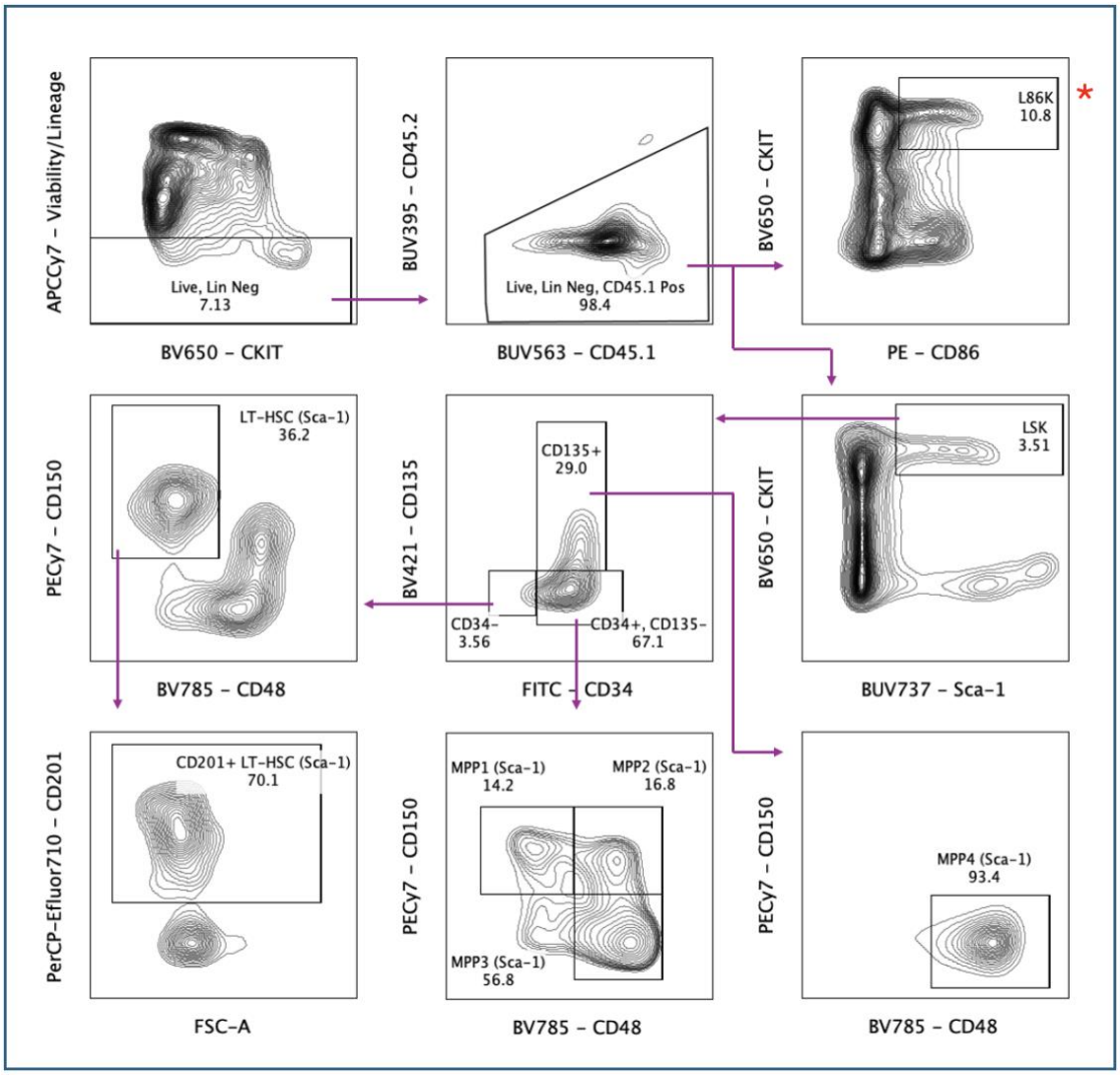



**Figure 3. 2:** Representative gating for haematopoietic stem cell (HSC) and multipotent progenitor (MPP) populations.

Gating shown is performed following debris and doublet exclusion. Gating is shown using Sca-1 as a backbone marker. Note that the gating down stream of c-Kit$^+$/CD86$^+$ cells (L86K), (labelled with a red asterisk) is identical to gating down stream of c-Kit$^+$/Sca-1$^+$ (LSK) and so is omitted for clarity.

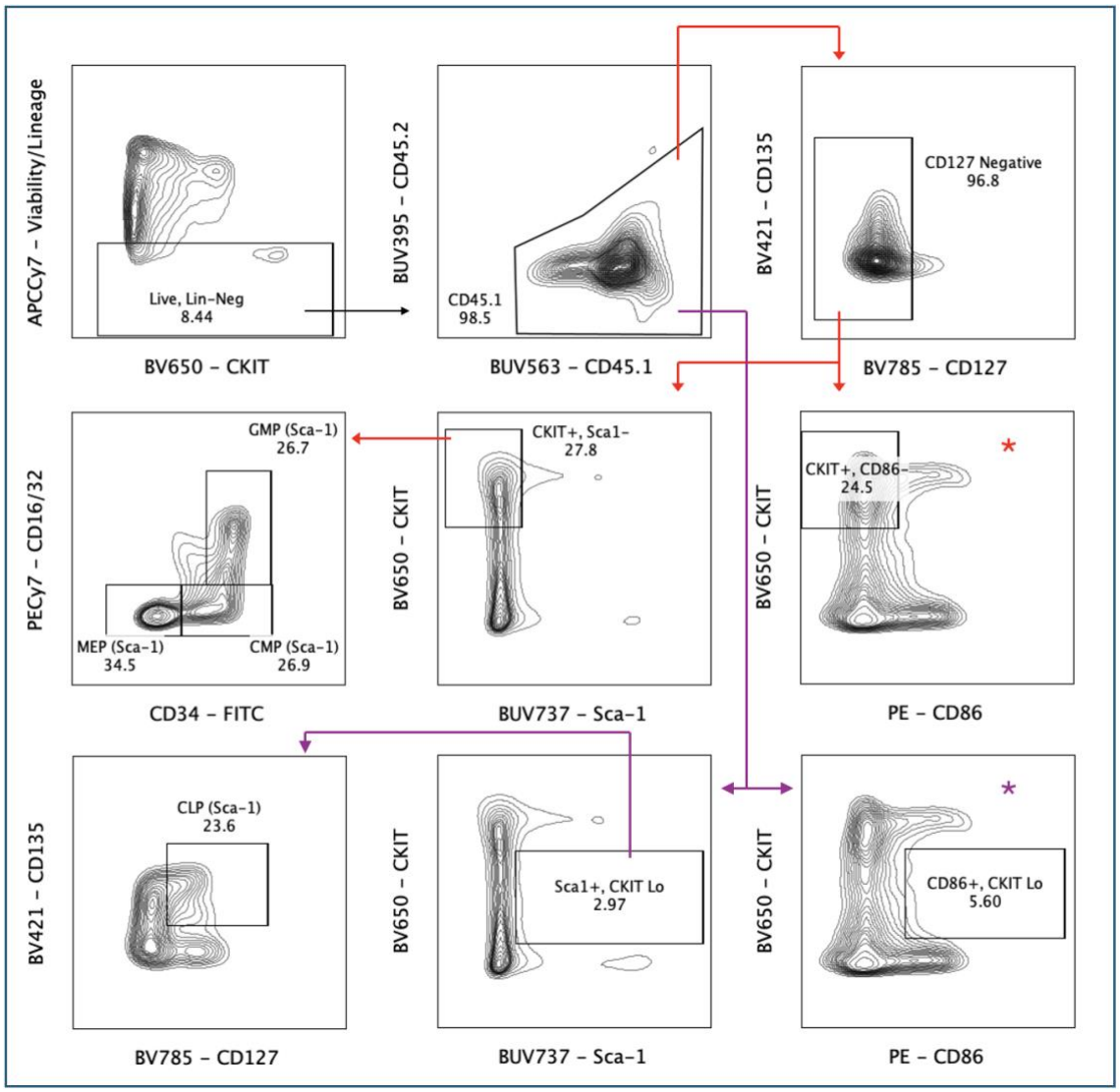



**Figure 3. 3:** Representative gating for lineage committed progenitor populations.

Gating shown is performed following debris and doublet exclusion. Red arrows demonstrate the gating strategy for defining myeloid populations. Purple arrows demonstrate the gating strategy for defining common lymphoid progenitors (CLPs). Note that gating down stream of c-Kit$^{+}$/CD86$^{-}$ (labelled with a red asterisk) is identical to gating down stream of c-Kit$^{+}$/Sca1$^{-}$ and so is omitted for clarity. Similarly, gating down stream of c-Kit$^{Lo}$/CD86$^{+}$ (labelled with a purple asterisk) is identical to gating down stream of c-Kit$^{Lo}$/Sca-1$^{+}$, and so is omitted for clarity.

A T cell panel was developed to facilitate the separate characterisation of residual recipient-derived T cells, graft T cells and donor HSC-derived T cells, identified based on differential CD45 isoform expression as described previously. The memory state of T cells was characterised by differential expression of the

adhesion molecules CD44 and CD62L (132). Figure 3.4 demonstrates representative T cell gating.

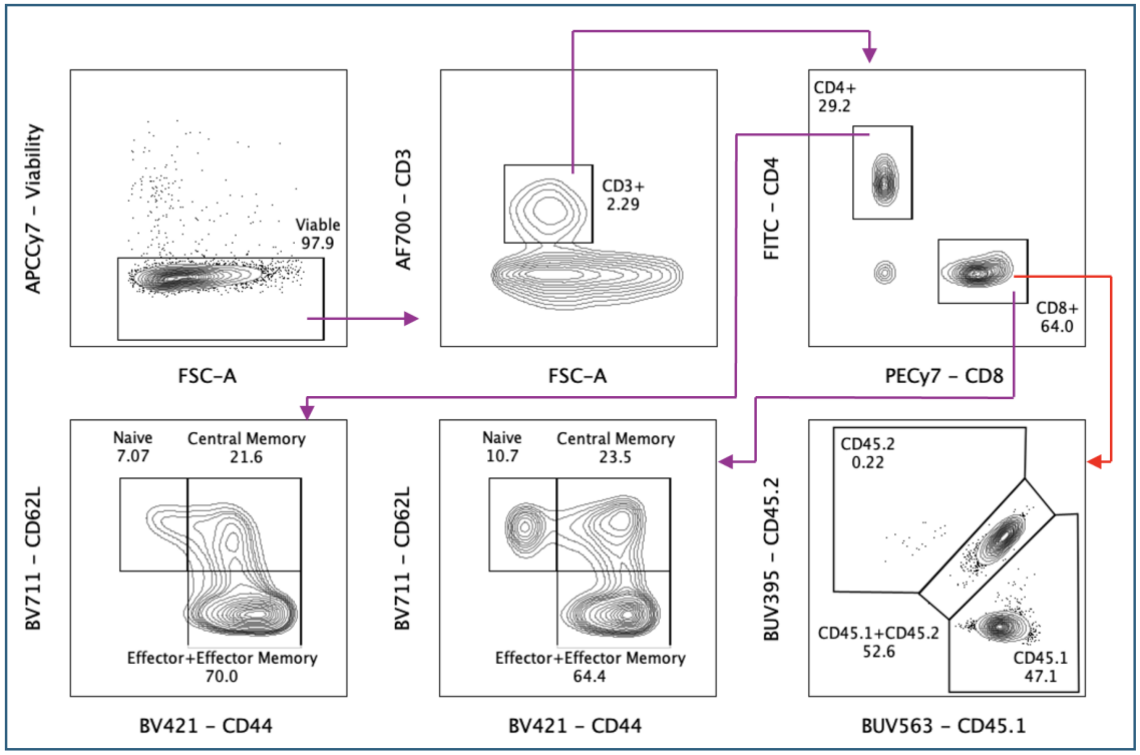



**Figure 3. 4:** Representative gating for bone marrow T cell populations.

Gating shown is performed following debris and doublet exclusion. Purple arrows demonstrate the gating strategy used to characterise the memory state of $CD4^+$ and $CD8^+$ populations. Red arrows demonstrate the gating strategy used to identify HSC-derived T cells ($CD45.1^+$), graft T cells ($CD45.1^+$ and $CD45.2^+$) and persistent recipient T cells ($CD45.2^+$). Chimerism gating is demonstrated down stream of $CD8^+$ T cells, but an identical approach was employed to characterise other populations of interest.

### 3.1.3 Radiation dose titration

An experiment was performed to determine a dose of radiation to condition animals for transplantation that would result in high donor chimerism in haematopoietic populations of interest, while minimising animal losses due to conditioning stress. Eight 129 mice were randomised to 7.5Gy or 9Gy doses of caesium-137 irradiation, prior to infusion of $0.5x10^6$ c-$Kit^+$ bone marrow cells from male B6 donors, with no

supplementary T cells. All animals were included in peripheral blood chimerism analyses, and two and three animals from the 7.5Gy and 9Gy cohorts respectively were included in the haematopoietic endpoint of this experiment.

Both radiation doses were well tolerated. No mice in this experiment died prior to the scheduled D56 endpoint, and no adverse effects bar transient weight loss were observed. The mean (+/- SD) maximum loss of weight from baseline in the 7.5Gy and 9Gy cohorts were 6.7% (+/- 3.5) and 9.9% (+/- 0.9) respectively.

Peripheral blood analyses are summarised in Figure 3.5. Peripheral CBCs were similar between cohorts at each timepoint analysed. A trend towards higher donor chimerism in B, T and myeloid cell was observed in the 9Gy cohort at all timepoints, though the differences between cohorts were small. At D56, B cell and myeloid chimerism were 86.9% (+/- 3.5) and 82.9% (+/- 9.5) vs 96.1% (+/- 0.4) and 88.6% (+/- 4.4) for the 7.5Gy and 9Gy cohorts respectively. As expected, D56 peripheral T cell donor chimerism was lower than other cell fractions at 49.4% (+/- 4.3) and 57.3% (+/- 2.3) in the 7.5Gy and 9Gy cohorts respectively.

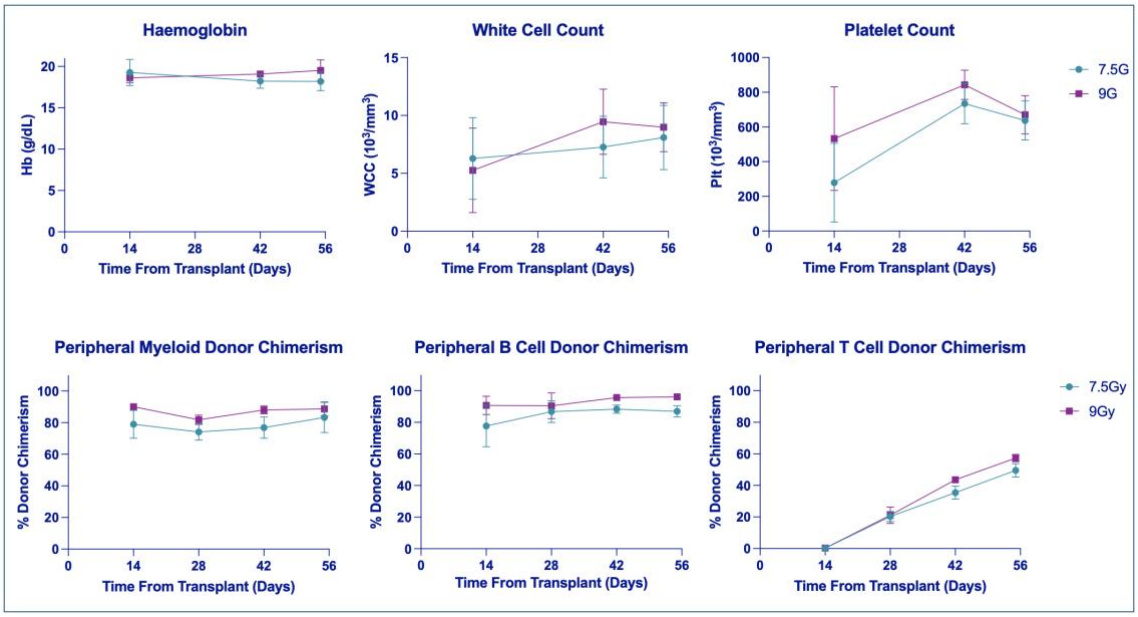



**Figure 3. 5:** Radiation dose titration peripheral blood analyses.

CBCs over time are shown for mice randomised to 7.5Gy (n=4) or 9Gy (n=4) radiation doses prior to transplantation. Note that CBCs are not shown for the D28 timepoint due to an analyser failure. Peripheral donor chimerism over time as determined by differential expression of CD45 isoforms is shown by radiation dose cohort.

Donor chimerism was evaluated at D56 in bone marrow haematopoietic subpopulations. As panels had been designed to characterise haematopoietic populations using either Sca-1 or CD86 as alternative back bone markers, analysis of chimerism was performed in subpopulations defined by each of these markers. Donor chimerism by cohort in bone marrow populations is summarised in Figure 3.6. Donor chimerism trended higher in the 9Gy cohort than the 7.5Gy cohort in all haematopoietic subpopulations. In the 9Gy cohort, mean donor chimerism at D56 was >80% in all populations, bar HSCs defined by Sca-1 gating, and megakaryocyte/erythroid biased MPP2 populations. As expected, donor chimerism was similar in populations defined by Sca-1 or CD86 gating strategies.

Based on these results, 9Gy was identified as an appropriate radiation dose for conditioning animals for transplantation in this model system.

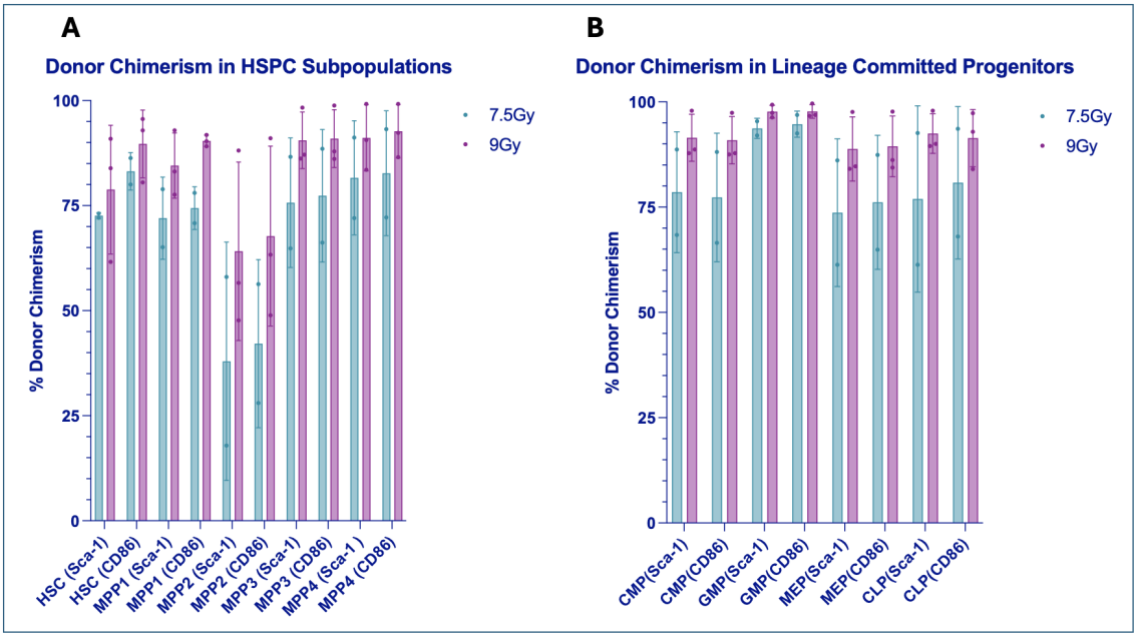



**Figure 3. 6:** Donor chimerism by radiation dose in haematopoietic subpopulations.

Donor chimerism by radiation dose in haematopoietic stem cell and multipotent progenitor populations **A** and lineage committed progenitor populations **B**. Populations defined by a Sca-1 or CD86 gating backbone are shown side by side. Two mice randomised to 7.5G (green) and three mice randomised to 9Gy (purple) were analysed in this experiment. Data are the mean +/- SD.

### 3.1.4 Syngeneic transplantation and aged matched litter mates

While well validated reference intervals for haematological parameters are published for C57/BL6 mice over time, there is evidence that differences between strains prevent the generalisation of these values to the 129S2/SvHsd recipients used in our model system (143, 144). To explore unperturbed haematopoiesis in our model, four non-transplanted mice age matched to our transplant recipients underwent serial evaluation of peripheral blood counts, followed by evaluation of the cellular architecture of haematopoietic and stromal bone marrow populations. These animals were aged 11 weeks at the beginning of the analysis period, and 19 weeks at experimental endpoint. CBC parameters at each timepoint in the non-transplanted cohort are summarised in Table 3.1.

**Table 3. 1:** Peripheral blood haematological parameters over time in non-transplanted 129S2/SvHSD mice.

| Age | Hb (g/dL) | +/- SD | WCC ($10^3$/mm$^3$) | +/- SD | Plt ($10^3$/mm$^3$) | +/- SD |
|---|---|---|---|---|---|---|
| 13 weeks | 19.6 | 0.4 | 6.1 | 0.9 | 270 | 210 |
| 15 weeks | 18.4 | 0.9 | 6.6 | 1.2 | 360 | 240 |
| 17 weeks | 19.1 | 0.5 | 11.5 | 3.5 | 690 | 70 |
| 19 weeks | 19.2 | 0.3 | 7.1 | 0.6 | 390 | 110 |

Peripheral blood haematological parameters in non-transplanted mice were largely stable over the time course of the analysis, with no observable trends over time. Marked variability in platelet count was observed between animals within the cohort at each timepoint. An increase in both white cell count, and platelet count at the 17 week timepoint compared with other timepoints was observed, with no identified systematic differences in animal husbandry, sample collection or handling to explain this variation.

As the mean value of haematological parameters within the cohort was largely stable over the time course of the experiment, an analysis of the reproducibility of serial measurements from each individual animal was performed (Figure 3.7). Serial measurements of haemoglobin and white cell count from each animal were similar over time, excluding the week 17 timepoint for white cell count, where high measurements were recorded from 2/4 animals. Serial measurements of platelet count from each individual animal demonstrated marked variability.

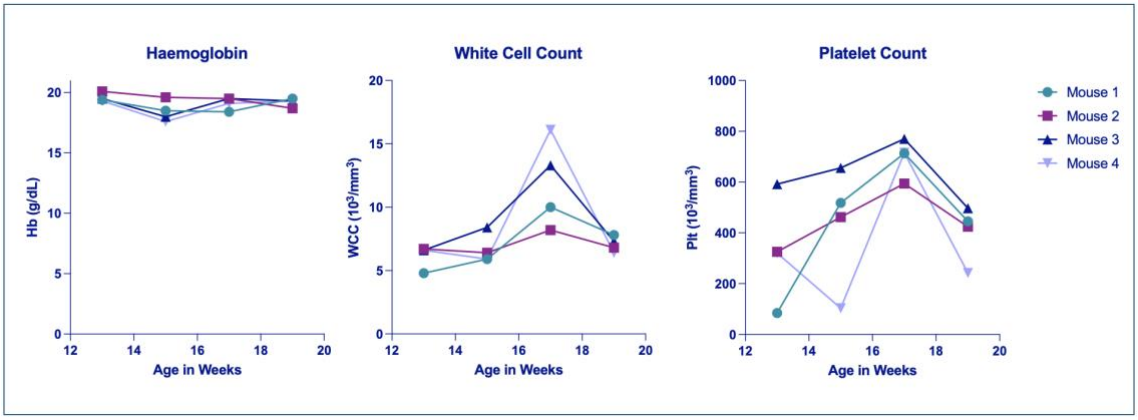



**Figure 3. 7:** Serial measurements of haematological parameters from individual non-transplanted 129 mice.

Peripheral blood was collected every 14 days from four 129 mice aged from age 13 weeks to 19 weeks by tail bleed. Serial CBCs from each animal are shown side by side.

To explore the impact of artifact from irradiation and transplantation on analyses in our model, four 129 litter mates of the non-transplanted cohort underwent syngeneic transplantation with $0.5x10^6$ c-Kit$^+$ cells from a 129 donor. Analyses of this cohort were performed in parallel to their non-transplanted litter mates, and haematopoietic parameters are summarised in Figure 3.8. The four animals in each cohort were included in all peripheral blood and bone marrow analyses in this experiment. Haemoglobin and platelet count were similar between syngeneic transplant and non-transplanted cohorts across the duration of follow up, except for the D42 time point when platelets were higher in the untransplanted cohort (mean +/- SD, 457 $10^3$/mm$^3$ +/- 136 vs 698 $10^3$/mm$^3$ +/- 74, $P$ = 0.03). White cell count was lower in transplanted animals compared with non-transplanted litter mates at early timepoints (Day 14 mean +/- SD, 4.0 $10^3$/mm$^3$ +/- 1.0 vs 6.2 $10^3$/mm$^3$ +/- 0.9, $P$ = 0.02; Day 28 mean +/- SD, 4.8 $10^3$/mm$^3$ +/- 1.1 vs 6.7 $10^3$/mm$^3$ +/- 1.2, $P$ = 0.06) but this difference had resolved by the D56 endpoint. The frequency of HSCs was lower in the transplanted cohort compared with untransplanted littermates. Typically

defined LT-HSCs as a proportion of live, lineage negative cells (mean +/- SD) were 0.048% +/- 0.02 vs 0.14% +/- 0.01 in transplanted and untransplanted cohorts respectively (*P*<0.001*)*. The proportions of CD201$^{+}$ LT-HSCs were 0.038% +/- 0.02 vs 0.12% +/- 0.01 (*P*<0.0001) in these respective cohorts. Other haematopoietic progenitor populations were similar between groups. Results were unchanged using a Sca-1 or CD86 gating backbone to define haematopoietic populations.

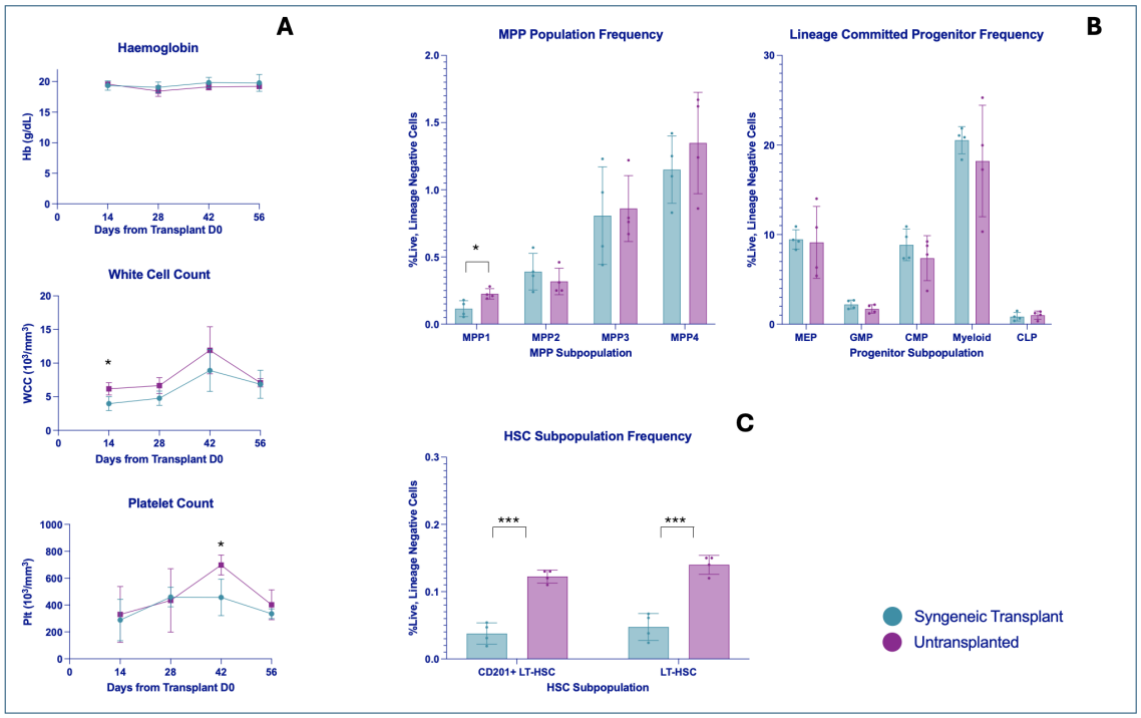



**Figure 3. 8:** Haematological parameters following syngeneic transplantation compared with non-transplanted litter mates.

**A** CBC parameters over time until D56 post-transplant in 129 mice undergoing syngeneic transplantation (n=4) and non-transplanted littermates (n=4). Bone marrow haematopoietic progenitor **B** and HSC **C** population frequencies at D56 post-transplantation compared with non-transplanted littermates. All bone marrow populations shown are defined using a Sca-1 gating backbone. Data are the mean +/- SD. *P* values calculated using student t-tests with no correction for multiple comparison. **P*<0.05, ****P*<0.001.

Stromal population architecture at the D56 endpoint was unchanged between groups (Figure 3.9). The proportion of LepR$^{+}$ MSCs expressing Sca-1$^{+}$, a marker of

niche inflammation, was increased in the transplanted cohort relative to untransplanted littermates; Sca-1 was expressed on 8.2% +/- 0.6 vs 4.8% +/- 1.0 of LepR$^+$ MSCs in these respective groups ($P$ = 0.0012).

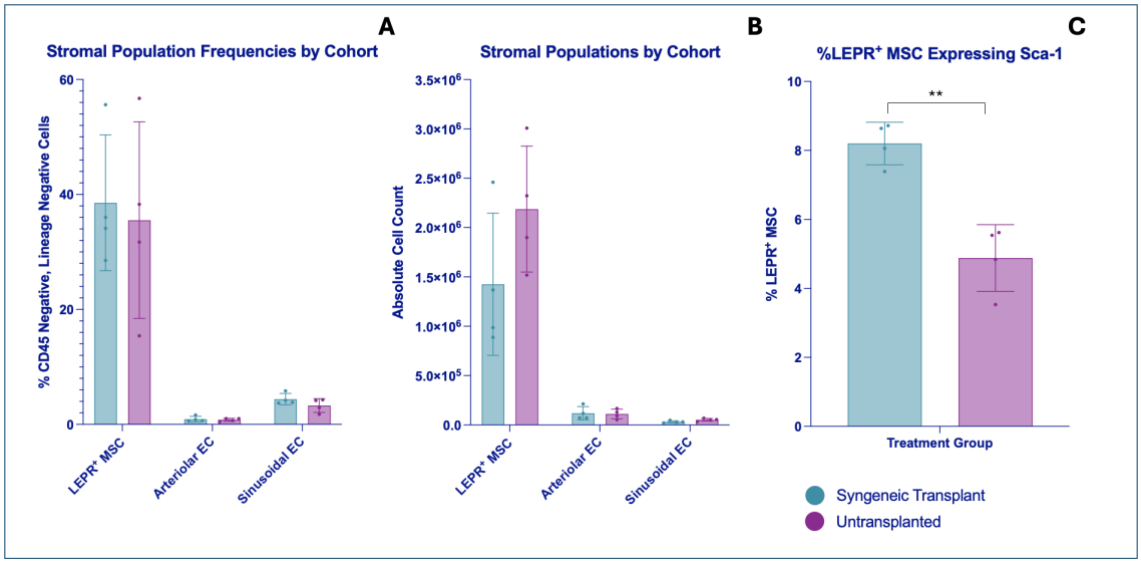



**Figure 3. 9:** Stromal population architecture and phenotype following syngeneic transplantation compared with non-transplanted litter mates.

Stromal cell populations by flow cytometry in 129 mice on D56 following syngeneic transplantation (n=4) and in non-transplanted littermates (n=4). **A** Frequency as a percentage of non-haematopoietic cells, **B** absolute cell counts, **C** % of LepR$^+$ MSCs expressing Sca-1 by cohort. Data are the mean +/- SD. $P$ values calculated using student t-tests with no correction for multiple comparison. ** $P$ <0.01.

### 3.1.5 T cell dose titration #1

An experiment was conducted to determine a dose of T cells that would result in sufficient GVHD to generate a reproducible haematopoietic phenotype, while still facilitating survival to a D56 endpoint for most recipients. Thirteen 129 recipients were randomised to a no T cell control group, or T cell doses ranging from 5x10$^4$ to 5x10$^5$ graft T cells. No mice died prior to the scheduled D56 endpoint. No adverse effects bar transient weight loss following irradiation were observed in any mice in

this experiment, including no clinical evidence of GVHD. No differences in weight were observed between cohorts at any timepoint.

Peripheral blood analyses for this experiment are summarised in Figure 3.10. No changes in CBCs were observed between groups at any timepoint. T cell donor chimerism trended higher in the cohort randomised to $5x10^5$ graft T cells compared with other groups at early timepoints, but this trend was less clear at D42 and D56. No other changes in peripheral blood chimerism were observed between groups. No changes in haematopoietic population architecture were observed between groups at the D56 endpoint. With only one mouse per group included in the stromal endpoint of this experiment, no conclusions could be drawn.

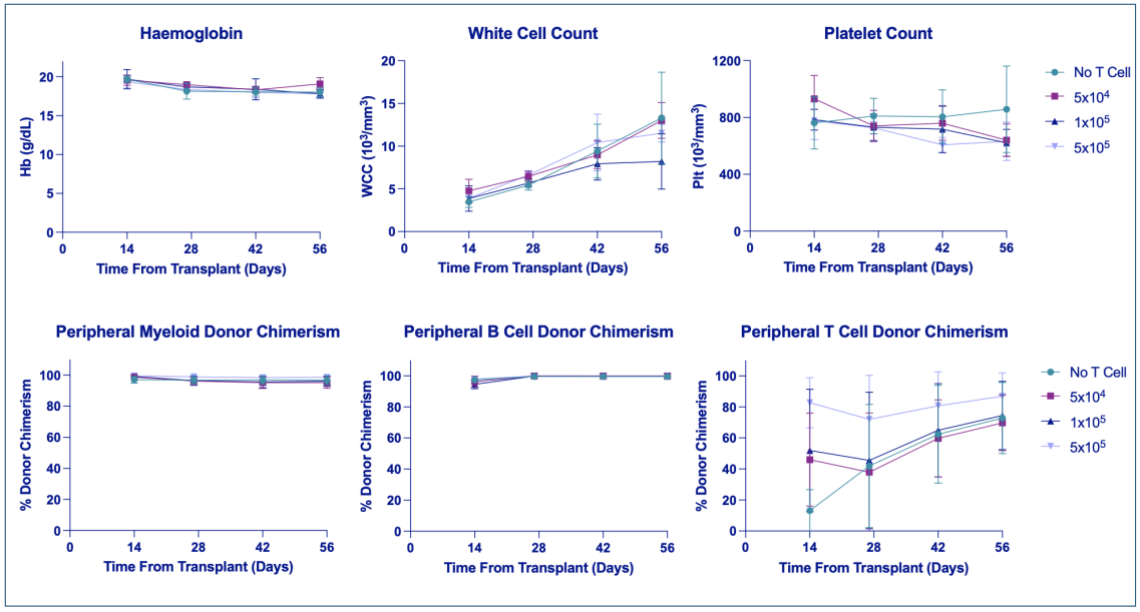



**Figure 3. 10:** Peripheral blood analyses from T cell dose titration #1.

CBCs over time are shown by T cell dose allocation, with no differences observed between groups. Peripheral blood donor chimerism in myeloid, B and T cell populations are shown over time between groups. Three mice were allocated to each of the no T cell control cohort, $5x10^4$ T cell cohort and $1x10^5$ T cell cohort. Four mice were allocated to the $5x10^5$ T cell cohort. Data are the mean +/- SD. Hypothesis testing was performed using student t-tests.

### 3.1.6 T cell dose titration #2

As the first T cell dose titration demonstrated no differences between groups and no clinical evidence of GVHD, the experiment was repeated using higher doses of graft T cells. Thirteen animals were allocated to a no graft T cell control (n=4), a $1x10^6$ T cell cohort (n=6) and a $5x10^6$ T cell cohort (n=3). An unexpectedly low yield of T cells at time of cellular product preparation led to an uneven distribution of mice between the two GVHD cohorts. Clinical evidence of GVHD was observed in this experiment (Figure 3.11). All mice in the $5x10^6$ cohort died within 20 days of transplantation, representing a significant reduction in median survival in this group despite the small number of mice allocated to this cohort ($P$=0.03). A sex difference appeared to be present in the $1x10^6$ T cell cohort, with two of three males in this cohort dying within 30 days of transplantation, compared with all three females in this cohort surviving to the scheduled D56 endpoint; given only two deaths occurred, this comparison did not reach statistical significance ($P$=0.11). One male in the control group died on day four, presumably due to stress from irradiation. Mild cutaneous GVHD was observed in the male randomised to the $1x10^6$ cohort that survived to the scheduled D56 endpoint, with no other end organ manifestations of GVHD observed. Mice randomised to GVHD dose cohorts had a lower mean weight at all time points than mice in the non-GVHD cohort, though at no timepoint did this comparison reach statistical significance.

As only one animal in the $5x10^6$ T cell cohort survived to the first peripheral blood analysis, comparisons for haematopoietic and stromal parameters in this experiment are made between the control group and $1x10^6$ T cell dose cohort (referred to as 'no GVHD' and 'GVHD' cohorts respectively). While it is likely that sex

differences exist in this model system, males and females are pooled in these analyses as the experiment was insufficiently powered to allow meaningful interpretation of data from males or females in isolation.

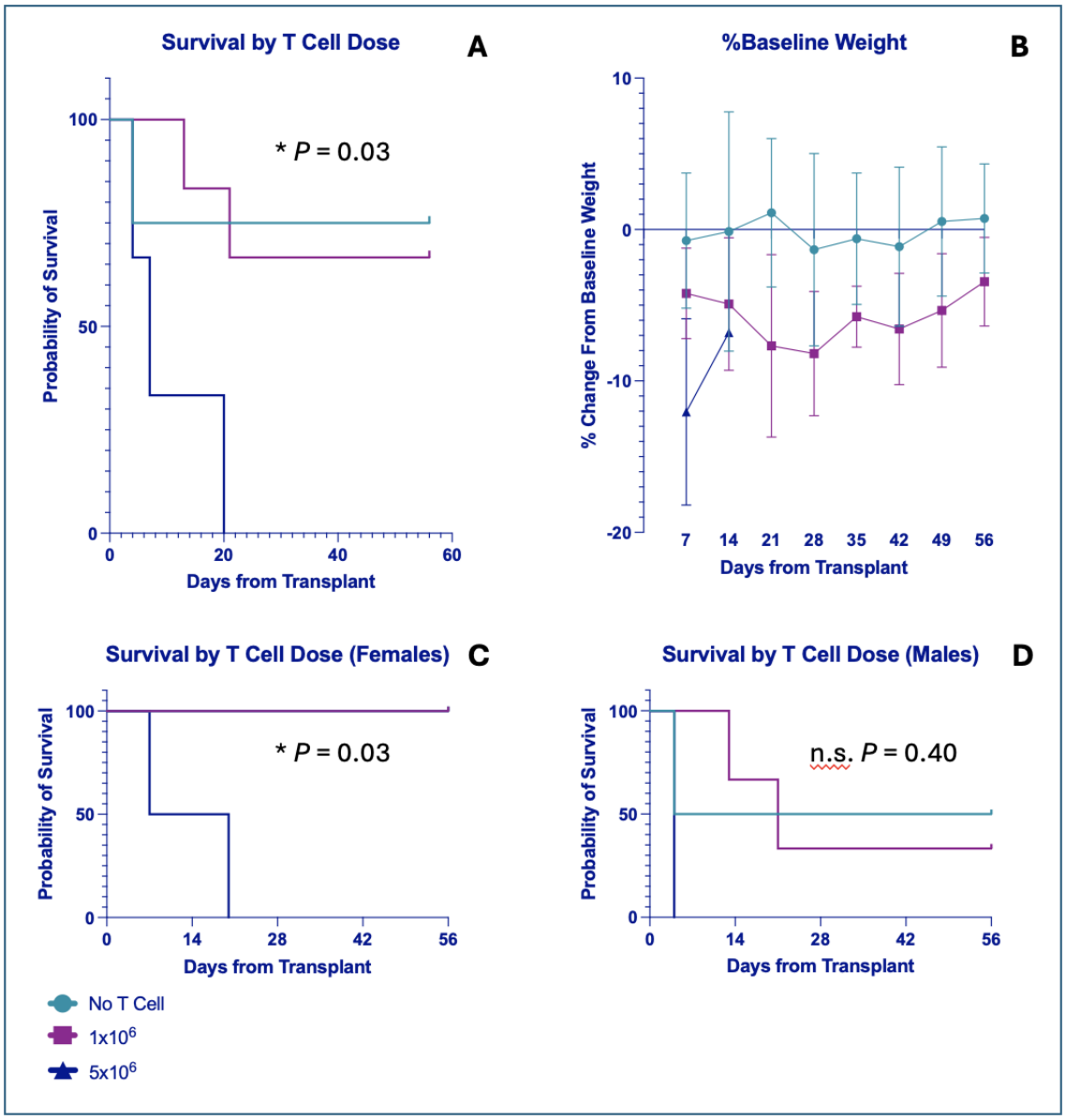



**Figure 3. 11:** Clinical parameters by T cell dose from T cell dose titration #2.

Thirteen animals were randomised to one of three T cell doses, no T cells (n=4), $1x10^6$ T cells (n=6) and $5x10^6$ T cells (n=3) . **A** Survival by T cell dose. **B** Weight as percentage of baseline weight by cohort. Both GVHD cohorts demonstrated loss of weight relative to control animals at all timepoints, though all comparisons were below the threshold of statistical significance. All surviving animals in each cohort are included at each timepoint. **C/D** Survival by T cell dose in female and male recipients respectively. All female mice randomised to the no T cell control and $1x10^6$ T cell cohort survived to the scheduled endpoint. Data are the mean +/- SD. Hypothesis testing for comparisons of weight was

performed using student t-tests. *P* values for survival analyses were calculated using a Log-rank test. * *P* <0.05.

Peripheral blood parameters are summarised in Figure 3.12. All surviving animals are included in each timepoint of this analysis. There was a reduction in haemoglobin in the GVHD cohort compared with the no GVHD cohort from D28 onwards. The difference between groups was most pronounced at D28, with a mean (+/- SD) Hb of 13.4 g/dL (+/- 1.0) and 17.5 g/dL (+/- 1.3) in the GVHD vs no GVHD cohorts respectively at this timepoint (*P*=0.005). White cell count was higher in the GVHD cohort vs the no GVHD cohort at all timepoints, with a rising white cell count over time observed in the GVHD cohort. The difference in white cell count was not statistically significant at any time point but trended towards significance at the D42 (*P*=0.06) and D52 (*P*=0.06). No differences were seen with regards to platelet count between groups. To explore the impact of GVHD on engrafting haematopoiesis, the output of the $CD45.1^+$ $c\text{-}Kit^+$ cells (referred to as HSC-derived haematopoiesis) was compared between groups over time. HSC-derived B cells were reduced in the GVHD cohort at D14 relative to controls, with a mean (+/- SD) B cell count of 0.08 $10^3/mm^3$ (+/- 0.05) vs 0.7 $10^3/mm^3$ (+/- 0.1) in these respective groups (*P*<0.0001). B cell quantification was similar between groups at later timepoints, with a trend towards an increase in the B cell count in the GVHD cohort relative to controls at D56 (*P* = 0.12). Peripheral blood HSC-derived myelopoiesis trended higher in the GVHD cohort at all timepoints, though this difference was statistically significant only at the D42 time point. HSC-derived T lymphocytes were higher in the GVHD cohort at D42 and D56, with a mean (+/- SD) $CD45.1^+$ T lymphocyte count at D56 of 3.2 $10^3/mm^3$ (+/-1.2) vs 1.2 $10^3/mm^3$ (+/- 0.1) in the GVHD vs no GVHD cohorts

respectively ($P$ = 0.03). No residual recipient-derived myeloid cells or B cells were identified in the peripheral blood at any timepoint.

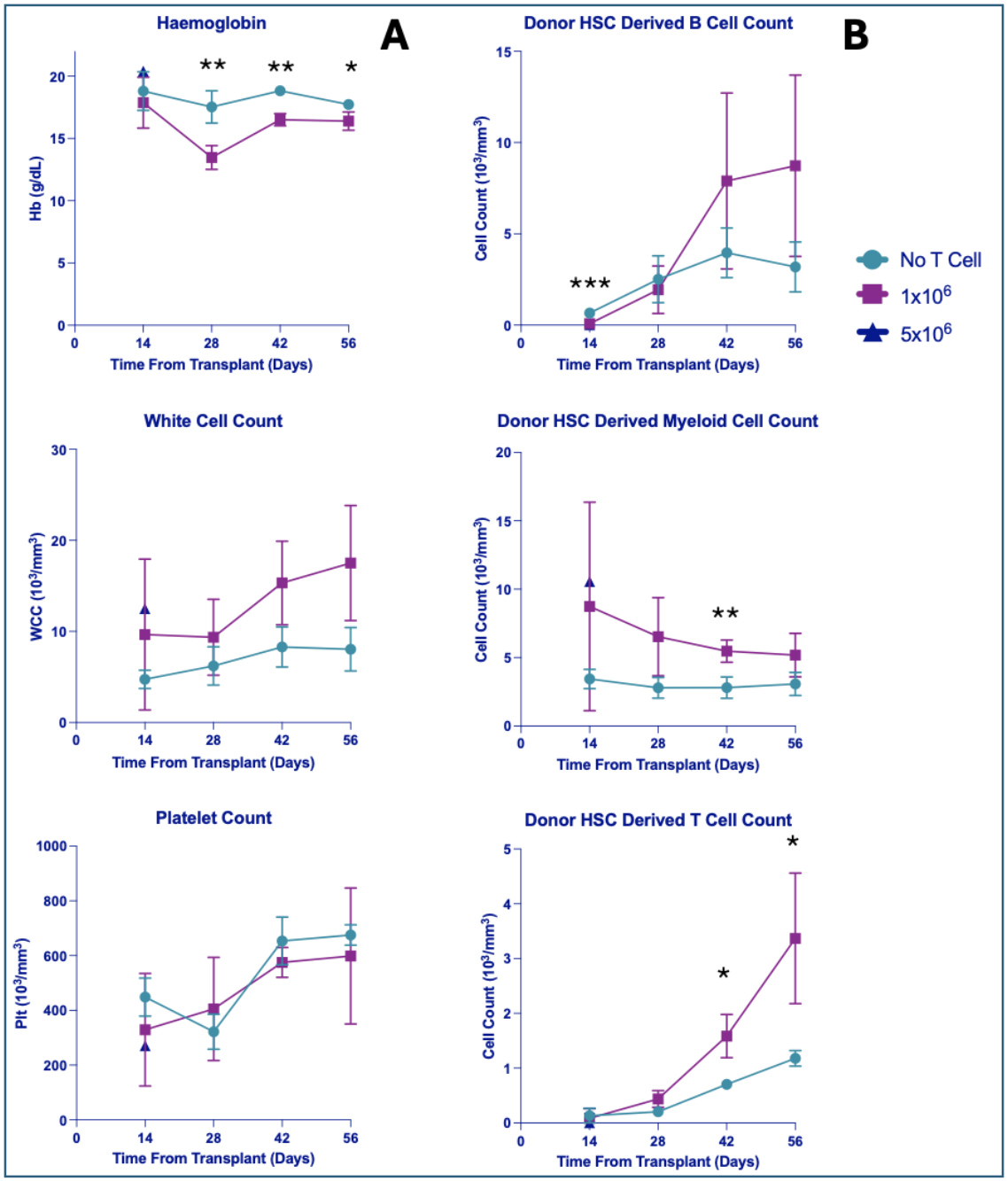



**Figure 3. 12:** Peripheral blood analyses from T cell dose titration #2.

Thirteen animals were randomised to one of three T cell doses, no T cells (green, n=4), 1x10$^6$ T cells (purple, n=6) and 5x10$^6$ T cells (blue, n=3). All surviving mice are included at each timepoint. Three mice in the no T cell cohort and four mice in the 1x10$^6$ T cell cohort survived to the D56 endpoint. **A** CBCs over time by cohort. **B** Donor HSC-derived peripheral B cell, myeloid cell and T cell counts over time by cohort. Data are the mean +/- SD. *P* values calculated using student t-tests with no correction for multiple comparison. * $P$<0.05, ** $P$ <0.01, *** $P$<0.01.

As both anaemia and weight loss in the GVHD cohort appeared to decline following D28, an analysis was performed to determine if graft T cells persisted in the GVHD cohort over the duration of the experiment (Figure 3.13). Residual recipient T cell chimerism in this cohort was <1% at the D14 timepoint, and undetectable at later timepoints. Peripheral blood graft T cells steadily declined over the duration of the experiment, from a mean (+/- SD) of 0.62 (+/- 0.48) $10^3/mm^3$ at D14 to 0.21 (+/- 0.046) $10^3/mm^3$ at D56. By D28 most peripheral blood T cells in the GVHD cohort were donor HSC-derived T cells, rather than persistent graft T cells.

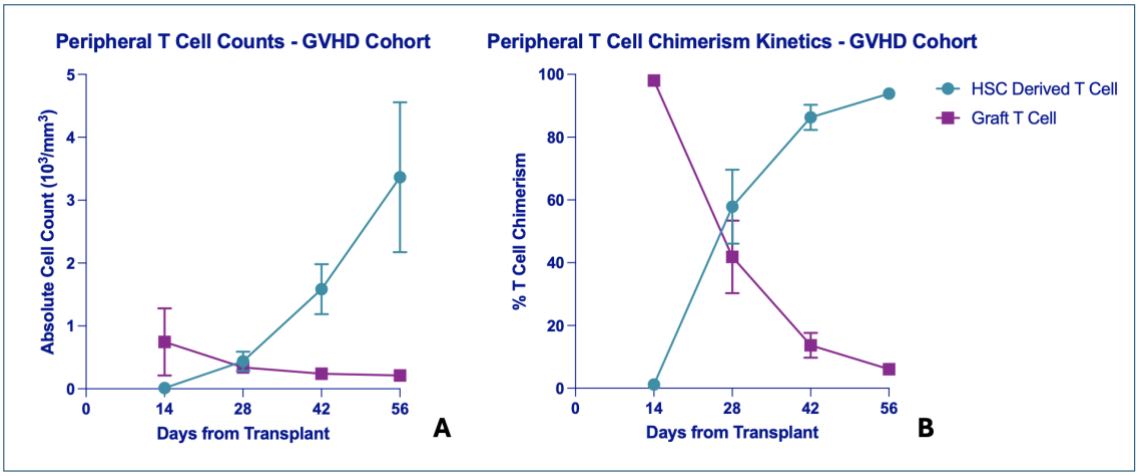



**Figure 3. 13:** Peripheral blood T cell kinetics in mice randomised to the GVHD cohort.

Six mice were randomised to receive $1x10^6$ graft T cells (CD45.1/CD45.2) in addition to $0.5x10^6$ c-Kit$^+$ cells (CD45.1) at time of transplantation, with four surviving until D56. Contributions to peripheral T cell counts by graft T cells and HSC-derived T cells in this cohort are presented over time. **A** Absolute peripheral T cell counts by T cell source over time. **B** Relative contributions of T cell sources to total peripheral T cell chimerism over time. Data are the mean +/- SD.

Three animals in the no GVHD and four animals in the GVHD cohort survived to the scheduled D56 endpoint and were included in bone marrow haematopoietic and stromal analyses. To facilitate like-with-like comparison, bone marrow haematopoietic parameters were assessed in the CD45.1$^+$ population derived from

donor HSCs, though residual recipient haematopoiesis was negligible in all animals at D56 in this experiment. Sca-1 and CD86 are both markers used to distinguish HSC/MPP populations from maturing haematopoiesis however Sca-1 is also expressed by lineage committed progenitors in the setting of inflammation. A relative increase in Sca-1$^+$ cells compared with CD86$^+$ cells is a marker of the frequency with which lineage committed progenitors are misclassified as HSC/MPP populations due to use of a Sca-1 gating backbone in the setting of inflammation (138). The ratio of the populations defined as lineage marker negative (lin$^-$), Sca-1$^+$/c-Kit$^+$ (LSK) and lin$^-$ CD86$^+$/c-Kit$^+$ (L86K) were calculated. The mean (+/- SD) ratio of LSK/L86K was 0.39 (+/- 0.11) and 0.25 (+/- 0.02) in the GVHD and no GVHD cohorts respectively ($P$=0.07). While not reaching the threshold of statistical significance, there is a trend towards an increase in the LSK/L86K ratio in the GVHD cohort. This suggests that misidentification of a lineage committed progenitor as a HSC or MPP due to the impact of inflammation on Sca-1 expression was more likely to occur in the GVHD cohort and could represent a confounder in the interpretation of experimental data using a Sca-1 gating backbone.

It has been demonstrated that in the setting of inflammation, long-term repopulating potential is largely restricted to the subpopulation of immunophenotypic LT-HSCs expressing CD201(33). While no difference in the frequency of the broader LT-HSC population was observed, using Sca-1 gating a trend towards a reduction in CD201$^+$ LT-HSCs was observed in the GVHD cohort ($P$=0.15). This trend was less apparent using a CD86 gating backbone ($P$=0.4). In the MPP compartment, Sca-1 gating demonstrated an increase in most MPP populations in the GVHD cohort, in particular the myeloid biased MPP2 and MPP3

subpopulations. These differences were below the threshold of statistical significance. These differences were not observed in MPPs defined by the inflammation-robust marker CD86. This suggests that any apparent differences in the frequency of MPPs due to GVHD in this model system may reflect an analytical artifact rather than a true change in population architecture. Among lineage committed progenitors, no differences between cohorts were seen in the frequency of any individual population. The ratio of combined myeloid progenitors including common myeloid progenitors (CMPs), GMPs and megakaryocyte erythroid progenitors (MEPs) to common lymphoid progenitors (CLPs) was unchanged between cohorts using a Sca-1 gating backbone. Using a CD86 gating backbone, this ratio was 29.0 (+/- 7.2) vs 19.8 (+/- 3.2) in the GVHD and no GVHD cohorts respectively ($P$ = 0.08). The haematopoietic endpoint of this experiment is summarised in Figure 3.14.

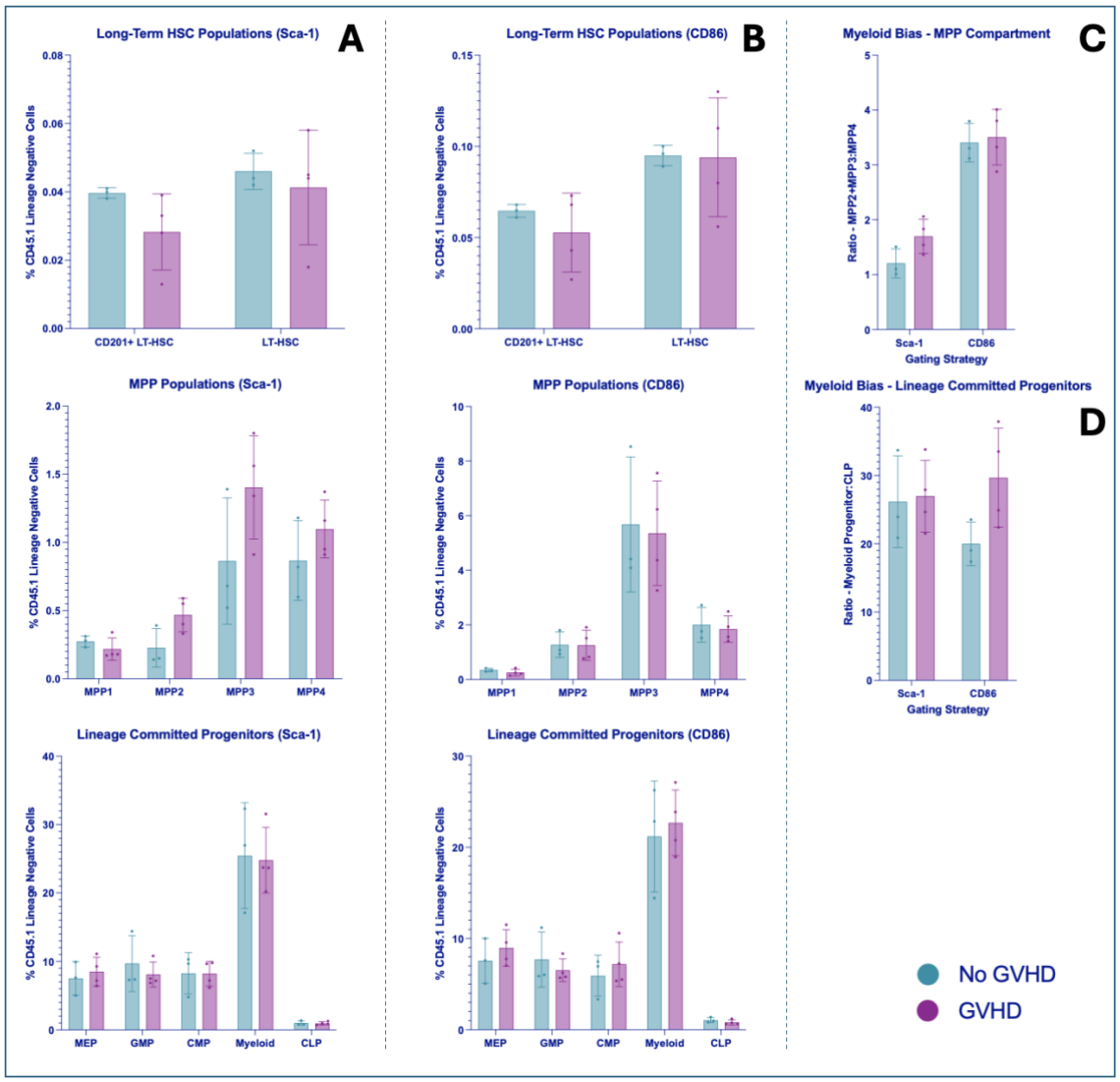



**Figure 3. 14:** Bone marrow haematopoietic populations between GVHD and no GVHD cohorts.

Bone marrow haematopoietic populations were defined by flow cytometry at D56 following transplantation. Three mice are included in the no GVHD cohort (green) and four mice in the GVHD cohort (purple). Frequencies of LT-HSCs, MPPs and lineage committed progenitors are shown by cohort, defined either by Sca-1 **A** or the inflammation-robust marker CD86 **B**. A myeloid biased lineage output is a hallmark of haematopoiesis in the setting of inflammation. Myeloid bias in the MPP compartment is explored by calculating the ratio of myeloid biased MPP2/3 populations to lymphoid biased MPP4s **C**. The ratio of myeloid lineage committed progenitors to common lymphoid progenitors is shown in **D**. Data are the mean +/- SD.

Stromal population architecture appeared to be impacted by GVHD (Figure 3.15). Stromal populations were quantified by flow cytometry, with representative gating shown in Figure 3.16. The frequencies of LepR$^{+}$ MSCs, arteriolar endothelial cells and sinusoidal endothelial cells all trended higher in the setting of GVHD relative to

the no GVHD cohort, though these differences were below the threshold of statistical significance. The mean (+/- SD) percentage of non-haematopoietic cells represented by each of these respective populations were 22.2% (+/- 14.8) vs 11.2% (+/- 3.8) (P=0.27), 2.1% (+/- 1.5) vs 0.7% (+/- 0.3) (*P* = 0.18), and 7.3% (+/- 3.3) vs 3.2% (+/- 0.9) (P=0.1). This trend was also observed in the absolute quantifications of each of these populations but was less apparent than when evaluated by frequency. This raises the possibility of a reduction in the frequency of a population not positively identified by the stromal endpoint panel in the setting of GVHD. Niche inflammation has been shown to induce a pro-inflammatory phenotype in LepR$^+$ MSCs, characterised by upregulation of surface Sca-1 (5). A trend for a higher proportion of LepR$^+$ MSCs expressing Sca-1 was observed in the GVHD cohort, with a mean percentage (+/-SD) of LepR$^+$ MSCs positive for Sca-1 of 30.4% (+/- 14.5) vs 11.1% (+/- 2.8) in the GVHD vs no GVHD cohorts respectively (*P* = 0.07).

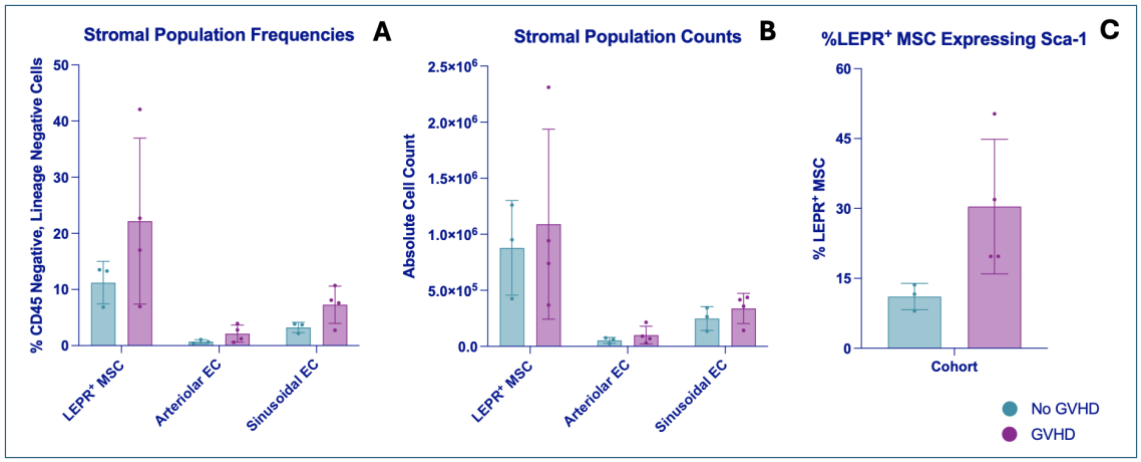



**Figure 3. 15:** Stromal population architecture between GVHD and no GVHD cohorts.

Bone marrow stromal populations were identified by flow cytometry following enzymatic digestion at D56 post transplantation. Population architecture by cohort is presented in terms of percentage of non-haematopoietic cells **A** and absolute cell counts **B**. Sca-1 expression identifies a population of pro-inflammatory LepR$^+$ MSCs. The percentages of LepR$^+$ MSCs expressing Sca-1 are shown by cohort **C**. Three mice are included in the no GVHD cohort (green) and four mice in the GVHD cohort (purple). Data are the mean +/- SD.

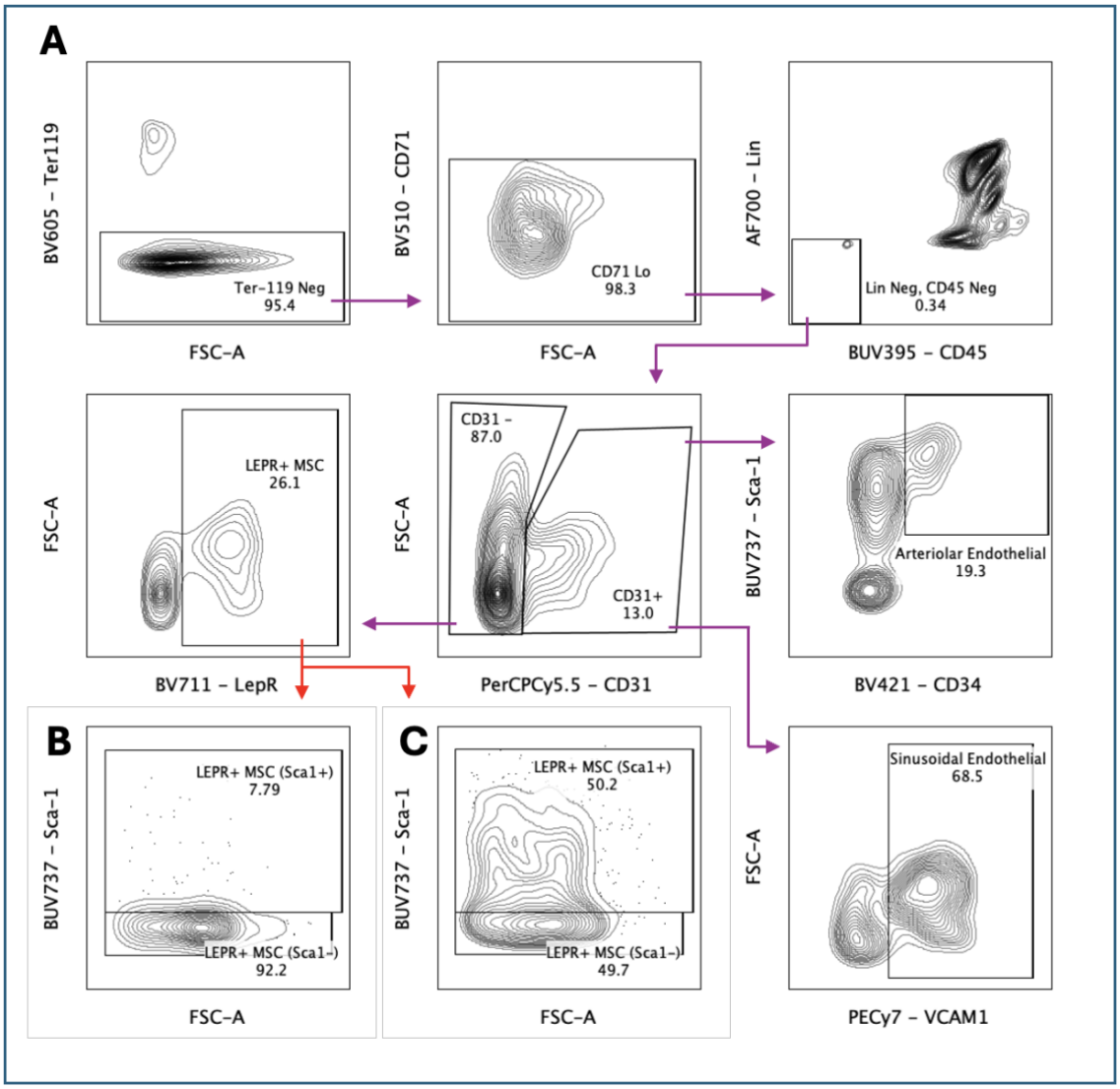



**Figure 3. 16:** Representative gating to define bone marrow stromal populations.

**A** Representative gating to define LepR$^+$ MSCs, arteriolar endothelial cells and sinusoidal endothelial cells from digested bone marrow stroma. Gating shown is following debris and doublet exclusion. **B,C** Percentage of LepR$^+$ MSCs expressing Sca-1, in representative mice from the no GVHD and GVHD cohorts respectively.

Bone marrow T cell results are summarised in Figure 3.17. As was observed in peripheral blood, bone marrow T cells were higher in the GVHD cohort relative to the non-GVHD cohort, with absolute CD3$^+$ counts of 4.5 (+/- 0.6) x$10^5$ and 2.4 (+/- 0.5) x $10^5$ respectively ($P$=0.005). HSC donor-derived T cell chimerism was similar between cohorts, at 58.3% (+/- 18.2) and 48.6% (+/- 8.3) in the GVHD and non-GVHD cohorts respectively. No residual recipient T cells were observed in the GVHD

cohort, and (as expected) no graft T cells were observed in the no GVHD cohort. Donor HSC-derived T cells reconstituted naïve, central memory and effector T cell populations in both cohorts. The majority of residual recipient T cells in the no GVHD cohort and persistent graft T cells in the GVHD cohort were skewed towards an effector/effector memory cell state.

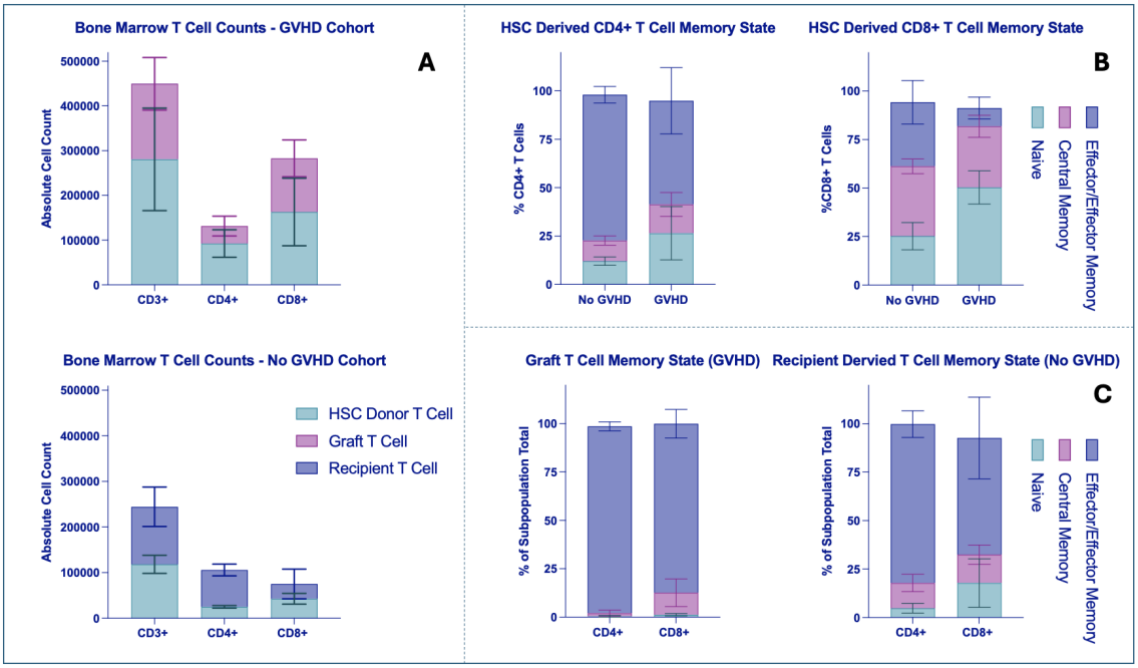



**Figure 3. 17:** Bone marrow T cell analyses between GVHD and no GVHD cohorts.

Bone marrow T cell populations were analysed by flow cytometry at D56 following transplantation. (A) Absolute T cell counts are increased in the GVHD cohort relative to the no GVHD cohort. (B) The cell state of donor HSC-derived $CD4^+$ and $CD8^+$ T cells are shown by cohort. Naïve, central memory and effector cells are observed in both cohorts. (C) No residual donor T cells were observed at D56 in the GVHD cohort. The cell states of persistent graft T cells, and residual donor T cells are shown for the GVHD (n=4) and no GVHD (n=3) cohorts respectively. Data are the mean +/- SD.

## 3.2 Discussion and Summary

This project aimed to develop a model characterised by peripheral cytopenias driven by GVHD. This attempt has not yet been successful, but the findings of these

preliminary studies can be used to inform the next steps towards model optimisation. It is important to note that the data presented represents a series of pilot studies and that caution should be taken in the over interpretation of these results prior to an appropriately powered validation experiment being performed to demonstrate reproducibility. Given our desired phenotype was not observed in these pilot experiments, further model optimisation is planned prior to committing resources to a validation experiment.

Several simple conclusions regarding this model system can be drawn from these results. The radiation dose titration experiment was informative, and 9Gy delivered in two split fractions is effective in our hands for conditioning 129 recipients for transplantation. Across four independent experiments using this radiation dose, 34 animals received a 9Gy dose of radiation, with all animals achieving adequate donor chimerism, and only one animal reaching a humane endpoint secondary to conditioning stress. A $5x10^6$ dose of graft T cells is too high to use in this model system. All animals randomised to this T cell dose demonstrated rapid weight loss and died within 20 days of transplantation. A key point of difference between the design of our model and prior studies analysing haematopoiesis in murine models of GVHD is that those prior studies have employed models characterised by severe systemic illness (101, 102). This limits the ability to attribute changes in the bone marrow niche to the activity of T cells specifically, due to the overlay of critical illness. A $5x10^6$ T cell dose in our model is sufficiently high to result in a severe GVHD phenotype similar to prior studies. It is likely that the $1x10^6$ T cell dose trialled in the second T cell dose titration is appropriate, and that further model

refinement will not be achieved through T cell dose titration alone without other modifications.

Biologically significant variation in GVHD phenotype appears to exist between male and female 129 recipients, and future experiments should be performed in recipients of one sex. Two of three male recipients of $1x10^6$ T cell dose died within 30 days of transplantation, compared with no deaths in the three female recipients in this cohort prior to the prespecified endpoint. The surviving male in this cohort also had clinical evidence of cutaneous GVHD, not observed in any female recipients. This variation is likely driven by host-vs-graft alloimmunity in female but not male recipients, directed at H-Y antigens expressed on male donor T lymphocytes. Alloreactivity from female T lymphocytes against male recipient tissues occurs in both human and murine transplantation, driven by well characterised immunogenic minor histocompatibility antigens expressed on the Y chromosome, known as H-Y antigens (145-147). To account for this most studies in mice using alloreactive T cells use donors and recipients of only one sex, frequently female -> female due to ease of husbandry. During model design, we made the decision to trial the use of recipients of both sexes to minimise wastage of pups from the recipient colony of the unused sex. With this in mind, we restricted donors to male only. This was to ensure the same cellular product could be used in all transplant recipients in each experiment, and to avoid H-Y antigen mediated alloimmunity impacting male recipients of a female cellular product. The assumption was made that the impact of anti-H-Y antigen reactivity by female recipient T cells against incoming graft T cells would be negligible. A possible explanation for the sex difference observed is that this assumption was incorrect,

and that the milder phenotype observed in female recipients is due to the impact of a host-vs-graft effect on incoming graft T cells. While restricting the model to only one sex may mean that sex differences are missed, reactivity to male antigens appears to be an important confounder. The increased variability introduced into this system by this sex variation is likely to impact on model interpretability. Either a male -> male or female -> female transplant system should be employed moving forwards.

The comparison of syngeneically transplanted mice with non-transplanted litter mates demonstrated few changes in peripheral blood or bone marrow populations at D56. The trends observed in this experiment were towards a decrease in LT-HSCs in the syngeneically transplanted cohort relative to non-transplanted littermates, and an increase in the proportion of $LepR^{+}$ MSCs expressing Sca-1, a marker of recent inflammation. The analysis of CBCs over time in non-transplanted 129 mice revealed marked variability in measurements of platelet count. This degree of variability is likely to limit the ability of this experimental system to detect small changes in platelet count.

A number of differences were observed in the second T cell dose titration experiment between the cohort randomised to $1x10^{6}$ cells and the no GVHD control population. Peripheral blood analyses revealed decreased haemoglobin, and a trend towards an increase in peripheral white cell count in the GVHD cohort. At later timepoints, this increase in white cell count was driven by an increase in HSC donor-derived T lymphocytes and myeloid cells, with a less clear difference in peripheral B cells between cohorts.

Bone marrow haematopoietic analyses in this study demonstrated a trend towards a decrease in CD201$^{+}$LT HSCs in the setting of GVHD, a subpopulation which has been previously shown to contain the majority of HSCs capable of long-term repopulation in the setting of inflammation (33). Analysis of other HSC/MPP populations using the inflammation-robust marker CD86 revealed no differences between conditions, however the analysis of MPP populations using Sca-1 was suggestive of an increase in the majority of MPP populations. A likely interpretation of the discrepancy between Sca-1 and CD86 gating strategies is that upregulation of Sca-1 on lineage committed progenitors occurred more frequently in the GVHD cohort, leading to the mischaracterisation of these maturing populations as HSC/MPP subpopulations (138). These finding highlight the value of developing inflammation-robust endpoint panels for this model system.

Changes were observed between GVHD and control cohorts with regards to the cellular architecture of bone marrow stromal populations. The relative frequency of LepR$^{+}$ MSCs, and both sinusoidal and arteriolar endothelial cells as a proportion of non-haematopoietic cells trended higher in the GVHD cohort relative to controls. While this trend was also present in absolute cell counts, it was much less prominent, which raises the possibility that GVHD led to the depletion of a stromal population not positively identified by our analysis panel. Given a loss of osteoblasts has been observed in both prior human and murine studies of bone marrow GVHD, it would be useful to positively identify osteo-lineage cells to explore the hypothesis that loss of this population in part explains our observed phenotype (98, 99, 101). Using a recently published method for defining a broader array of bone marrow stromal populations by flow cytometry, it is likely that exploration of the

impact of T cell mediated inflammation on osteogenic progenitors could achieved by minor modifications to our current endpoint workflows (5, 83).

Recent studies have demonstrated that the expression of Sca-1 by $LepR^+$ MSCs identifies a population which can be induced by inflammatory stimuli, and which produce proinflammatory cytokines capable of modulating the function of local myeloid populations (5, 83). In the second T cell dose titration, a trend was observed towards an increase in the proportion of $LepR^+$ MSCs expressing Sca-1. 28.1% (+/- 14.8%) of $LepR^+$ MSCs in the GVHD cohort expressed Sca-1, compared with only 10.8% (+/- 2.8%) in the control cohort.

Given our phenotype of interest has not yet been observed, further optimisation of this model system will be required. Considering these results within the context of previously published murine models of bone marrow failure and GVHD will inform the next steps that should be taken towards developing a useful model of T cell mediated injury to the haematopoietic niche.

# 4. Contributions to a Human iPSC-Derived Bone Marrow Organoid Model of Stromal Graft-vs-Host Disease

## 4.0 Introduction

While *in vivo* murine models provide critical insights both into haematopoietic niche physiology and T cell function, there are limitations to murine systems for modelling the human diseases contributed to by T cell mediated injury to the bone marrow niche. Different evolutionary pressures shape the adaptive immune systems of long-lived mammals like humans and short-lived animals such as mice. Fundamental differences in lymphocyte biology have been highlighted as underpinning the challenge of translating pre-clinical insights from murine models into the care of patients with GVHD (148, 149). In the context of this project, an additional complexity is that while there is increasing consensus regarding the key stromal populations in the haematopoietic niche in mice, the degree of functional equivalence between murine and human MSC populations remains unclear (2). It is challenging to resolve these potential differences through the analysis of clinical samples, given the complexity, rarity and heterogeneity of relevant patients.

HiPSC-derived organoids represent a novel and attractive system for addressing these limitations, as they can form the foundation of tractable models using human tissue. In the setting of a complex systemic disease like GVHD, the ability to study an organ or tissue in a reductionist context abstracted from the broader animal can also be useful. *Ex vivo* organoids have recently provided important insights into the pathophysiology of gut and bile duct GVHD (150, 151).

Our colleagues in the Psaila group have recently developed a novel model of hiPSC-derived bone marrow organoids. A yet unpublished collaboration between the Psaila and Chakraverty groups led by Chiara Cox (MSc student – Chakraverty Group), Zoe Wong (DPhil student – Psaila group) and Andrew McIntyre (postdoctoral fellow, Chakraverty group), demonstrated evidence of alloreactivity in primary donor T cells co-cultured with bone marrow organoids. Organoids provided by the Psaila group were engrafted with primary donor T cells and co-cultured for 7 days, prior to digestion and analysis by flow cytometry. Compared with T cells cultured in organoid condition-media, organoid engrafted T cells showed enhanced proliferation and a bias towards an effector cell state. These changes are consistent with an alloreactive response against organoid populations by primary donor T cells. It is likely that a major MHC mismatch would be present between the vast majority of randomly selected primary T cell donors and the donor from whom a commercially available hiPSC line was developed. It has been long recognised that 1-10% of peripheral blood T cells will react to non-self MHC molecules in the setting of a major MHC mismatch (152).

The Chakraverty group aims to establish a model of T cell mediated injury to haematopoietic niche populations using hiPSC-derived organoids, based on this alloimmune response from primary donor T cells (Figure 4.1). This model will involve engrafting organoids with primary donor T cells and measuring the impact this has on bone marrow stromal populations using flow cytometry, scRNAseq and florescence microscopy. By employing a gene-editing approach to manipulate the T cell and hiPSCs in the system, this model will represent a sophisticated but tractable *in vitro* system for mechanistically unpicking the tissue targets and T cell

effector machinery which underpin T cell mediated injury to the human bone marrow niche. This will complement the murine model developed in Chapter 3 in three key domains. Firstly, it is likely to represent a significantly lower cost and higher throughput system than the murine model. Secondly, it facilitates mechanistic experimentation using human tissue, facilitating bidirectional validation of insights from *in vivo* murine and *in vitro* human model systems. Finally, organoids are inherently reductionist systems and will facilitate exploration of the impact of alloimmune T cells on bone marrow niche populations without the overlay of injury to other GVHD target tissues and subsequent systemic inflammation.

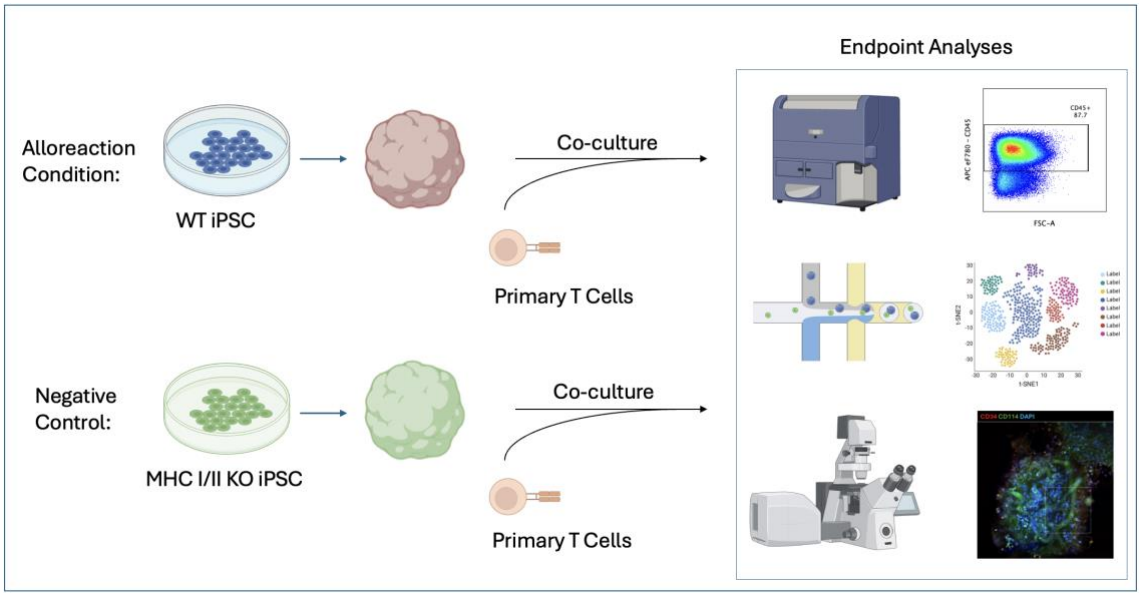



**Figure 4. 1:** Schematic of a bone marrow organoid T cell injury model.

Injury to bone marrow stromal populations by alloreactive T cells will be modelled by co-culturing hiPSC-derived bone marrow organoids with primary donor T cells. An MHC class I/II K/O hiPSC line will be used to generate hypoimmune organoids as a negative control. Flow cytometry, fluorescence microscopy and scRNAseq will be employed as complimentary endpoint technologies to characterise T cell mediated injury to the bone marrow niche *in vitro* both in a spatial context, and at single cell resolution. Figure created using BioRender.com. Confocal image of a bone marrow organoid was generated by Gareth Purvis in the Channon laboratory and is reproduced with permission.

While establishing this model system is beyond the scope of the currently presented project, two foundational objectives towards this goal were attempted:

1. Establish the techniques for hiPSC maintenance and bone marrow organoid differentiation within the laboratory.
2. Develop organoids from MHC class I/II dual K/O hiPSC lines for use as a negative control and determine if they share a similar cellular architecture to wild-type organoids.

Another finding of the preliminary collaboration between the Chakraverty and Psaila groups was that T cells cultured in organoid condition media showed changes compared with T cells cultured in media alone. $CD4^+$ T cells showed increased expression of the activation marker CD25, and increased CD28 co-expression was observed in all T cells between these conditions. It is likely that the cytokine and metabolic environment in the organoid culture system has an impact on T cell phenotype, and so consideration needs to be given to the appropriate controls to facilitate attributing observed changes in stromal populations to interactions between these populations and T cells. In experimental systems leveraging alloreactivity to model T cell responses, a syngeneic condition is typically employed as a key negative control. For our proposed bone marrow organoid model, a syngeneic control is unlikely to be available. Generating hiPSCs from a donor available for repeat donation of primary T cells has ethical and pragmatic limitations and readily accessing T cells MHC matched to a commercially available hiPSC line is also likely to be non-feasible. While protocols exist for differentiating T cells from hiPSCs, this technology is currently insufficiently mature to generate T cells with the appropriate education to be fit for purpose in this model system (153). Protocols for

the generation of hypoimmune hiPSCs have recently been published, with validated guides for CRISPR-Cas9 mediated deletion of *β2m* and *Ciita* to remove MHC class I and II respectively (134). Use of hypoimmune organoids as a negative control will allow the isolation of sequalae of cognate interactions between donor T cells and wild-type organoids. While *in vivo* HSC function has been shown to be impacted by MHC mediated T cell interactions, we hypothesise that MHC K/O organoids will be similar to wild type organoids prior to perturbation, due to the lack of NK cells and mature T cells in the organoid culture system (154).

This chapter will detail the successful establishment of a protocol for bone marrow organoid differentiation in our laboratory, and the attempts to generate an MHC K/O hiPSC line in collaboration with the WIMM transgenic core facility.

## 4.1 Results

### 4.1.1 Organoid differentiation technique replication

Organoids were differentiated as described in Chapter 2. Figure 4.2 demonstrates the progressive development of the organoids via serial imaging of representative samples.

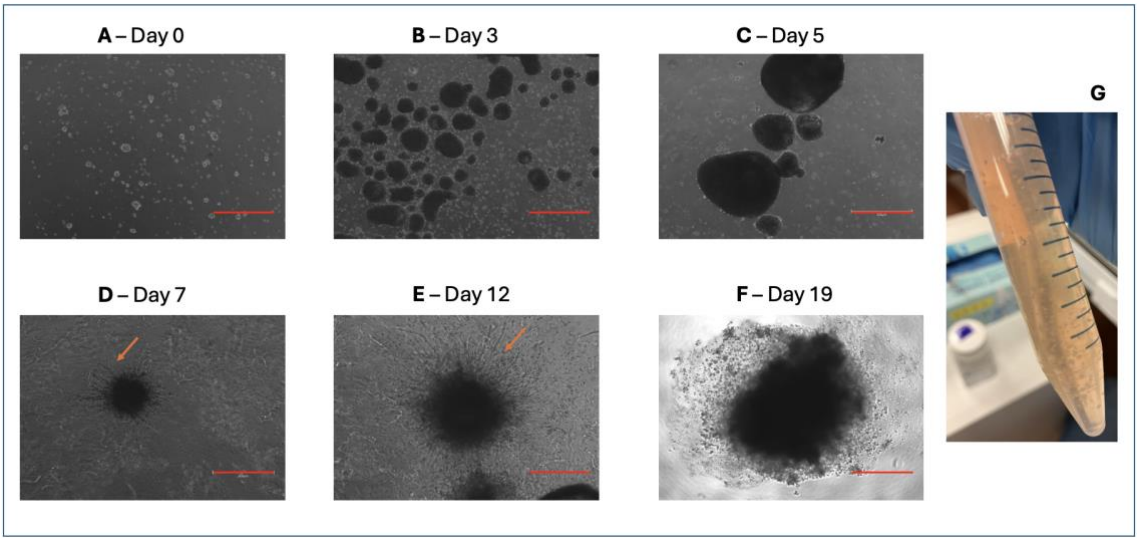



**Figure 4. 2:** Sequential images of developing organoids.

**A-F**: Representative images of developing bone marrow organoids, taken with an EVOS5000 microscope. Red scale bars represent 600μm. **A** – HiPSCs forming discrete clusters after plating in ultra-low attachment plates. **B** – Following mesodermal commitment, discrete aggregates of ~250μm were observed. **C** – Immediately prior to hydrogel embedding, spheroids with defined edges of 400-600μm diameter had developed. **D** – Early vascular sprouts (orange arrow) were observed on D7 following hydrogel embedding. **E** – Immediately prior to hydrogel extraction on D12, organoids had developed dense vascular networks (orange arrow) with associated haematopoietic cells. **F** – A bright field image of a discrete organoid in isolation in the base of a 96-well plate. Haematopoietic cells surround the organoid. **G** – Following hydrogel extraction on D12, organoids are discrete structures clearly visible to the naked eye.

To evaluate whether this represented a successful replication of the organoid differentiation protocol, D21 organoids underwent digestion and analysis by flow cytometry to characterise the cellular architecture of haematopoietic and stromal

populations within the organoids. This was compared with results obtained from a prior D21 analysis of 'exemplar' organoids differentiated from the same hiPSC line by the Psaila group who had initially developed the organoid differentiation protocol (Figure 4.3). All three technical replicates from this differentiation were similar in their haematopoietic and stromal composition to exemplar organoids differentiated by the Psaila group. Representative gating for organoid analysis is shown in Figure 4.4.

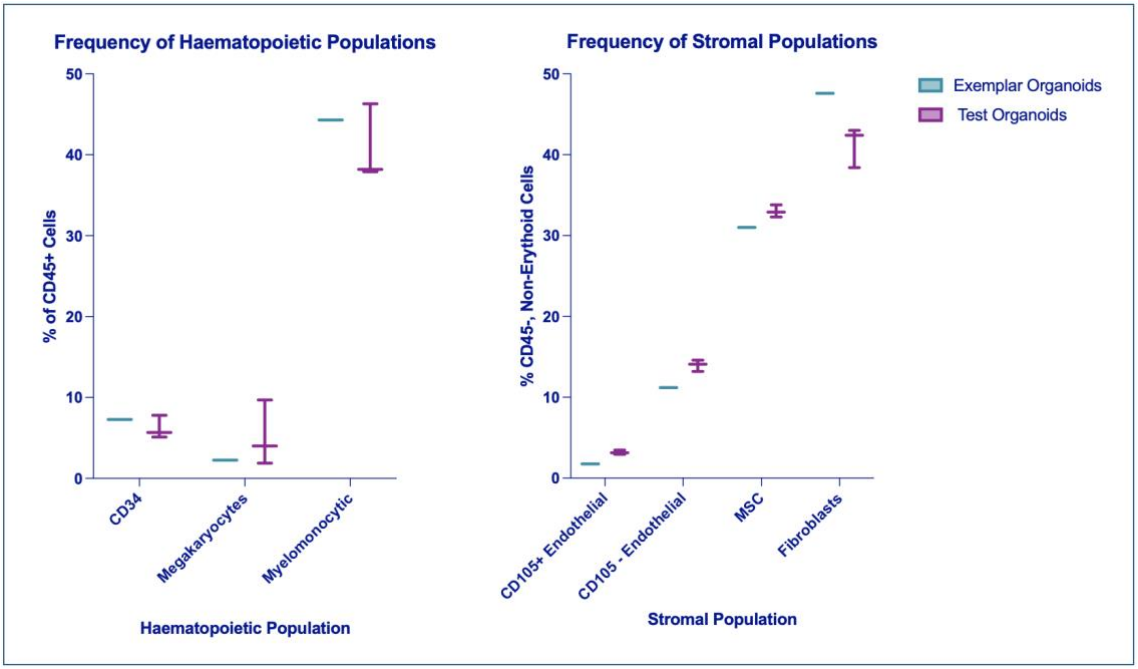



**Figure 4. 3:** Cellular architecture of organoids by flow cytometry.

On D21 organoids were digested and analysed by flow cytometry. Twelve organoids were pooled for each technical replicate of the analysis. Analyses were compared to exemplar data provided by collaborators in the Psaila group. Exemplar organoid data is shown in green, and data from this differentiation is shown in purple.

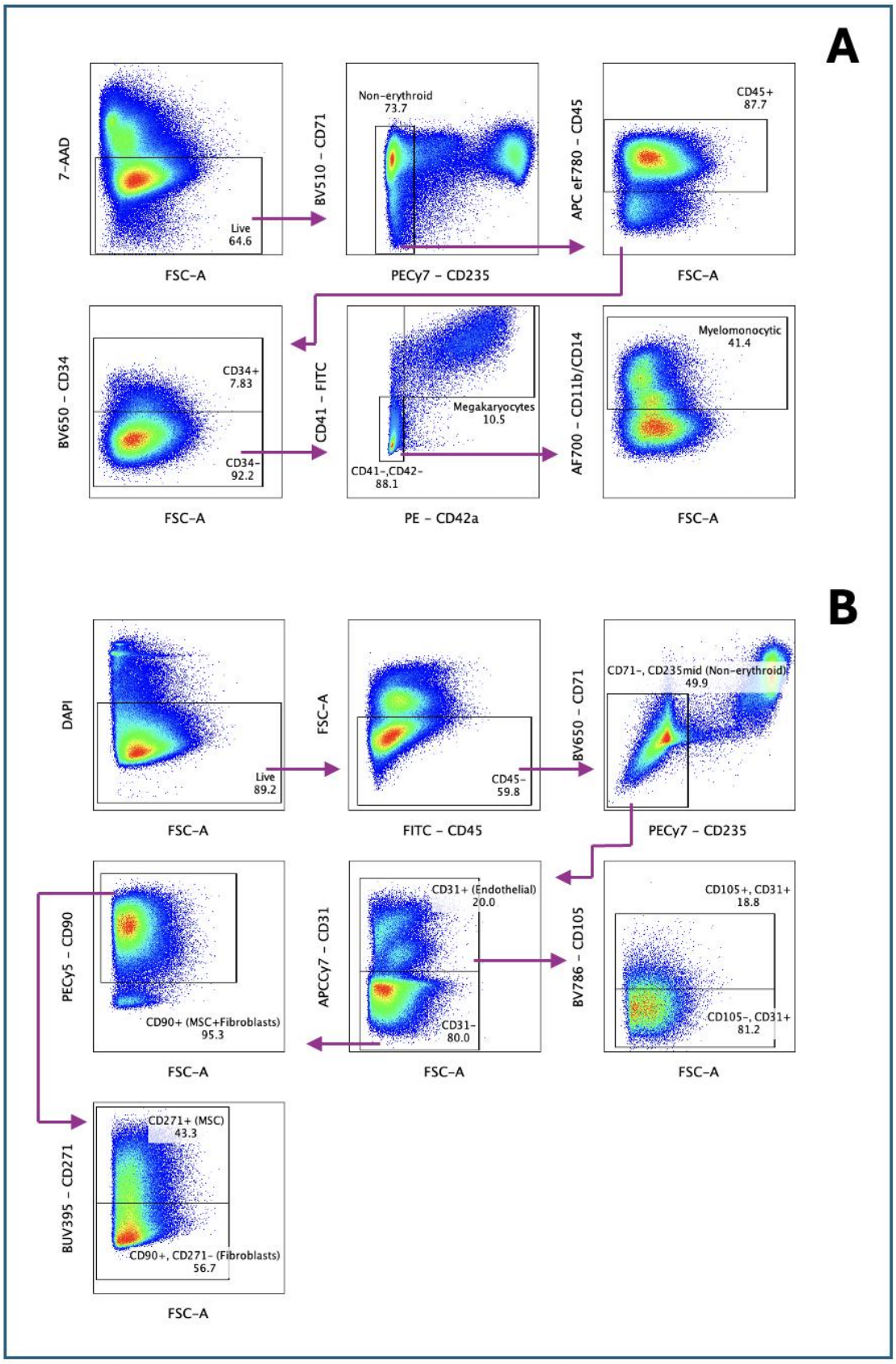



**Figure 4. 4:** Representative gating for hiPSC-derived bone marrow organoids.

Gating performed following doublet and debris exclusion. Organoids were digested and stained for flow cytometry analysis on D21. **A** – Haematopoietic populations from hiPSC-derived bone marrow organoids. **B** – Stromal populations.

### 4.1.2 MHC class I/II K/O hiPSC editing

The results presented in the following section were generated by the WIMM transgenic core facility, who led the collaborative effort to generate a dual MHC class I/II biallelic K/O hiPSC line using previously published CRISPR-Cas9 guides (134). These results are reproduced here with permission. Following hiPSC editing as detailed in Chapter 2, Sanger sequencing was performed on bulk hiPSCs, and editing efficiency was estimated using the Synthego ICE bioinformatic platform. Editing efficiencies of 30% and 5-10% were estimated from the bulk cell pool for *Ciita* and *β2m* respectively.

100 colonies were generated from single cells within this cell pool and screened for the presence of a successful dual K/O by Sanger sequencing. No dual edited colonies were identified, and no colonies with successful *β2m* editing were identified. Four colonies with monoallelic K/O of *Ciita* were identified. No biallelic *Ciita* colonies were present.

## 4.2 Discussion

HiPSC-derived organoids represent a novel platform for generating a tractable model of interactions between T cells and human bone marrow stromal populations. In this project I have established the workflows for the differentiation of bone marrow organoids in our laboratory. Analysis of the cellular architecture of organoids generated in this differentiation were similar to organoids differentiated from the same hiPSC line by the laboratory where the technique was developed. The

next step in developing an experimental system to model our pathophysiology of interest is establishing an appropriate negative control.

The attempt to generate a dual MHC class I/II K/O hiPSC line has been unsuccessful to date, despite the use of guides previously optimised for this purpose (134). The analysis of bulk hiPSCs post editing suggested that successful biallelic editing had been achieved for *Ciita* in 30% of cells, and *β2m* for 5-10% of cells. Despite this, none of the 100 colonies derived from this bulk population had evidence of biallelic editing. This suggests that while editing has been achieved, there is a selection pressure against successfully establishing colonies from hiPSC containing biallelic edits. This may be attributable to a failure of homology directed repair (HDR), the process by which a double-strand break is repaired precisely using a sister chromatid as a template (155). HDR has been shown to be inefficient in CRISPR edited hiPSCs compared with immortalised cell lines (156). A number of methods have been proposed in the literature to overcome this limitation, including techniques to optimise high-throughput screening of large numbers of clones to identify rare successful edits (157). The number of clones screened prior to identifying a successful edit in the paper from which guides were sourced was not reported, and it may be that the 100 clones screened in our editing attempt was too few to facilitate successful identification of a rare event.

Prior reports have identified that a 24h period of incubation at 32°C can improve the efficiency of hiPSC editing by increasing the rate of successful HDR, without compromising pluripotency (158). The WIMM transgenic core have discussed the optimisation of this editing with colleagues within the National Institutes of Health (NIH) iPSC core facility and have received advice that using a

multiplexed editing approach with 5 or more redundant guides for each target locus may improve editing efficiency. In addition, the NIH iPSC core have adopted the use of laminin 521 rather than Geltrex as a basement membrane for the culture of hiPSCs post editing, due to experience with both biomatrices leading to a perception that laminin 521 reduces the drop-out of clones due to stress following editing. A future editing attempt is planned, incorporating these new insights. Cells will be edited using 5 guides per locus, and colonies will be cultured on laminin 521 at 32°C for the 24 hours following editing. A larger number of colonies will also be screened for successful editing.

Given the challenges encountered in the generation of this K/O hiPSC line, alternative approaches to generating a negative control for this experimental system require consideration. Commercial MHC I/II K/O hiPSC lines are now available, though currently these suppliers do not market the WT hiPSCs from which these lines were derived. Without access to paired WT hiPSCs, these are unlikely to be an appropriate solution, as variability is observed between organoids derived from different hiPSC lines (130). An editing approach could be taken to the T cells rather than the hiPSCs in our planned model. Comparing T cell receptor (TCR) K/O T cells to sham-edited T cells represents an alternative strategy that would allow conclusions to be drawn regarding the impact on stromal populations of T cells due to cognate interactions via the TCR.

# 5 Discussion

## 5.0 Findings and Limitations

### 5.0.1 Murine Model – Limitations due to underpowered experiments

The experiments performed in the development of this mouse model were conceived as pilot studies and not powered to detect statistically significant differences between treatment groups. While pilot studies have a role in the early exploration of model systems under development, the reliance of this work on unpowered experiments impacts the interpretability of results. Small but biologically relevant effects are likely to be masked due to the small number of mice included in each experimental condition. Furthermore, the iterative refinement of a model system based on underpowered pilot experiments definitionally involves the interpretation of results with a high risk of type 1 error. This approach risks compounding errors in early results by the incorporation of these findings into the design of subsequent experiments. The results presented here should be interpreted with appropriate caution until they are found to be reproducible in an appropriately powered validation study.

The small scale of the experiments performed reflects pragmatic limitations in the availability of skilled personal to conduct this work. This work was led by an early career researcher without prior laboratory experience, largely supported by colleagues without prior exposure to animal work. Experiments were designed to be as large in scale as possible, while still being able to be safely and successfully executed considering these limitations. The increasing skill of the laboratory in the

execution of these experiments acquired over the course of this project and refinement of labour-intensive workflows will help facilitate larger-scale experiments moving forward. Power studies should be performed prior to embarking on large-scale experiments in this project. It will be important to ensure that the objectives of future experiments are aligned with available resources.

### 5.0.2 Murine Model – Peripheral blood phenotype

This project set out to use GVHD to develop a murine model of T cell mediated injury to the bone marrow niche, characterised by peripheral cytopenias. Prior studies of the impact of GVHD on haematopoiesis in mouse models observed bone marrow failure, with peripheral pancytopenia and the depletion of bone marrow haematopoietic populations (101, 102). Where these studies employed a severe GVHD model associated with critical systemic illness and short survival, we took steps to design a model characterised by milder GVHD, and used a later endpoint. These differences in experimental design may inform why pancytopenia was not observed in our model system.

In the second T cell dose titration, a trend towards anaemia was observed in the GVHD cohort relative to the non-GVHD control cohort. Anaemia is frequently observed in patients suffering from chronic inflammatory conditions, which is referred to as the anaemia of chronic disease (ACD) or anaemia of inflammation (159). Rather than a manifestation of HSC dysfunction or exhaustion as occur in bone marrow failure syndromes, ACD is increasingly understood as a response of lineage committed erythroid progenitors to inflammatory stress. The function of erythroid progenitors is controlled by signalling via receptors for inflammatory

cytokines including IL-6, IFN-γ and IL-33, all of which act directly on this population to inhibit erythropoiesis (160-162).

Prior studies in mice have demonstrated that megakaryopoiesis in particular is disrupted by GVHD (102). aGVHD is also a risk factor for persistent thrombocytopenia and reduced megakaryopoiesis in patients post allograft (93). In our model, no difference in platelet count was observed between GVHD and non-GVHD cohorts, which in part may reflect the high degree of variability in the measurements of platelet count in this study. Serial measurements of platelet count taken from a cohort of non-transplanted 129 mice demonstrated marked differences even between samples collected from the same animals. With this degree of background variability, it is likely that unless a large effect was present it would not be detected given the small cohort sizes used in these pilot experiments. This variability in platelet count may reflect genuine biological variation, or technical artifact from sample collection and handling. Diurnal variation has been observed in mouse platelet counts, with up to 50% differences observed between peak platelet counts measured during rest periods, and platelet nadirs observed during nocturnal active periods (163). This was not controlled for in these experiments, and most sampling was performed in the hours immediately following the night to day transition when diurnal changes are likely to be most impactful on data reproducibility. CBCs were collected by tail vein incision, a technique which some but not all animal technicians in our institution perform following prewarming to facilitate peripheral vasodilation and ease of collection. There is evidence that platelet counts collected from cold tails consistently measure higher than those collected from pre-warmed tails, and that both of these techniques consistently

measure higher and with less reproducibility than is observed using cardiac puncture under terminal anaesthesia (164). It is likely that variability in platelet count measurements could be reduced by standardisation of the timing of sampling, and consistent sampling by the same technician. Quantification of bone marrow megakaryocytes at experimental endpoint may also be informative, given peripheral platelet counts in the setting of T cell mediated inflammation may reflect both changes in peripheral turnover and platelet production.

A trend towards an increase in white cell count was observed in the GVHD cohort of the second T cell titration experiment, due to an increase both in peripheral myeloid and T cell counts. This contrasts with prior studies in murine models of GVHD, which demonstrated a decrease in peripheral white cell count in the context of bone marrow failure (101, 102). GVHD is likely to have resulted in inflammation in our experiment, and the increase in myeloid cells in this cohort may reflect emergency myelopoiesis occurring in the setting of this inflammation (4).

In our experiments a difference in B cell counts between GVHD and control cohorts was observed only at the early D14 timepoint, with no clear trend observed at later timepoints. This contrasts with existing evidence that B cell reconstitution is impacted by GVHD. Decreased and abnormal B cell lymphopoiesis is a consistent finding in murine models of both acute and chronic GVHD (101, 165). This has also been demonstrated in human studies. A recent study profiling B cell populations in patients following alloSCT by mass cytometry demonstrated that on unbiased dimensionality reduction patient samples segregated into two distinct populations, with a past history of GVHD discriminating between these groups (166). The group enriched for patients with GVHD was characterised by a global decrease in bone

marrow B cells, with a particular depletion of early B cell precursors. A study of B cell reconstitution following allogeneic transplantation identified acute GVHD as a key risk factor for delayed B cell recovery (167). This study of B cell reconstitution kinetics also demonstrated an association between delayed B cell recovery and bone marrow infiltration by T cells, with an associated decrease in bone marrow osteoblasts. Similar results were observed in a study prospectively following a cohort of 51 alloSCT patients to explore the relationship between GVHD and peripheral blood cytopenias, which independently demonstrated a link between chronic GVHD, peripheral blood cytopenias including B cell lymphopenia and a decrease in bone marrow osteoblasts (98). Osteoblasts have been previously highlighted as a source of cytokines supportive of B cell development, and osteoblast depletion by alloreactive T cells has been proposed as a mechanism to explain the link between B cell lymphopenia and GVHD (168). B cell development has also been shown to be impaired in patients with HLH, another syndrome characterised by T cell mediated inflammation (169). Given that an impairment of B cell lymphopoiesis is a reproducible feature observed across the pathophysiological contexts we are attempting to model, its absence from our pilot experiments beyond the D14 timepoint should prompt further model optimisation.

In the second T cell dose titration GVHD was associated with an increase in T cell lymphopoiesis driven not by persistence or expansion of graft T cells, but by an increase in HSC-derived T cell lymphopoiesis. This has not been observed in prior mouse models of GVHD, which demonstrated delayed peripheral blood and splenic T cell reconstitution (101, 102). The difference between our observations and prior murine studies may reflect the shorter period of follow-up facilitated by those model

systems, as the increase in peripheral T cells in the GVHD cohort of the T cell dose titration did not become apparent until the week six timepoint. An association between GVHD and delayed T cell reconstitution has been observed in prior clinical studies. An analysis of single-joint T cell receptor excision circles in patients post alloSCT demonstrated that aGVHD was associated with a delay in the recovery of thymic output post-transplant, with an associated delay in both recovery of $CD4^+$ lymphocyte counts and T cell repertoire diversity (170). Indeed, thymic epithelial cells are able to prime and activate naïve allospecific T cells and are sensitive to depletion in the setting of aGVHD (171).

### 5.0.3 Murine Model – T cell kinetics and endpoint timing

Prior studies have demonstrated that aGVHD in murine models is a rapid process, with peak expansion of T cells seen around D6 following transplantation, prior to mass apoptosis of alloreactive T cells via activation induced cell death resulting in declining numbers of graft T cells from the second week post-transplant onwards (172, 173). This is consistent with peripheral blood T cell kinetics we observed in the second T cell dose titration experiment. The first peripheral blood timepoint was measured at D14, and graft T cells declined on each sequential measurement after this timepoint. By D28, donor HSC derived-T cells were more numerous in peripheral blood than persistent graft T cells and HSC derived-T cells constituted 93% of peripheral T cells by D56. Unlike persistent graft T cells which were heavily skewed towards a T effector cell state, donor HSC-derived T cells showed prominent naïve and central memory populations. Peripheral blood donor HSC-derived T cells will

have been subject to central tolerance in the recipient thymus and may be less likely to contribute to ongoing aGVHD than persistent graft T cells. It may be the case that the majority of inflammation and tissue injury in this experiment had occurred in the first month post-transplant. The nadir in haemoglobin and weight observed in the GVHD cohort at D28 is consistent with this interpretation. This may in part explain the modest effect size observed between the GVHD and control cohorts at our prespecified D56 endpoint.

### 5.0.4 Murine Model – Bone marrow haematopoietic and stromal findings

Important differences observed in our experiment in the GVHD cohort relative to controls were a trend towards a decrease in $CD201^+$ LT-HSCs, and changes to stromal populations. Using both a CD86 and Sca-1 gating back bone, there was a trend towards a decrease in $CD201^+$ LT-HSCs in the setting of GVHD, but no evidence of a change in the frequency of the broader LT-HSC population. A prior study demonstrated that 20 days of IL-1β decreased the frequency of $CD201^+$ LT-HSCs, while increasing $CD201^-$ LT-HSCs. Unlike $CD201^+$ LT-HSCs, $CD201^-$ LT-HSCs had limited long term repopulating potential (33). If found to be reproducible, a loss in $CD201^+$ LT-HSCs in the setting of GVHD would raise the possibility that GVHD depletes functional HSCs in our model system. This could be validated functionally with a secondary transplant assay.

All stromal populations positively identified by our panel had an increase in relative frequency in the setting of GVHD, with a less clear difference between

groups observed with regards to absolute counts. This result differs from some prior studies exploring the impact of T cell mediated inflammation on bone marrow stroma, in which a decrease in LepR$^+$ MSCs were observed. A prior study using an MHC mismatched murine model of GVHD with a severe systemic phenotype demonstrated a 36-fold reduction in LepR$^+$ MSCs in GVHD relative to control animals at D21 post transplantation (99). A study exploring the impact of LCMV infection on bone marrow stromal and haematopoietic populations demonstrated that infection was associated with marked disruption of LepR$^+$ MSC populations due to their depletion by viral specific CD8$^+$ T cells (121). The impact of LCMV infection on LepR$^+$ MSCs peaked at D7, improved by D56 and had resolved by D112. It may be informative to quantify LepR$^+$ MSCs at an earlier timepoint in our model system, to explore if there is a reduction in this population that had resolved by the D56 experimental endpoint.

An important consideration is that only a small proportion of stromal cells are released into a single cell suspension, even after enzymatic digestion. Prior studies quantifying LepR$^+$ MSCs in a spatial context within whole mouse bones have estimated that <5% of these cells are quantified by flow cytometry (174). While the assumption is frequently made that the sample of stromal cells captured for analysis by flow cytometry is representative of the broader population, it is plausible that interactions could exist between an experimental condition like GVHD and the efficiency with which cells are released into single cell suspension by processing and enzymatic digestion. It would be important to validate any quantitative conclusions regarding stromal population architecture in a spatial context using imaging.

The clearest trend observed in the stromal analysis of this experiment was towards an increase in the proportion of LepR$^+$ MSCs expressing Sca-1, a marker of a proinflammatory phenotype (5). This mirrors the findings seen in analysis of the impact of LCMV infection on LepR$^+$ MSCs (121). Following infection, both type I & II IFN levels returned to baseline by D14, but transcriptomic analysis of LepR$^+$ MSCs demonstrated a persistent gene expression profile suggestive of an IFN-driven inflammatory program at D56. This included markedly increased expression of IL-1β, a cytokine implicated in driving myeloid skewed HSC proliferation at the expense of self-renewal and functional fitness (65).

Prior publications using mouse models to explore the impact of GVHD on haematopoiesis reported an increase in LSK cells in GVHD cohorts compared with controls (101, 102). This finding was also observed in our study; using a standard Sca-1 gating backbone the MPP populations which comprise the LSK gate were increased in the setting of GVHD. Sca-1 can become upregulated on myeloid progenitors in the setting of inflammation (138). The difference in MPP frequency between GVHD and control cohorts disappeared on reanalysis using CD86, an inflammation robust alternative to Sca-1. This discrepancy between Sca-1 and CD86 gating strategies suggests that the apparent change in MPP frequency reflects upregulation of Sca-1 on lineage committed progenitors in the setting of inflammation rather than a true change in population architecture. It is possible that prior studies reporting an increase in HSC/MPP populations in the setting of GVHD may be impacted by this artifact, due to their use of a Sca-1 gating strategy (101, 102). This possibility was noted by Shono and colleagues, but alternatives to Sca-1 gating were less well characterised at the time of their publication.

The changes in lineage committed progenitors between control and GVHD cohorts in the second T cell dose titration are the inverse of the trend observed in MPP populations. Prior studies have demonstrated a myeloid bias among lineage committed progenitors is a feature of the output of myeloid biased HSCs, a distinct HSC subset that emerge in the setting of aging or prior inflammatory stress (175-177). Gating using Sca-1 revealed no difference between cohorts with regards to these populations, whereas CD86 gating demonstrated a trend towards an increase in myeloid progenitors (MEPs, CMPs and GMPs) relative to CLPs in the setting of GVHD. Given the small scale of this experiment and subtle effect size, these findings should be interpreted with caution until they are demonstrated to be both statistically robust and reproducible.

### 5.0.5 Organoid model – progress and limitations

In this project I have established a recently published protocol for the differentiation of hiPSC-derived bone marrow organoids within our laboratory. We plan to use MHC class I/II K/O hiPSCs to generate hypoimmune organoids to use as a negative control in an experimental system analysing the impact of alloreactive primary T cells on bone marrow stromal populations. The initial attempt to generate gene-edited hiPSCs in collaboration with the WIMM transgenic core facility has been unsuccessful, but as discussed in Chapter 4 plans are in place to reattempt this editing with modifications designed to improve the survival and recovery of successfully edited clones.

It is important to consider the anticipated limitations of this experimental system. HiPSC-derived organoids are not patient samples, and do not generate the full diversity of cell types observed in the human bone marrow. In cell composition they are most representative of a central marrow niche, with $CXCL12^+$ MSCs, sinusoidal endothelial cells, $CD34^+$ HSPCs and maturing myelopoiesis (129). While the bone marrow populations subject to injury in GVHD and other T cell mediated conditions are incompletely characterised, prior studies have highlighted B cell lymphopoiesis and osteoblasts as potential target populations (101, 166). The fact neither osteogenesis nor lymphopoiesis is present in these organoids will limit the ability to study these populations of interest. An iterative update to the organoid protocol has recently been published in preprint, and has been shown to generate maturing lymphopoiesis and $ALP^+$ osteolineage cells (178). With minor modifications to the workflows developed in this project, this updated protocol could be used as the foundation of our planned experimental system.

In our murine model, graft T cells do not exhibit alloreactivity against engrafting donor haematopoiesis as they come from syngeneic donors. This facilitates studying the indirect impact on haematopoiesis of GVHD directed at host tissues. In our planned organoid experiments, both haematopoietic and stromal compartments will be organoid derived, and MHC mismatched to the primary T cells introduced to the culture system. It is likely that the changes observed in haematopoietic populations in our organoid model will reflect direct interactions with alloreactive T cells; this may limit the capacity of this system to explore the impact on haematopoiesis of changes in stromal populations caused by GVHD. To circumvent this limitation, it may be possible to refine our organoid model to

incorporate primary human T cells and $CD34^+$ cells from the same donor, as these cell types are both present in apheresis cones collected by the NHS blood and transplant service.

Consideration needs to be given to the mechanism of T cell activation in our planned model system. Alloimmune injury to organoid populations will be induced by reacting purified primary donor T cells against organoids, based on the overwhelming likelihood of a major MHC mismatch between the organoid hiPSC donor and any individual peripheral blood donor. Indeed, analysis of T cell phenotype in a preliminary collaboration between the Psaila and Chakraverty groups was very suggestive of alloimmune activation of primary donor T cells after organoid co-culture. The only haematopoietic antigen presenting cells (APCs) in this model system are organoid derived monocyte and dendritic cell populations. While these APCs share a transcriptomic signature similar to normal bone marrow resident populations, no functional evaluation of these populations has yet been performed. It should be noted that non-haematopoietic APCs have been shown to be sufficient for the initiation of GVHD, and human bone marrow MSCs have been shown to function as APCs *in vitro* (179, 180). A reductionist approach to resolve the issue of T cell activation in this model would be to pre-activate T cells with $CD3^+/CD28^+$ synthetic stimulation beads prior to organoid co-culture.

## 5.1 Future Directions

### 5.1.1 Murine model optimisation

This project set out to develop a model of peripheral cytopenias using a mouse model of GVHD, to explore the impact of T cell mediated inflammation on stromal and haematopoietic populations within the bone marrow niche. To date, the desired phenotype has not been achieved, so future experiments in this project should be informed by consideration of two questions:

1. What further optimisation could be performed to generate our phenotype of interest using this model system?
2. What alternative questions could be addressed using this model system?

Peripheral pancytopenia and bone marrow failure are observed in previously published mouse models of severe GVHD (101, 102). It is likely that the lack of pancytopenia observed in our experiments reflects the decision to employ a model characterised by a milder GVHD phenotype. While this limitation could be overcome by increasing the severity of the GVHD in our model, our work would then carry the same limitation as prior studies exploring haematopoiesis in the setting of GVHD: confounding by severe systemic illness. Looking to an alternative model system where chronic inflammation drives bone marrow failure and pancytopenia may be informative regarding how this could be overcome.

Using a model of chronic mycobacterium infection, Baldrige and colleagues at the Baylor College of Medicine demonstrated that despite increased turnover of peripheral immune cells in the setting of infection, absolute numbers of peripheral cells are kept stable due to increased production by intermediate progenitors. These

intermediate progenitors in turn are replenished by quiescent LT-HSCs entering the cell cycle under the influence of IFN-γ; a process that maintains haematopoietic homeostasis, but at the expense of HSC functional fitness (64). In a follow up study, the same group demonstrated that with prolonged infection the capacity of the haematopoietic system to maintain this homeostasis decompensates (10). Over four to six months of infection HSCs were progressively depleted both numerically and functionally. Ultimately the capacity of HSCs to backfill intermediate progenitors was compromised, leading to haematopoietic collapse and peripheral pancytopenia.

While mechanisms of HSC loss may be different in chronic infection and GVHD, it may be the case that peripheral cytopenias in models of GVHD also reflect a failure of homeostasis occurring when the pool of functional HSCs is depleted. This raises the possibility that reducing the dose of HSCs transplanted may facilitate peripheral cytopenias in our model system. It may be the case that with a restricted HSC pool, HSC exhaustion and haematopoietic decompensation could be achieved without employing a more severe GVHD phenotype. Extreme limiting dilution assays performed using HSCs harvested from mice with LCMV infection demonstrated an increase in the HSC dose required from infected donors to demonstrate equivalent functional fitness (121). While the $0.5x10^6$ c-Kit$^+$ cells given to recipients in this study resulted in successful engraftment in all recipients, it is possible that a cell dose could be identified which results in stable engraftment in the absence of GVHD but results in graft failure in the setting of GVHD.

The next experiments to optimise this model system will aim to identify this c-Kit$^+$ cell dose (Figure 5.1). Recipients will be randomised to GVHD or no-GVHD

cohorts, and then randomised to variable doses of c-Kit$^+$ cells. Both peripheral blood and bone marrow populations will be analysed, with the aim of identifying a c-Kit$^+$ cell dose which results in peripheral cytopenias only in the presence of GVHD. Other insights from prior experiments to date will also be incorporated. GVHD will be induced with 1x10$^6$ graft T cells, a D28 endpoint will be used and to minimise variability introduced by sex differences all transplants will be performed with female donors and recipients.

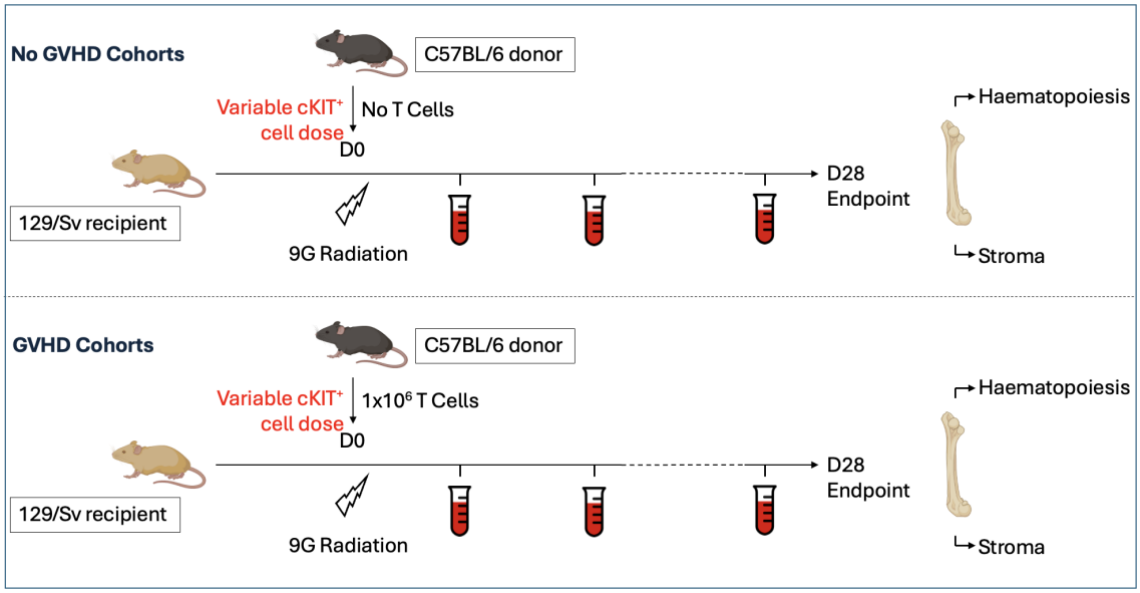



**Figure 5. 1:** Schematic representation of planned c-Kit$^+$ dose titration experiment.

An experiment will be performed to identify a dose of c-Kit$^+$ cells which results in graft failure in the presence of GVHD, but not in the absence of GVHD. Mice will be randomised first to a GVHD cohort,or no-GVHD control. Within these groups, animals will be randomised to variable doses of c-Kit$^+$ cells. A c-Kit$^+$ cell dose which results in pancytopenia in the GVHD group but not the control group will be taken forward for further validation. Figure created using BioRender.com.

While to date our murine model does not develop pancytopenia and so does not represent a functional model of T cell mediated bone marrow failure, it may be the case that it can be employed to answer different questions. An increase in the

proportion of LepR$^+$ MSCs expressing Sca-1, a marker of a proinflammatory phenotype, was observed at D56 in GVHD mice. This change in LepR$^+$ MSCs was observed despite a suspicion that most of the tissue injury due to GVHD in this model had occurred in the early period post-transplant. This raises the possibility that this proinflammatory phenotype persists independently of ongoing GVHD. A hallmark of treatment refractory GVHD is the persistence of tissue dysfunction beyond the initial T cell mediated injury, due to disruption of mechanisms of tissue regeneration and repair (181). Recent work has demonstrated that GVHD induces epigenetic changes in intestinal stem cells which persist in the absence of ongoing T cell mediated injury. These epigenetic alterations were shown to result in reduced proliferative function and persistent metabolic changes (150). It is unclear if similar mechanisms of inflammatory memory exist in bone marrow stromal populations. By depleting T cells after the establishment of GVHD, it would be possible to test if the induced proinflammatory stromal phenotype we observe in this model persists in the absence of graft T cells. If this was the case, this model may represent an opportunity to explore a mechanism of persistent inflammation within the haematopoietic niche.

We aim to develop a model characterised by peripheral cytopenias so that the interplay between haematopoiesis, T cells and stromal populations leading to these cytopenias can be characterised in a tractable system. If it proves unfeasible to reproducibly generate pancytopenia in this model, it would still be of value to study the interactions between T cells and bone marrow stromal populations *in vivo*, as a complement to our bone marrow organoid model.

### 5.1.2 Organoid model development

We aim to develop our organoid model into a tractable system for mechanistically exploring the specific interactions underpinning T cell mediated injury to the bone marrow stroma. It is likely that our generation of MHC class I/II K/O hiPSC lines will lead to the development of clones with successful editing of only one or the other locus. We will perform experiments co-culturing T cells from the same donor against organoids derived from WT, double K/O, and individual MHC class I and MHC class II K/O hiPSC lines. This will allow us to identify what changes to the stromal compartment are attributable to cognate interactions specifically with $CD4^+$ or $CD8^+$ T cells, or the synergistic action of both populations. By applying a gene-editing approach to donor T cells, we will explore the contributions of specific elements of T cell effector machinery to our phenotypes of interest. By editing donor T cells and knocking-out proteins such as perforin, granzyme, Fas-L or cytokines including IFN-$\gamma$, we will explore which processes are essential and which are dispensable for bone marrow GVHD in this model system. It is also possible that changes to stromal populations caused by T cells will lead to the amplification of tissue injury within the niche, and once our workflows for editing hiPSCs are optimised, we will be able to manipulate these mechanisms directly. An example of a hypothesis to explore is if recipient cells including bone marrow MSCs become a source of IL-1$\beta$ in the setting of T cell mediated inflammation, and if IL-1$\beta$ signalling contributes to tissue injury in this context (5). An *IL-1B* K/O hiPSC line could be used to generate organoids capable of exploring this question.

## 5.2 Conclusion

T cell mediated injury to the haematopoietic niche contributes to a number of diseases, including complications of cellular therapies such as poor graft function following alloSCT, and ICAHT following CAR-T therapy. Those patients who do not recover haematopoietic function with currently available treatments have poor outcomes and represent an area of unmet clinical need. A barrier to developing novel therapeutic strategies in this space is a lack of tractable pre-clinical models to develop mechanistic insights into these diseases.

I have completed the foundational work towards the development of two complementary pre-clinical models of T cell mediated injury to the haematopoietic niche. Steps have been taken towards developing a murine model of cytopenias driven by GVHD. While further optimisation of this system is required, the results of this project provide direction for ongoing model development. This project has also established the workflows for the differentiation of hiPSC-derived bone marrow organoids in our laboratory, which will form the basis of a novel *in vitro* model system.

Once they have been developed, these experimental models will complement one another. The mouse model will facilitate the simultaneous evaluation of T cell, stromal and haematopoietic populations, and how they interact. Analysing these populations using flow cytometry and scRNAseq, we will identify target mechanisms for further exploration. The organoid model will allow these candidate mechanisms to be perturbed and understood in a tractable high throughput *in vitro* system in human tissue. Employed in parallel, these models will

provide a platform for the identification of targetable mechanisms underpinning T cell mediated injury to the haematopoietic niche. It is our hope that these insights will be translatable into novel therapeutic strategies to improve the outcomes of patients suffering from haematological toxicities of cellular therapeutics, and related conditions.

# Appendices

## Appendix 1 – Flow Cytometry Panels

**Appendix 1 – Table 1 –** Peripheral Blood Leukocyte Chimerism

| Fluorochrome | Antigen | Product Code | Titre |
|---|---|---|---|
| BV421 | CD45.2 | Invitrogen 48-0454-82 | 3:1000 |
| Zombie Green™ (FITC) | Live/Dead | Biolegend 423111 | 1:1000 |
| PE | CD11b | Biolegend 101208 | 1:2000 |
| PE | GR1/Ly6G | Biolegend 108408 | 1:2000 |
| PECy7 | CD45.1 | Biolegend 110730 | 1:400 |
| APC | CD4 | Biolegend 100516 | 1:2000 |
| APC | CD8 | Biolegend 100712 | 1:2000 |
| APCCy7 | CD45R/B220 | Biolegend 103224 | 1:1000 |

**Appendix 1 – Table 2 –** HSC/MPP Panel

| Fluorochrome | Antigen | Product Code | Titre |
|---|---|---|---|
| BUV395 | CD45.2 | BD Horizon 564616 | 1:100 |
| BUV563 | CD45.1 | BD OptiBuild 741274 | 1:100 |
| BUV737 | Sca-1 | BD OptiBuild 741708 | 1:200 |
| BV421 | CD135 | Biolegend 135313 | 2.5:100 |
| BV650 | c-Kit | Biolegend 105853 | 1:400 |
| BV785 | CD48 | Biolegend 103449 | 1:100 |
| FITC | CD34 | eBioscience 11-0341-82 | 1:100 |
| PerCP-eFluor710 | CD201 | Invitrogen 46-2012-80 | 1:400 |
| PE | CD86 | Biolegend 105008 | 1:400 |
| PECy7 | CD150 | Biolegend 115914 | 1:400 |
| Fixable Viability 780 | Live/Dead | BD Horizon 565388 | 1:1000 |
| APCCy7 | Streptavidin* | Biolegend 405208 | 1:400 |

*Cells pre-incubated with biotinylated lineage antigen cocktail prior to staining

**Appendix 1 – Table 3 –** Lineage Committed Progenitor Panel

| Fluorochrome | Antigen | Product Code | Titre |
|---|---|---|---|
| BUV395 | CD45.2 | BD Horizon 564616 | 1:100 |
| BUV563 | CD45.1 | BD OptiBuild 741274 | 1:100 |
| BUV737 | Sca-1 | BD OptiBuild 741708 | 1:200 |
| BV421 | CD135 | Biolegend 135313 | 2.5:100 |
| BV650 | c-Kit | Biolegend 105853 | 1:400 |
| BV785 | CD127 | Biolegend 135037 | 1:100 |
| FITC | CD34 | eBioscience 11-0341-82 | 1:100 |
| PE | CD86 | Biolegend 105008 | 1:400 |
| PECy7 | CD16/32* | Biolegend 101317 | 1:400 |
| Fixable Viability 780 | Live/Dead | BD Horizon 565388 | 1:1000 |
| APCCy7 | Streptavidin** | Biolegend 405208 | 1:400 |

*Staining with this antibody is performed prior to applying the staining master-mix

**Cells are pre-incubated with biotinylated lineage antigen cocktail prior to staining

**Appendix 1 – Table 4 –** Bone Marrow T Cell Panel

| Fluorochrome | Antigen | Product Code | Titre |
|---|---|---|---|
| BUV395 | CD45.2 | BD Horizon 564616 | 1:100 |
| BUV563 | CD45.1 | BD OptiBuild 741274 | 1:100 |
| BV421 | CD44 | Biolegend 103029 | 1:100 |
| BV711 | CD62L | Biolegend 104445 | 1:400 |
| FITC | CD4 | Biolegend 100405 | 1:100 |
| PECy7 | CD8 | Biolegend 100721 | 1:400 |
| AF700 | CD3 | Biolegend 100216 | 1:200 |
| Fixable Viability 780 | Live/Dead | BD Horizon 565388 | 1:1000 |

**Appendix 1 – Table 5 –** Bone Marrow Stroma Panel

| Fluorochrome | Antigen | Product Code | Titre |
|---|---|---|---|
| BUV395 | CD45* | BD Horizon 564279 | 1:100 |
| BUV737 | Sca-1 | BD OptiBuild 741708 | 1:800 |
| BV421 | CD34 | BD Horizon 562608 | 1:200 |
| BV510 | CD71 | Biolegend 113823 | 1:100 |
| BV605 | Ter119 | Biolegend 116239 | 1:200 |
| Biotin | LepR | R&D systems BAF497 | 1:100 |
| BV711 | Streptavidin** | Biolegend 405241 | 1:200 |
| PerCPCy5.5 | CD31 | Biolegend 102522 | 1:200 |
| PE/Cy7 | VCAM-1 | Biolegend 105720 | 1:200 |
| AF700 | Gr-1*** | Biolegend 108422 | 1:200 |
| AF700 | CD11b*** | Biolegend 101222 | 1:200 |
| AF700 | CD3*** | Biolegend 100216 | 1:200 |
| AF700 | CD45R/B220*** | Biolegend 103232 | 1:200 |
| Fixable Viability 780 | Live/Dead | BD Horizon 565388 | 1:1000 |

*CD45 staining performed separately to master-mix in 200µL volume
**Streptavidin-BV711 staining performed following LepR-biotin staining in master-mix
***Lineage antigens

**Appendix 1 – Table 6 –** Biotinylated Lineage Antibody Cocktail

| Antigen | Product Code | Titre | Volume in 375µL working stock* |
|---|---|---|---|
| Ter119 | Biolegend 116203 | 1:7 | 50µL |
| Gr-1/Ly-6G | Biolegend 108404 | 1:7 | 50µL |
| CD45R/B220 | Biolegend 103204 | 1:14 | 25µL |
| CD4 | Biolegend 100508 | 1:28 | 12.5µL |
| CD8 | Biolegend 100704 | 1:28 | 12.5µL |
| CD11b | Invitrogen 12-0112-81 | 1:28 | 12.5µL |

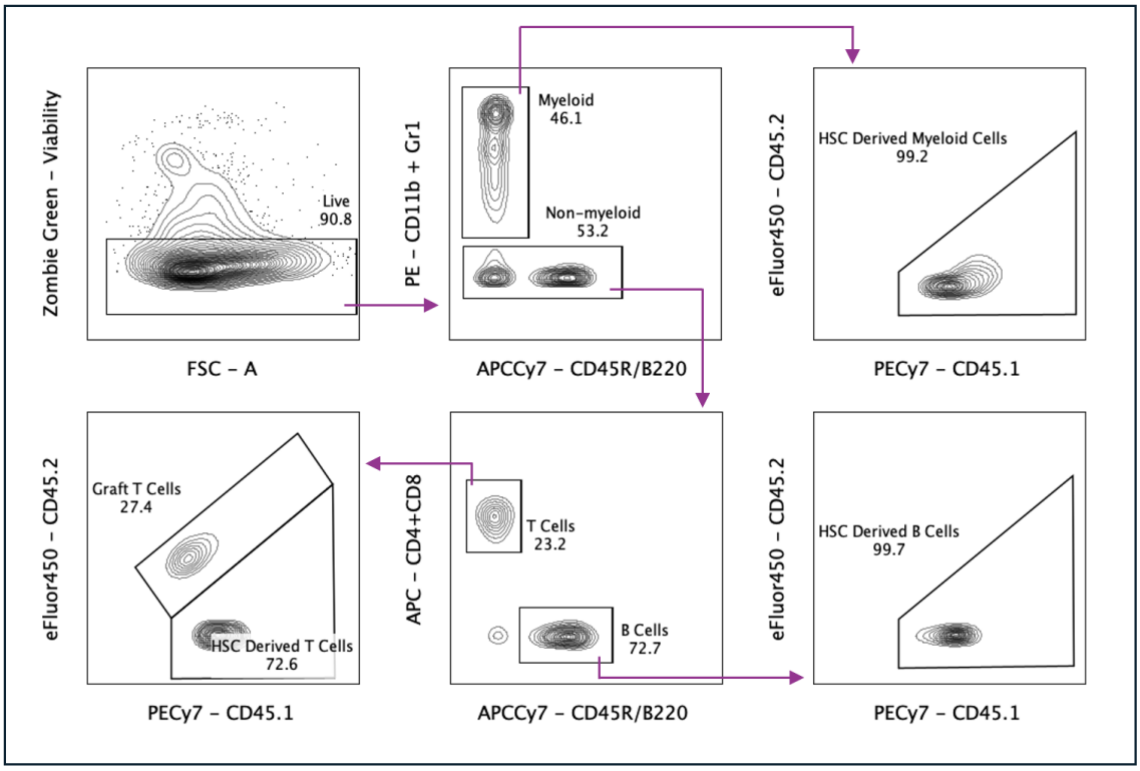
*375µL Working stock made fresh every three months, with 187.5µL sterile PBS as a dilutant

**Appendix 1 – Table 7 –** Organoid Haematopoiesis Panel

| Fluorochrome | Antigen | Product Code | Titre |
|---|---|---|---|
| BV510 | CD71 | BD OptiBuild 744926 | 1:100 |
| BV650 | CD34 | Biolegend 343624 | 1:100 |
| FITC | CD41 | Biolegend 303704 | 1:100 |
| PE | CD42a | BD Pharmingen 558819 | 1:100 |
| PECy7 | CD235 | Biolegend 306620 | 1:200 |
| AF700 | CD11b | Biolegend 301355 | 1:200 |
| AF700 | CD14 | Biolegend 367113 | 1:200 |
| APCeF780 | CD45 | Biolegend 368516 | 1:200 |
| 7-AAD | Live/Dead | Cayman Chemical 11397 | - |

**Appendix 1 – Table 8 –** Organoid Stromal Panel

| Fluorochrome | Antigen | Product Code | Titre |
|---|---|---|---|
| BUV395 | CD271 | BD OptiBuild 743362 | 1:100 |
| BV650 | CD71 | Biolegend 334116 | 1:100 |
| BV786 | CD105 | BD OptiBuild 742571 | 1:100 |
| AF488 | CD45 | Biolegend 304017 | 1:100 |
| PECy5 | CD90 | Biolegend 328112 | 1:100 |
| PECy7 | CD235 | Biolegend 306620 | 1:200 |
| APCCy7 | CD31 | Biolegend 303120 | 1:100 |
| DAPI | Live/Dead | Life Technologies D3571 | - |




**Appendix 1, Figure 1:** Representative gating for peripheral blood flow

Gating shown following doublet and debris exclusion. Peripheral blood was analysed every 14 days during transplant experiments by flow cytometry. HSC donor-derived haematopoiesis, recipient haematopoiesis and graft T cells were identified based on differential expression of congenic CD45 isoforms.

# Appendix 2 – Organoid Reagents

## Appendix 2 Section 1 – Component Reagents

| | |
|---|---|
| Media | |
| APEL 2 | SCT Cat: 05275 |
| Ham's F12 | ThermoFisher Cat: 11765054 |
| 10x Dulbecco's modified Eagle medium (DMEM) | ThermoFisher Cat: 12491023 |
| StemPro-34 | ThermoFisher Cat: 10639011 |
| | |
| Media Supplements | |
| HEPES Buffer | ThermoFisher Cat: 15630080 |
| Glutamax | ThermoFisher Cat: 35050061 |
| Heparin Salt | Sigma Cat: H3393 |
| NaOH 7.5% Solution | ThermoFisher Cat: 25080094 |
| Sodium Acetate | Sigma Cat: S8750 |
| Glacial acetic acid | Merck Cat: A6283-100ML |
| Chemically Defined Lipids (CDL) | ThermoFisher Cat: 11905031 |
| KnockOut serum replacement | ThermoFisher Cat: 10828028 |
| Thrombin | Merck Cat: 605157 – 1KU |
| | |
| Biomatrices | |
| VitroCol® (Type I Collagen Solution) | Advanced Biomatrix Cat: 5007 |
| Lyophilised Type I Collagen | Advanced Biomatrix Cat: 5008 |
| Lyophilised Type IV Collagen | Advanced Biomatrix Cat: 5022 |
| Matrigel® | Corning Cat: 354230 |
| Fibrinogen | MPBio Cat: 9001-32-5 |
| | |
| Cytokines and Small Molecules | |
| FGF2 | PeproTech Cat: 100-18B |
| VEGFA(165) | PeproTech Cat: 100-20 |
| VEGFC | PeproTech Cat: 100-20D |
| EPO | PeproTech Cat: 100-64 |
| BMP4 | PeproTech Cat: 120-05 |
| IL3 | PeproTech Cat: 200-03 |
| IL6 | PeproTech Cat: 200-6 |
| hSCF | PeproTech Cat: 300-07 |
| TPO | PeproTech Cat: 300-18 |
| Flt3 Ligand | PeproTech Cat: 300-19 |
| GCSF | SCT Cat: 78012 |
| CHIR99021 | Merck Cat: SML1046 |

## Appendix 2 Section 2 – Reagent Production

Collagen Dilutant

100mL 0.01% sodium acetate in sterile water
+ 250uL glacial acetic acid

Collagen Type I + Type IV Mix

Step 1 – reconstitute 15mg lyophilised collagen type I in 5mL collagen dilutant
- Incubate overnight on a shaker at 4°C

Step 2 – add the solution from Step 1 to 5mg of lyophilised collagen type IV
- Incubate overnight on a shaker at 4°C

Step 3 – mix vigorously to complete resuspension of collagens

Final mix: 3mg/mL collagen type I, 1mg/mL collagen type IV

Hydrogel Dilutant

100mL Total Volume:

| | |
|---|---|
| 71.34mL | Ham's F12 |
| 1.89mL | Glutamax |
| 3.14mL | 7.5% NaOH |
| 3.96mL | HEPES Buffer |
| 19.67mL | 10x DMEM |

**Appendix 2 – Table 1 –** Hydrogel Layer Composition

| Reagent | Stock [] | Hydrogel Base Layer Volume in 500µL Well | Hydrogel Organoid Layer Volume in 500µL Well |
|---|---|---|---|
| Hydrogel dilutant | Neat | 133.8µL | 25µL |
| Fibrinogen | 20mg/mL | 31.3µL | 20.8µL |
| Vitrocol (I) | 3mg/mL | 333.3µL | 100µL |
| Collagen I+IV Mix | Neat | - | 150µL |
| Matrigel | Neat | - | 200uL |
| NaOH | 1M | 1.3µL | 4.7µL |
| Thrombin | 2U/µL | 0.3µL | 0.2µL |

**Appendix 2 – Table 2 –** Organoid Media Composition

| Media | Base Media | Supplements | Cytokines/Small Molecules |
|---|---|---|---|
| Phase 1 | APEL2 | - | 50ng/mL BMP4, VEGFA, FGF2<br>3uM CHIR99021 |
| Phase 2 | APEL2 | | 50ng/mL BMP4, VEGFA, FGF2<br>25ng/mL hSCF, Flt3L |
| Phase 3A | APEL2 | K/O serum (5%)<br>Heparin 5U/mL | 100ng/mL VEGFA<br>50ng/mL VEGFC, FGF2, BMP4, TPO<br>50ng/mL EPO, cGCSF, Flt3L, hSCF<br>20ng/mL IL3, IL6 |
| Phase 3B | APEL2 | K/O serum (5%)<br>Heparin 5U/mL | 50ng/mL VEGFA<br>25ng/mL VEGFC, FGF2, BMP4, TPO<br>25ng/mL EPO, cGCSF, Flt3L, hSCF<br>10ng/mL IL3, IL6 |
| Phase 3C | APEL2 | K/O serum (5%)<br>Heparin 5U/mL | 50ng/mL VEGFA<br>25ng/mL VEGFC, FGF2, TPO, EPO<br>25ng/mL Flt3L, hSCF<br>10ng/mL IL3, IL6 |
| Extraction | StemPro-34 | Glutamax (1%)<br>K/O serum (2%)<br>CDL (2%) | 25ng/mL VEGFA, VEGFC, FGF2<br>25ng/mL hSCF, Flt3L<br>10ng/mL TPO, EPO, IL3, IL6 |
| Phase 4 | StemPro-34 | Glutamax (1%)<br>K/O serum (2%)<br>CDL (2%) | 5ng/mL EPO<br>1ng/mL TPO |

# References


1. Comazzetto S, Shen B, Morrison SJ. Niches that regulate stem cells and hematopoiesis in adult bone marrow. Developmental Cell. 2021;56(13):1848-60.
2. Pereira AL, Galli S, Nombela-Arrieta C. Bone marrow niches for hematopoietic stem cells. Hemasphere. 2024;8(8):e133.
3. Cheshier SH, Prohaska SS, Weissman IL. The effect of bleeding on hematopoietic stem cell cycling and self-renewal. Stem Cells Dev. 2007;16(5):707-17.
4. Swann JW, Olson OC, Passegué E. Made to order: emergency myelopoiesis and demand-adapted innate immune cell production. Nature Reviews Immunology. 2024;24(8):596-613.
5. Mitchell CA, Verovskaya EV, Calero-Nieto FJ, Olson OC, Swann JW, Wang X, et al. Stromal niche inflammation mediated by IL-1 signalling is a targetable driver of haematopoietic ageing. Nature Cell Biology. 2023;25(1):30-41.
6. Valletta S, Thomas A, Meng Y, Ren X, Drissen R, Sengül H, et al. Micro-environmental sensing by bone marrow stroma identifies IL-6 and TGFβ1 as regulators of hematopoietic ageing. Nature Communications. 2020;11(1):4075.
7. Boettcher S, Ziegler P, Schmid MA, Takizawa H, van Rooijen N, Kopf M, et al. Cutting edge: LPS-induced emergency myelopoiesis depends on TLR4-expressing nonhematopoietic cells. J Immunol. 2012;188(12):5824-8.
8. de Jong MME, Kellermayer Z, Papazian N, Tahri S, Hofste op Bruinink D, Hoogenboezem R, et al. The multiple myeloma microenvironment is defined by an inflammatory stromal cell landscape. Nature Immunology. 2021;22(6):769-80.
9. Avagyan S, Henninger JE, Mannherz WP, Mistry M, Yoon J, Yang S, et al. Resistance to inflammation underlies enhanced fitness in clonal hematopoiesis. Science. 2021;374(6568):768-72.
10. Matatall KA, Jeong M, Chen S, Sun D, Chen F, Mo Q, et al. Chronic Infection Depletes Hematopoietic Stem Cells through Stress-Induced Terminal Differentiation. Cell Rep. 2016;17(10):2584-95.
11. Shallis RM, Ahmad R, Zeidan AM. Aplastic anemia: Etiology, molecular pathogenesis, and emerging concepts. Eur J Haematol. 2018;101(6):711-20.
12. Prabahran A, Koldej R, Chee L, Ritchie D. Clinical features, pathophysiology, and therapy of poor graft function post-allogeneic stem cell transplantation. Blood Adv. 2022;6(6):1947-59.
13. Rejeski K, Jain MD, Shah NN, Perales M-A, Subklewe M. Immune effector cell-associated haematotoxicity after CAR T-cell therapy: from mechanism to management. The Lancet Haematology. 2024;11(6):e459-e70.
14. Paolino J, Berliner N, Degar B. Hemophagocytic lymphohistiocytosis as an etiology of bone marrow failure. Frontiers in Oncology. 2022;12.
15. Purton LE, Scadden DT. Limiting Factors in Murine Hematopoietic Stem Cell Assays. Cell Stem Cell. 2007;1(3):263-70.
16. Ho TT, Warr MR, Adelman ER, Lansinger OM, Flach J, Verovskaya EV, et al. Autophagy maintains the metabolism and function of young and old stem cells. Nature. 2017;543(7644):205-10.
17. Wilson A, Laurenti E, Oser G, van der Wath RC, Blanco-Bose W, Jaworski M, et al. Hematopoietic Stem Cells Reversibly Switch from Dormancy to Self-Renewal during Homeostasis and Repair. Cell. 2008;135(6):1118-29.

18. Simsek T, Kocabas F, Zheng J, Deberardinis RJ, Mahmoud AI, Olson EN, et al. The distinct metabolic profile of hematopoietic stem cells reflects their location in a hypoxic niche. Cell Stem Cell. 2010;7(3):380-90.
19. Laurenti E, Göttgens B. From haematopoietic stem cells to complex differentiation landscapes. Nature. 2018;553(7689):418-26.
20. Pietras Eric M, Reynaud D, Kang Y-A, Carlin D, Calero-Nieto Fernando J, Leavitt Andrew D, et al. Functionally Distinct Subsets of Lineage-Biased Multipotent Progenitors Control Blood Production in Normal and Regenerative Conditions. Cell Stem Cell. 2015;17(1):35-46.
21. Oguro H, Ding L, Morrison SJ. SLAM family markers resolve functionally distinct subpopulations of hematopoietic stem cells and multipotent progenitors. Cell Stem Cell. 2013;13(1):102-16.
22. Akashi K, Traver D, Miyamoto T, Weissman IL. A clonogenic common myeloid progenitor that gives rise to all myeloid lineages. Nature. 2000;404(6774):193-7.
23. Pronk CJ, Rossi DJ, Månsson R, Attema JL, Norddahl GL, Chan CK, et al. Elucidation of the phenotypic, functional, and molecular topography of a myeloerythroid progenitor cell hierarchy. Cell Stem Cell. 2007;1(4):428-42.
24. Kondo M, Weissman IL, Akashi K. Identification of clonogenic common lymphoid progenitors in mouse bone marrow. Cell. 1997;91(5):661-72.
25. Höfer T, Rodewald H-R. Differentiation-based model of hematopoietic stem cell functions and lineage pathways. Blood. 2018;132(11):1106-13.
26. Schoedel KB, Morcos MNF, Zerjatke T, Roeder I, Grinenko T, Voehringer D, et al. The bulk of the hematopoietic stem cell population is dispensable for murine steady-state and stress hematopoiesis. Blood. 2016;128(19):2285-96.
27. Sun J, Ramos A, Chapman B, Johnnidis JB, Le L, Ho Y-J, et al. Clonal dynamics of native haematopoiesis. Nature. 2014;514(7522):322-7.
28. Weinreb C, Rodriguez-Fraticelli A, Camargo FD, Klein AM. Lineage tracing on transcriptional landscapes links state to fate during differentiation. Science. 2020;367(6479):eaaw3381.
29. Velten L, Haas SF, Raffel S, Blaszkiewicz S, Islam S, Hennig BP, et al. Human haematopoietic stem cell lineage commitment is a continuous process. Nat Cell Biol. 2017;19(4):271-81.
30. Olsson A, Venkatasubramanian M, Chaudhri VK, Aronow BJ, Salomonis N, Singh H, et al. Single-cell analysis of mixed-lineage states leading to a binary cell fate choice. Nature. 2016;537(7622):698-702.
31. Carrelha J, Meng Y, Kettyle LM, Luis TC, Norfo R, Alcolea V, et al. Hierarchically related lineage-restricted fates of multipotent haematopoietic stem cells. Nature. 2018;554(7690):106-11.
32. Safina K, van Galen P. New frameworks for hematopoiesis derived from single-cell genomics. Blood. 2024;144(10):1039-47.
33. Rabe JL, Hernandez G, Chavez JS, Mills TS, Nerlov C, Pietras EM. CD34 and EPCR coordinately enrich functional murine hematopoietic stem cells under normal and inflammatory conditions. Exp Hematol. 2020;81:1-15.e6.
34. Kiel MJ, Yilmaz ÖH, Iwashita T, Yilmaz OH, Terhorst C, Morrison SJ. SLAM Family Receptors Distinguish Hematopoietic Stem and Progenitor Cells and Reveal Endothelial Niches for Stem Cells. Cell. 2005;121(7):1109-21.

35. Acar M, Kocherlakota KS, Murphy MM, Peyer JG, Oguro H, Inra CN, et al. Deep imaging of bone marrow shows non-dividing stem cells are mainly perisinusoidal. Nature. 2015;526(7571):126-30.
36. Czechowicz A, Kraft D, Weissman IL, Bhattacharya D. Efficient transplantation via antibody-based clearance of hematopoietic stem cell niches. Science. 2007;318(5854):1296-9.
37. Thorén LA, Liuba K, Bryder D, Nygren JM, Jensen CT, Qian H, et al. Kit regulates maintenance of quiescent hematopoietic stem cells. J Immunol. 2008;180(4):2045-53.
38. Barker JE. Early transplantation to a normal microenvironment prevents the development of Steel hematopoietic stem cell defects. Exp Hematol. 1997;25(6):542-7.
39. Matsuoka S, Facchini R, Luis TC, Carrelha J, Woll PS, Mizukami T, et al. Loss of endothelial membrane KIT ligand affects systemic KIT ligand levels but not bone marrow hematopoietic stem cells. Blood. 2023;142(19):1622-32.
40. Nakatani T, Nagasawa T. Bone marrow niches for hematopoietic stem cells in homeostasis and aging. Exp Hematol. 2025;144:104749.
41. Broxmeyer HE, Orschell CM, Clapp DW, Hangoc G, Cooper S, Plett PA, et al. Rapid mobilization of murine and human hematopoietic stem and progenitor cells with AMD3100, a CXCR4 antagonist. J Exp Med. 2005;201(8):1307-18.
42. Sugiyama T, Kohara H, Noda M, Nagasawa T. Maintenance of the Hematopoietic Stem Cell Pool by CXCL12-CXCR4 Chemokine Signaling in Bone Marrow Stromal Cell Niches. Immunity. 2006;25(6):977-88.
43. Ding L, Morrison SJ. Haematopoietic stem cells and early lymphoid progenitors occupy distinct bone marrow niches. Nature. 2013;495(7440):231-5.
44. Nakatani T, Sugiyama T, Omatsu Y, Watanabe H, Kondoh G, Nagasawa T. Ebf3+ niche-derived CXCL12 is required for the localization and maintenance of hematopoietic stem cells. Nature Communications. 2023;14(1):6402.
45. Pinho S, Frenette PS. Haematopoietic stem cell activity and interactions with the niche. Nature Reviews Molecular Cell Biology. 2019;20(5):303-20.
46. Baryawno N, Przybylski D, Kowalczyk MS, Kfoury Y, Severe N, Gustafsson K, et al. A Cellular Taxonomy of the Bone Marrow Stroma in Homeostasis and Leukemia. Cell. 2019;177(7):1915-32.e16.
47. Ding L, Saunders TL, Enikolopov G, Morrison SJ. Endothelial and perivascular cells maintain haematopoietic stem cells. Nature. 2012;481(7382):457-62.
48. Cordeiro Gomes A, Hara T, Lim VY, Herndler-Brandstetter D, Nevius E, Sugiyama T, et al. Hematopoietic Stem Cell Niches Produce Lineage-Instructive Signals to Control Multipotent Progenitor Differentiation. Immunity. 2016;45(6):1219-31.
49. Emoto T, Lu J, Sivasubramaniyam T, Maan H, Khan AB, Abow AA, et al. Colony stimulating factor-1 producing endothelial cells and mesenchymal stromal cells maintain monocytes within a perivascular bone marrow niche. Immunity. 2022;55(5):862-78.e8.
50. Himburg HA, Termini CM, Schlussel L, Kan J, Li M, Zhao L, et al. Distinct Bone Marrow Sources of Pleiotrophin Control Hematopoietic Stem Cell Maintenance and Regeneration. Cell Stem Cell. 2018;23(3):370-81.e5.
51. Zhou BO, Yue R, Murphy MM, Peyer JG, Morrison SJ. Leptin-receptor-expressing mesenchymal stromal cells represent the main source of bone formed by adult bone marrow. Cell Stem Cell. 2014;15(2):154-68.

52. Méndez-Ferrer S, Michurina TV, Ferraro F, Mazloom AR, MacArthur BD, Lira SA, et al. Mesenchymal and haematopoietic stem cells form a unique bone marrow niche. Nature. 2010;466(7308):829-34.
53. Kunisaki Y, Bruns I, Scheiermann C, Ahmed J, Pinho S, Zhang D, et al. Arteriolar niches maintain haematopoietic stem cell quiescence. Nature. 2013;502(7473):637-43.
54. Méndez-Ferrer S, Bonnet D, Steensma DP, Hasserjian RP, Ghobrial IM, Gribben JG, et al. Bone marrow niches in haematological malignancies. Nat Rev Cancer. 2020;20(5):285-98.
55. Sanjuan-Pla A, Macaulay IC, Jensen CT, Woll PS, Luis TC, Mead A, et al. Platelet-biased stem cells reside at the apex of the haematopoietic stem-cell hierarchy. Nature. 2013;502(7470):232-6.
56. Pinho S, Marchand T, Yang E, Wei Q, Nerlov C, Frenette PS. Lineage-Biased Hematopoietic Stem Cells Are Regulated by Distinct Niches. Developmental Cell. 2018;44(5):634-41.e4.
57. Kokkaliaris KD, Kunz L, Cabezas-Wallscheid N, Christodoulou C, Renders S, Camargo F, et al. Adult blood stem cell localization reflects the abundance of reported bone marrow niche cell types and their combinations. Blood. 2020;136(20):2296-307.
58. Stone AP, Nascimento TF, Barrachina MN. The bone marrow niche from the inside out: how megakaryocytes are shaped by and shape hematopoiesis. Blood. 2022;139(4):483-91.
59. Hirata Y, Furuhashi K, Ishii H, Li HW, Pinho S, Ding L, et al. CD150high Bone Marrow Tregs Maintain Hematopoietic Stem Cell Quiescence and Immune Privilege via Adenosine. Cell Stem Cell. 2018;22(3):445-53.e5.
60. Golan K, Singh AK, Kollet O, Bertagna M, Althoff MJ, Khatib-Massalha E, et al. Bone marrow regeneration requires mitochondrial transfer from donor Cx43-expressing hematopoietic progenitors to stroma. Blood. 2020;136(23):2607-19.
61. Medzhitov R. Origin and physiological roles of inflammation. Nature. 2008;454(7203):428-35.
62. Wu Q, Zhang J, Kumar S, Shen S, Kincaid M, Johnson CB, et al. Resilient anatomy and local plasticity of naive and stress haematopoiesis. Nature. 2024;627(8005):839-46.
63. Nagai Y, Garrett KP, Ohta S, Bahrun U, Kouro T, Akira S, et al. Toll-like Receptors on Hematopoietic Progenitor Cells Stimulate Innate Immune System Replenishment. Immunity. 2006;24(6):801-12.
64. Baldridge MT, King KY, Boles NC, Weksberg DC, Goodell MA. Quiescent haematopoietic stem cells are activated by IFN-gamma in response to chronic infection. Nature. 2010;465(7299):793-7.
65. Pietras EM, Mirantes-Barbeito C, Fong S, Loeffler D, Kovtonyuk LV, Zhang S, et al. Chronic interleukin-1 exposure drives haematopoietic stem cells towards precocious myeloid differentiation at the expense of self-renewal. Nature Cell Biology. 2016;18(6):607-18.
66. Yamashita M, Passegué E. TNF-α Coordinates Hematopoietic Stem Cell Survival and Myeloid Regeneration. Cell Stem Cell. 2019;25(3):357-72.e7.
67. Maeda K, Malykhin A, Teague-Weber BN, Sun X-H, Farris AD, Coggeshall KM. Interleukin-6 aborts lymphopoiesis and elevates production of myeloid cells in systemic lupus erythematosus–prone B6.Sle1.Yaa animals. Blood. 2009;113(19):4534-40.

68. Mitroulis I, Kalafati L, Hajishengallis G, Chavakis T. Myelopoiesis in the Context of Innate Immunity. J Innate Immun. 2018;10(5-6):365-72.
69. Schuettpelz LG, Borgerding JN, Christopher MJ, Gopalan PK, Romine MP, Herman AC, et al. G-CSF regulates hematopoietic stem cell activity, in part, through activation of Toll-like receptor signaling. Leukemia. 2014;28(9):1851-60.
70. Rieger MA, Hoppe PS, Smejkal BM, Eitelhuber AC, Schroeder T. Hematopoietic cytokines can instruct lineage choice. Science. 2009;325(5937):217-8.
71. Zhao JL, Ma C, O'Connell RM, Mehta A, DiLoreto R, Heath JR, et al. Conversion of danger signals into cytokine signals by hematopoietic stem and progenitor cells for regulation of stress-induced hematopoiesis. Cell Stem Cell. 2014;14(4):445-59.
72. Kang Y-A, Paik H, Zhang SY, Chen JJ, Olson OC, Mitchell CA, et al. Secretory MPP3 reinforce myeloid differentiation trajectory and amplify myeloid cell production. Journal of Experimental Medicine. 2023;220(8).
73. Reynaud D, Pietras E, Barry-Holson K, Mir A, Binnewies M, Jeanne M, et al. IL-6 controls leukemic multipotent progenitor cell fate and contributes to chronic myelogenous leukemia development. Cancer Cell. 2011;20(5):661-73.
74. Hérault A, Binnewies M, Leong S, Calero-Nieto FJ, Zhang SY, Kang Y-A, et al. Myeloid progenitor cluster formation drives emergency and leukaemic myelopoiesis. Nature. 2017;544(7648):53-8.
75. Esplin BL, Shimazu T, Welner RS, Garrett KP, Nie L, Zhang Q, et al. Chronic exposure to a TLR ligand injures hematopoietic stem cells. J Immunol. 2011;186(9):5367-75.
76. de Bruin AM, Demirel Ö, Hooibrink B, Brandts CH, Nolte MA. Interferon-γ impairs proliferation of hematopoietic stem cells in mice. Blood. 2013;121(18):3578-85.
77. Wang J, Erlacher M, Fernandez-Orth J. The role of inflammation in hematopoiesis and bone marrow failure: What can we learn from mouse models? Front Immunol. 2022;13:951937.
78. Bogeska R, Mikecin A-M, Kaschutnig P, Fawaz M, Büchler-Schäff M, Le D, et al. Inflammatory exposure drives long-lived impairment of hematopoietic stem cell self-renewal activity and accelerated aging. Cell Stem Cell. 2022;29(8):1273-84.e8.
79. Mansell E, Lin DS, Loughran SJ, Milsom MD, Trowbridge JJ. New insight into the causes, consequences, and correction of hematopoietic stem cell aging. Experimental Hematology. 2023;125-126:1-5.
80. Basu S, Zhang HH, Quilici C, Dunn AR. Candida albicans can stimulate stromal cells resulting in enhanced granulopoiesis. Stem Cells Dev. 2004;13(1):39-50.
81. Chou DB, Sworder B, Bouladoux N, Roy CN, Uchida AM, Grigg M, et al. Stromal-derived IL-6 alters the balance of myeloerythroid progenitors during Toxoplasma gondii infection. J Leukoc Biol. 2012;92(1):123-31.
82. Boettcher S, Gerosa RC, Radpour R, Bauer J, Ampenberger F, Heikenwalder M, et al. Endothelial cells translate pathogen signals into G-CSF-driven emergency granulopoiesis. Blood. 2014;124(9):1393-403.
83. Swann JW, Zhang R, Verovskaya EV, Calero-Nieto FJ, Wang X, Proven MA, et al. Inflammation perturbs hematopoiesis by remodeling specific compartments of the bone marrow niche. bioRxiv. 2024:2024.09.12.612751.
84. Singh AK, McGuirk JP. Allogeneic Stem Cell Transplantation: A Historical and Scientific Overview. Cancer Res. 2016;76(22):6445-51.

85. Sweeney C, Vyas P. The Graft-Versus-Leukemia Effect in AML. Frontiers in Oncology. 2019;Volume 9 - 2019.
86. Akahoshi Y, Spyrou N, Hogan WJ, Ayuk F, DeFilipp Z, Weber D, et al. Incidence, clinical presentation, risk factors, outcomes, and biomarkers in de novo late acute GVHD. Blood Advances. 2023;7(16):4479-91.
87. Hill GR, Betts BC, Tkachev V, Kean LS, Blazar BR. Current Concepts and Advances in Graft-Versus-Host Disease Immunology. Annual Review of Immunology. 2021;39(1):19-49.
88. Lee KH, Lee JH, Choi SJ, Lee JH, Kim S, Seol M, et al. Failure of trilineage blood cell reconstitution after initial neutrophil engraftment in patients undergoing allogeneic hematopoietic cell transplantation – frequency and outcomes. Bone Marrow Transplantation. 2004;33(7):729-34.
89. Cuadrado MM, Szydlo RM, Watts M, Patel N, Renshaw H, Dorman J, et al. Predictors of recovery following allogeneic CD34+-selected cell infusion without conditioning to correct poor graft function. Haematologica. 2020;105(11):2639-46.
90. Al-Ramahi JS, Shahzad M, Nguyen A, Li K, Amin MK, Ahmed N, et al. Favorable outcomes following CD34-selected stem cell boost for poor graft function after allogeneic hematopoietic stem cell transplantation. Bone Marrow Transplantation. 2024;59(1):134-7.
91. Shapiro RM, Kim HT, Dulery R, Liney D, Garrity HM, Panaro K, et al. Active infection at the time of CD34+ selected stem cell boost is associated with treatment failure and poor overall survival. Blood Advances. 2024;8(17):4729-37.
92. von Bonin M, Bornhäuser M. Concise Review: The Bone Marrow Niche as a Target of Graft Versus Host Disease. STEM CELLS. 2014;32(6):1420-8.
93. Huang A, Zhao X, Li M, Tang G, Fei Y, Wang R, et al. Suppression of Hematopoietic Primitive Cells in Patients with Secondary Failure of Platelet Recovery after Acute Graft-versus-Host Disease. Biology of Blood and Marrow Transplantation. 2020;26(10):1840-54.
94. Sacchetti B, Funari A, Michienzi S, Di Cesare S, Piersanti S, Saggio I, et al. Self-Renewing Osteoprogenitors in Bone Marrow Sinusoids Can Organize a Hematopoietic Microenvironment. Cell. 2007;131(2):324-36.
95. Kong Y, Chang Y-J, Wang Y-Z, Chen Y-H, Han W, Wang Y, et al. Association of an Impaired Bone Marrow Microenvironment with Secondary Poor Graft Function after Allogeneic Hematopoietic Stem Cell Transplantation. Biology of Blood and Marrow Transplantation. 2013;19(10):1465-73.
96. Wang YT, Kong Y, Song Y, Han W, Zhang YY, Zhang XH, et al. Increased Type 1 Immune Response in the Bone Marrow Immune Microenvironment of Patients with Poor Graft Function after Allogeneic Hematopoietic Stem Cell Transplantation. Biol Blood Marrow Transplant. 2016;22(8):1376-82.
97. Kong Y, Wang Y-T, Cao X-N, Song Y, Chen Y-H, Sun Y-Q, et al. Aberrant T cell responses in the bone marrow microenvironment of patients with poor graft function after allogeneic hematopoietic stem cell transplantation. Journal of Translational Medicine. 2017;15(1):57.
98. Shono Y, Shiratori S, Kosugi-Kanaya M, Ueha S, Sugita J, Shigematsu A, et al. Bone Marrow Graft-versus-Host Disease: Evaluation of Its Clinical Impact on Disrupted Hematopoiesis after Allogeneic Hematopoietic Stem Cell Transplantation. Biology of Blood and Marrow Transplantation. 2014;20(4):495-500.

99. Lin Y, Gu Q, Lu S, Pan Z, Yang Z, Li Y, et al. Ruxolitinib improves hematopoietic regeneration by restoring mesenchymal stromal cell function in acute graft-versus-host disease. J Clin Invest. 2023;133(15).
100. Yao Y, Song X, Cheng H, Tang G, Hu X, Zhou H, et al. Dysfunction of Bone Marrow Vascular Niche in Acute Graft-Versus-Host Disease after MHC-Haploidentical Bone Marrow Transplantation. PLOS ONE. 2014;9(8):e104607.
101. Shono Y, Ueha S, Wang Y, Abe J, Kurachi M, Matsuno Y, et al. Bone marrow graft-versus-host disease: early destruction of hematopoietic niche after MHC-mismatched hematopoietic stem cell transplantation. Blood. 2010;115(26):5401-11.
102. Lin Y, Hu X, Cheng H, Pang Y, Wang L, Zou L, et al. Graft-versus-Host Disease Causes Broad Suppression of Hematopoietic Primitive Cells and Blocks Megakaryocyte Differentiation in a Murine Model. Biology of Blood and Marrow Transplantation. 2014;20(9):1290-300.
103. Cappell KM, Kochenderfer JN. Long-term outcomes following CAR T cell therapy: what we know so far. Nature Reviews Clinical Oncology. 2023;20(6):359-71.
104. Rejeski K, Subklewe M, Aljurf M, Bachy E, Balduzzi A, Barba P, et al. Immune effector cell–associated hematotoxicity: EHA/EBMT consensus grading and best practice recommendations. Blood. 2023;142(10):865-77.
105. Rejeski K, Wang Y, Hansen DK, Iacoboni G, Bachy E, Bansal R, et al. Applying the EHA/EBMT grading for ICAHT after CAR-T: comparative incidence and association with infections and mortality. Blood Advances. 2024;8(8):1857-68.
106. Cordeiro A, Bezerra ED, Hirayama AV, Hill JA, Wu QV, Voutsinas J, et al. Late Events after Treatment with CD19-Targeted Chimeric Antigen Receptor Modified T Cells. Biology of Blood and Marrow Transplantation. 2020;26(1):26-33.
107. Rejeski K, Perez A, Sesques P, Hoster E, Berger C, Jentzsch L, et al. CAR-HEMATOTOX: a model for CAR T-cell–related hematologic toxicity in relapsed/refractory large B-cell lymphoma. Blood. 2021;138(24):2499-513.
108. Aoki K, Kurashige M, Ichii M, Higaki K, Sugiyama T, Kaito T, et al. Identification of CXCL12-abundant reticular cells in human adult bone marrow. Br J Haematol. 2021;193(3):659-68.
109. Kitamura W, Asada N, Naoi Y, Abe M, Fujiwara H, Ennishi D, et al. Bone marrow microenvironment disruption and sustained inflammation with prolonged haematologic toxicity after CAR T-cell therapy. Br J Haematol. 2023;202(2):294-307.
110. Strati P, Li X, Deng Q, Marques-Piubelli ML, Henderson J, Watson G, et al. Prolonged cytopenia following CD19 CAR T cell therapy is linked with bone marrow infiltration of clonally expanded IFNγ-expressing CD8 T cells. Cell Rep Med. 2023;4(8):101158.
111. Young NS. Aplastic Anemia. N Engl J Med. 2018;379(17):1643-56.
112. Deng XZ, Du M, Peng J, Long JX, Zheng CJ, Tan Y, et al. Associations between the HLA-A/B/DRB1 polymorphisms and aplastic anemia: evidence from 17 case-control studies. Hematology. 2018;23(3):154-62.
113. Katagiri T, Sato-Otsubo A, Kashiwase K, Morishima S, Sato Y, Mori Y, et al. Frequent loss of HLA alleles associated with copy number-neutral 6pLOH in acquired aplastic anemia. Blood. 2011;118(25):6601-9.
114. Ben Hamza A, Welters C, Stadler S, Brüggemann M, Dietze K, Brauns O, et al. Virus-reactive T cells expanded in aplastic anemia eliminate hematopoietic progenitor cells by molecular mimicry. Blood. 2024;143(14):1365-78.

115. Peffault de Latour R, Kulasekararaj A, Iacobelli S, Terwel SR, Cook R, Griffin M, et al. Eltrombopag Added to Immunosuppression in Severe Aplastic Anemia. N Engl J Med. 2022;386(1):11-23.
116. Vaht K, Göransson M, Carlson K, Isaksson C, Lenhoff S, Sandstedt A, et al. Incidence and outcome of acquired aplastic anemia: real-world data from patients diagnosed in Sweden from 2000-2011. Haematologica. 2017;102(10):1683-90.
117. Griffin G, Shenoi S, Hughes GC. Hemophagocytic lymphohistiocytosis: An update on pathogenesis, diagnosis, and therapy. Best Practice & Research Clinical Rheumatology. 2020;34(4):101515.
118. Jordan MB, Hildeman D, Kappler J, Marrack P. An animal model of hemophagocytic lymphohistiocytosis (HLH): CD8+ T cells and interferon gamma are essential for the disorder. Blood. 2004;104(3):735-43.
119. Rosenfeld SJ, Young NS. Viruses and bone marrow failure. Blood Reviews. 1991;5(2):71-7.
120. Morinet F, Leruez-Ville M, Pillet S, Fichelson S. Concise Review: Anemia Caused by Viruses. Stem Cells. 2011;29(11):1656-60.
121. Isringhausen S, Mun Y, Kovtonyuk L, Kräutler NJ, Suessbier U, Gomariz A, et al. Chronic viral infections persistently alter marrow stroma and impair hematopoietic stem cell fitness. J Exp Med. 2021;218(12).
122. Groarke EM, Feng X, Aggarwal N, Manley AL, Wu Z, Gao S, et al. Efficacy of JAK1/2 inhibition in murine immune bone marrow failure. Blood. 2023;141(1):72-89.
123. McCabe A, Smith JNP, Costello A, Maloney J, Katikaneni D, MacNamara KC. Hematopoietic stem cell loss and hematopoietic failure in severe aplastic anemia is driven by macrophages and aberrant podoplanin expression. Haematologica. 2018;103(9):1451-61.
124. Bloom ML, Wolk AG, Simon-Stoos KL, Bard JS, Chen J, Young NS. A mouse model of lymphocyte infusion-induced bone marrow failure. Experimental Hematology. 2004;32(12):1163-72.
125. Patel BA, Giudice V, Young NS. Immunologic effects on the haematopoietic stem cell in marrow failure. Best Practice & Research Clinical Haematology. 2021;34(2):101276.
126. Rodriguez S, Chora A, Goumnerov B, Mumaw C, Goebel WS, Fernandez L, et al. Dysfunctional expansion of hematopoietic stem cells and block of myeloid differentiation in lethal sepsis. Blood. 2009;114(19):4064-76.
127. Kumar BV, Connors TJ, Farber DL. Human T Cell Development, Localization, and Function throughout Life. Immunity. 2018;48(2):202-13.
128. Mestas J, Hughes CCW. Of Mice and Not Men: Differences between Mouse and Human Immunology. The Journal of Immunology. 2004;172(5):2731-8.
129. Khan AO, Rodriguez-Romera A, Reyat JS, Olijnik A-A, Colombo M, Wang G, et al. Human Bone Marrow Organoids for Disease Modeling, Discovery, and Validation of Therapeutic Targets in Hematologic Malignancies. Cancer Discovery. 2023;13(2):364-85.
130. Olijnik A-A, Rodriguez-Romera A, Wong ZC, Shen Y, Reyat JS, Jooss NJ, et al. Generating human bone marrow organoids for disease modeling and drug discovery. Nature Protocols. 2024.
131. Wilkinson AC, Ishida R, Nakauchi H, Yamazaki S. Long-term ex vivo expansion of mouse hematopoietic stem cells. Nature Protocols. 2020;15(2):628-48.

132. Hengel RL, Thaker V, Pavlick MV, Metcalf JA, Dennis G, Jr., Yang J, et al. Cutting edge: L-selectin (CD62L) expression distinguishes small resting memory CD4+ T cells that preferentially respond to recall antigen. J Immunol. 2003;170(1):28-32.
133. Cooke KR, Kobzik L, Martin TR, Brewer J, Delmonte J, Crawford JM, et al. An Experimental Model of Idiopathic Pneumonia Syndrome After Bone Marrow Transplantation: I. The Roles of Minor H Antigens and Endotoxin. Blood. 1996;88(8):3230-9.
134. Deuse T, Hu X, Gravina A, Wang D, Tediashvili G, De C, et al. Hypoimmunogenic derivatives of induced pluripotent stem cells evade immune rejection in fully immunocompetent allogeneic recipients. Nature Biotechnology. 2019;37(3):252-8.
135. Choi EY, Yoshimura Y, Christianson GJ, Sproule TJ, Malarkannan S, Shastri N, et al. Quantitative analysis of the immune response to mouse non-MHC transplantation antigens in vivo: the H60 histocompatibility antigen dominates over all others. J Immunol. 2001;166(7):4370-9.
136. Dertschnig S, Evans P, Santos ESP, Manzo T, Ferrer IR, Stauss HJ, et al. Graft-versus-host disease reduces lymph node display of tissue-restricted self-antigens and promotes autoimmunity. J Clin Invest. 2020;130(4):1896-911.
137. Mills TS, Kain B, Burchill MA, Danis E, Lucas ED, Culp-Hill R, et al. A distinct metabolic and epigenetic state drives trained immunity in HSC-derived macrophages from autoimmune mice. Cell Stem Cell. 2024;31(11):1630-49.e8.
138. Kanayama M, Izumi Y, Yamauchi Y, Kuroda S, Shin T, Ishikawa S, et al. CD86-based analysis enables observation of bona fide hematopoietic responses. Blood. 2020;136(10):1144-54.
139. Ooi AG, Karsunky H, Majeti R, Butz S, Vestweber D, Ishida T, et al. The adhesion molecule esam1 is a novel hematopoietic stem cell marker. Stem Cells. 2009;27(3):653-61.
140. Flutter B, Edwards N, Fallah-Arani F, Henderson S, Chai JG, Sivakumaran S, et al. Nonhematopoietic antigen blocks memory programming of alloreactive CD8+ T cells and drives their eventual exhaustion in mouse models of bone marrow transplantation. J Clin Invest. 2010;120(11):3855-68.
141. Choi EY, Christianson GJ, Yoshimura Y, Jung N, Sproule TJ, Malarkannan S, et al. Real-time T-cell profiling identifies H60 as a major minor histocompatibility antigen in murine graft-versus-host disease. Blood. 2002;100(13):4259-64.
142. Tan JKH, O'Neill HC. Investigation of Murine Spleen as a Niche for Hematopoiesis. Transplantation. 2010;89(2).
143. White JR, Gong H, Colaizy TT, Moreland JG, Flaherty H, McElroy SJ. Evaluation of hematologic variables in newborn C57/BL6 mice up to day 35. Vet Clin Pathol. 2016;45(1):87-95.
144. Mazzaccara C, Labruna G, Cito G, Scarfò M, De Felice M, Pastore L, et al. Age-Related Reference Intervals of the Main Biochemical and Hematological Parameters in C57BL/6J, 129SV/EV and C3H/HeJ Mouse Strains. PLoS One. 2008;3(11):e3772.
145. Scott DM, Ehrmann IE, Ellis PS, Bishop CE, Agulnik AI, Simpson E, et al. Identification of a mouse male-specific transplantation antigen, H-Y. Nature. 1995;376(6542):695-8.
146. Umino K, Morita K, Ikeda T, Kawaguchi S-i, Nagayama T, Ito S, et al. Antibody-mediated pathogenesis of chronic GVHD through DBY/HLA class II complexes and induction of a GVL effect. Blood. 2023;142(11):1008-21.

147. Popli R, Sahaf B, Nakasone H, Lee JY, Miklos DB. Clinical impact of H-Y alloimmunity. Immunol Res. 2014;58(2-3):249-58.
148. Zeiser R, Blazar BR. Preclinical models of acute and chronic graft-versus-host disease: how predictive are they for a successful clinical translation? Blood. 2016;127(25):3117-26.
149. Socié G, Kean LS, Zeiser R, Blazar BR. Insights from integrating clinical and preclinical studies advance understanding of graft-versus-host disease. The Journal of Clinical Investigation. 2021;131(12).
150. Zhao D, Ravikumar V, Leach TJ, Kraushaar D, Lauder E, Li L, et al. Inflammation-induced epigenetic imprinting regulates intestinal stem cells. Cell Stem Cell. 2024;31(10):1447-64.e6.
151. Arnhold V, Chang WY, Jansen SA, Thangavelu G, Calafiore M, Vinci P, et al. Corticosteroids impair epithelial regeneration in immune-mediated intestinal damage. The Journal of Clinical Investigation. 2024;134(7).
152. Koyama M, Hill GR. Mouse Models of Antigen Presentation in Hematopoietic Stem Cell Transplantation. Frontiers in Immunology. 2021;Volume 12 - 2021.
153. Netsrithong R, Garcia-Perez L, Themeli M. Engineered T cells from induced pluripotent stem cells: from research towards clinical implementation. Front Immunol. 2023;14:1325209.
154. Hernández-Malmierca P, Vonficht D, Schnell A, Uckelmann HJ, Bollhagen A, Mahmoud MAA, et al. Antigen presentation safeguards the integrity of the hematopoietic stem cell pool. Cell Stem Cell. 2022;29(5):760-75.e10.
155. Liao H, Wu J, VanDusen NJ, Li Y, Zheng Y. CRISPR-Cas9-mediated homology-directed repair for precise gene editing. Molecular Therapy Nucleic Acids. 2024;35(4).
156. Mali P, Yang L, Esvelt KM, Aach J, Guell M, DiCarlo JE, et al. RNA-Guided Human Genome Engineering via Cas9. Science. 2013;339(6121):823-6.
157. Miyaoka Y, Chan AH, Judge LM, Yoo J, Huang M, Nguyen TD, et al. Isolation of single-base genome-edited human iPS cells without antibiotic selection. Nature Methods. 2014;11(3):291-3.
158. Guo Q, Mintier G, Ma-Edmonds M, Storton D, Wang X, Xiao X, et al. 'Cold shock' increases the frequency of homology directed repair gene editing in induced pluripotent stem cells. Scientific Reports. 2018;8(1):2080.
159. Weiss G, Ganz T, Goodnough LT. Anemia of inflammation. Blood. 2019;133(1):40-50.
160. Libregts SF, Gutiérrez L, de Bruin AM, Wensveen FM, Papadopoulos P, van Ijcken W, et al. Chronic IFN-γ production in mice induces anemia by reducing erythrocyte life span and inhibiting erythropoiesis through an IRF-1/PU.1 axis. Blood. 2011;118(9):2578-88.
161. McCranor BJ, Kim MJ, Cruz NM, Xue Q-L, Berger AE, Walston JD, et al. Interleukin-6 directly impairs the erythroid development of human TF-1 erythroleukemic cells. Blood Cells, Molecules, and Diseases. 2014;52(2):126-33.
162. Swann JW, Koneva LA, Regan-Komito D, Sansom SN, Powrie F, Griseri T. IL-33 promotes anemia during chronic inflammation by inhibiting differentiation of erythroid progenitors. J Exp Med. 2020;217(9).
163. Hartley PS. Mice housed in groups of 4-6 exhibit a diurnal surge in their platelet count. Platelets. 2013;24(5):412-4.

164. Hoggatt J, Hoggatt AF, Tate TA, Fortman J, Pelus LM. Bleeding the laboratory mouse: Not all methods are equal. Exp Hematol. 2016;44(2):132-7.e1.
165. Kolupaev OV, Dant TA, Bommiasamy H, Bruce DW, Fowler KA, Tilley SL, et al. Impaired bone marrow B-cell development in mice with a bronchiolitis obliterans model of cGVHD. Blood Advances. 2018;2(18):2307-19.
166. Bordenave J, Gajda D, Michonneau D, Vallet N, Chevalier M, Clappier E, et al. Deciphering bone marrow engraftment after allogeneic stem cell transplantation in humans using single-cell analyses. The Journal of Clinical Investigation. 2024;134(20).
167. Mensen A, Jöhrens K, Anagnostopoulos I, Demski S, Oey M, Stroux A, et al. Bone marrow T-cell infiltration during acute GVHD is associated with delayed B-cell recovery and function after HSCT. Blood. 2014;124(6):963-72.
168. Hughes AM, Kuek V, Kotecha RS, Cheung LC. The Bone Marrow Microenvironment in B-Cell Development and Malignancy. Cancers (Basel). 2022;14(9).
169. Shim J, Park S, Venkateswaran S, Kumar D, Prince C, Parihar V, et al. Early B-cell development and B-cell maturation are impaired in patients with active hemophagocytic lymphohistiocytosis. Blood. 2023;142(23):1972-84.
170. Clave E, Busson M, Douay C, Peffault de Latour R, Berrou J, Rabian C, et al. Acute graft-versus-host disease transiently impairs thymic output in young patients after allogeneic hematopoietic stem cell transplantation. Blood. 2009;113(25):6477-84.
171. Hauri-Hohl MM, Keller MP, Gill J, Hafen K, Pachlatko E, Boulay T, et al. Donor T-cell alloreactivity against host thymic epithelium limits T-cell development after bone marrow transplantation. Blood. 2007;109(9):4080-8.
172. Beilhack A, Schulz S, Baker J, Beilhack GF, Wieland CB, Herman EI, et al. In vivo analyses of early events in acute graft-versus-host disease reveal sequential infiltration of T-cell subsets. Blood. 2005;106(3):1113-22.
173. Brochu S, Rioux-Massé B, Roy J, Roy D-C, Perreault C. Massive Activation-Induced Cell Death of Alloreactive T Cells With Apoptosis of Bystander Postthymic T Cells Prevents Immune Reconstitution in Mice With Graft-Versus-Host Disease. Blood. 1999;94(2):390-400.
174. Gomariz A, Helbling PM, Isringhausen S, Suessbier U, Becker A, Boss A, et al. Quantitative spatial analysis of haematopoiesis-regulating stromal cells in the bone marrow microenvironment by 3D microscopy. Nature Communications. 2018;9(1):2532.
175. Mann M, Mehta A, de Boer CG, Kowalczyk MS, Lee K, Haldeman P, et al. Heterogeneous Responses of Hematopoietic Stem Cells to Inflammatory Stimuli Are Altered with Age. Cell Reports. 2018;25(11):2992-3005.e5.
176. Ross JB, Myers LM, Noh JJ, Collins MM, Carmody AB, Messer RJ, et al. Depleting myeloid-biased haematopoietic stem cells rejuvenates aged immunity. Nature. 2024;628(8006):162-70.
177. Rundberg Nilsson A, Soneji S, Adolfsson S, Bryder D, Pronk CJ. Human and Murine Hematopoietic Stem Cell Aging Is Associated with Functional Impairments and Intrinsic Megakaryocytic/Erythroid Bias. PLoS One. 2016;11(7):e0158369.
178. Shen Y, Benlabiod C, Rodriguez-Romera A, Watson E, Reyat JS, Gurashi K, et al. comBO: A combined human bone and lympho-myeloid bone marrow organoid for pre-clinical modelling of haematopoietic disorders. bioRxiv. 2025:2025.02.16.638505.
179. Chan JL, Tang KC, Patel AP, Bonilla LM, Pierobon N, Ponzio NM, et al. Antigen-presenting property of mesenchymal stem cells occurs during a narrow window at low levels of interferon-gamma. Blood. 2006;107(12):4817-24.

180. Koyama M, Kuns RD, Olver SD, Raffelt NC, Wilson YA, Don AL, et al. Recipient nonhematopoietic antigen-presenting cells are sufficient to induce lethal acute graft-versus-host disease. Nat Med. 2011;18(1):135-42.
181. Chakraverty R, Teshima T. Graft-versus-host disease: a disorder of tissue regeneration and repair. Blood. 2021;138(18):1657-65.